05 Apr 1995, 9:00 am - 10:00 am

Simple Physical Models for Foundation Dynamics

John P. Wolf

Swiss Federal Institute of Technology Lausanne, Lausanne, Switzerland

Proceedings: Third International Conference on Recent Advances in Geotechnical Earthquake Engineering and Soil Dynamics, April 2–7, 1995, Volume II, St. Louis, Missouri

Simple Physical Models for Foundation Dynamics

Paper No. SOA9

(State of the Art Paper)

John P. Wolf
Institute of Hydraulics and Energy, Dept. of Civil Engineering, Swiss Federal Institute of Technology Lausanne, Lausanne, Switzerland

SYNOPSIS As an alternative to rigorous boundary-element solutions, simple physical models can be used to determine e.g. the interaction force-displacement relationship (dynamic stiffness) of foundations and the seismic effective foundation input motion. Translational and rotational cones and their corresponding lumped-parameter models together with simple one-dimensional wave patterns in the horizontal plane allow surface, embedded and pile foundations even for a layered site to be analyzed and thus form a major step towards developing a strength-of-materials approach to foundation-vibration analysis. The analysis can mostly be performed directly in the time domain. The physical models provide physical insight which is often obscured by the mathematical complexity of rigorous solutions, offer simplicity in application as well as in the physics and in the rigorous mathematical solution of the physical model, are sufficiently general to enable reasonably complicated practical cases to be solved, exhibit adequate accuracy, allow physical features to be demonstrated and offer the potential for generalizations.

1. INTRODUCTION

A key aspect of any foundation vibration or dynamic soil-structure interaction analysis is the calculation of the interaction force-displacement relationship (dynamic stiffness) on the basemat-soil interface. To discuss the concepts, a specific case is addressed (Fig. 1): the vertical degree of freedom with the force P_0 and displacement u_0 of a rigid, massless disk of radius r_0 on a soil layer of depth d resting on a flexible rock halfspace. G represents the shear modulus, υ Poisson's ratio and ρ the mass density, from which the dilatational wave velocity c_p follows. Indices L and R are introduced to identify constants associated with the layer and the rock respectively.

To determine the P_0-u_0 relationship, *rigorous methods* exist: either the region of the layer and part of the halfspace are modeled with axisymmetric finite elements and sophisticated *consistent transmitting boundaries* are introduced to represent wave propagation towards infinity or the *boundary-element method* is applied whereby the free surface and the interface between the layer and the halfspace must be discretized when the fundamental solution of the full space is used. In these rigorous methods a formidable theoretical background is required. A considerable amount of expertise in idealizing the actual dynamic system is necessary [8], and a significant amount of data preparation has to be performed. The computational expense for just one run is large, making it difficult from an economical point of view to perform the necessary parametric studies. A false sense of security could thus be provided to the user. The engineer tends to be intimidated by these procedures. The effort to interpret the results is also significant. These rigorous methods with their mathematical complexity obscure the physical insight and belong more to the discipline of applied computational mechanics than to civil engineering. They should only be used for large projects of critical facilities such as nuclear-power plants, bunkered military constructions, dams, etc. with the corresponding budget and available time to perform the analysis. For all other projects, the most majority, the *simple physical models to represent the unbounded soil* summarized in this paper should be used.

For instance, the soil below the disk is modeled as a truncated rod (bar) with its area varying as in a *cone* (Fig. 2). The vertical force $P_0(t)$ produces an incident dilatational wave propagating with the velocity c_p^L (for $\upsilon_L \le 1/3$) along a cone (with Apex 1) with mass density ρ_L and a specific opening angle determined by z_0^L downwards from the disk. At the beginning of the excitation before the wave reaches the soil-rock interface, the wave pattern in the layer will be the same as that occurring in a halfspace. The corresponding displacement in the truncated semi-infinite cone is inversely proportional to the distance from apex 1

$$u(z,t) = \frac{z_0^L}{z_0^L + z} f\left(t - \frac{z}{c_p^L}\right) \tag{1}$$

with z measured from the free surface. Apex 1 is specified in such a way as to yield the same static-stiffness coefficients for the truncated semi-infinite cone $\rho\left(c_p^L\right)^2 \pi r_0^2 / z_0^L$ and the disk on a homogeneous halfspace with the material properties of the layer $4G_L r_0/(1-\nu_L)$, yielding

$$\frac{z_0^L}{r_0} = \frac{\pi}{2}\frac{(1-\upsilon_L)^2}{1-2\upsilon_L} \tag{2}$$

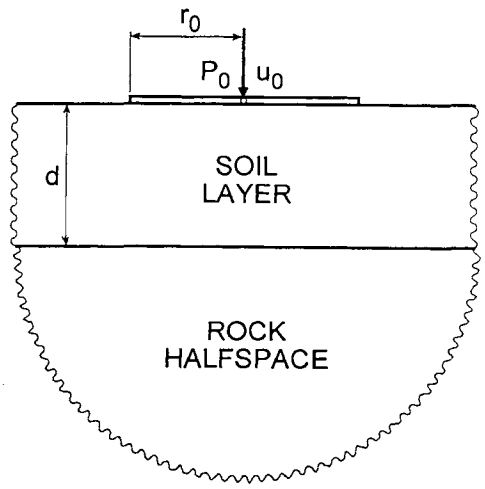

Fig. 1 Vertical motion of disk on surface layer resting on flexible rock halfspace.

At the interface of the layer and the rock (z=d) the incident wave f will lead to a refracted wave h propagating in the rock in the same direction as the incident wave along its own cone with the apex distance-to-radius ratio $z_0^R/\left(r_0\left(z_0^L+d\right)/z_0^L\right)$ (apex 2, dotted line). (Note that the aspect ratio of the rock's cone is generally different from that of the layer's cone. However, in the special case $\upsilon_R=\upsilon_L$, both cones have the same proportions and z_0^R equals z_0^L+d). The displacement in the rock $u_R(z,t)$ is formulated as

$$u_R(z,t)=\frac{\frac{z_0^L z_0^R}{z_0^L+d}}{z_0^R-d+z}\,h\left(t-\frac{d}{c_p^L}+\frac{d}{c_p^R}-\frac{z}{c_p^R}\right) \qquad (3)$$

with the numerator chosen for convenience. In addition, a reflected wave g is created propagating back through the layer along the indicated cone (apex 3) in the opposite upward direction. The resulting displacement in the layer $u_L(z,t)$ then equals

$$u_L(z,t)=\frac{z_0^L}{z_0^L+z}\,f\left(t-\frac{z}{c_p^L}\right)+\frac{z_0^L}{z_0^L+2d-z}\,g\left(t-\frac{2d}{c_p^L}+\frac{z}{c_p^L}\right) \qquad (4)$$

Notice that the denominators in Eqs. 3 and 4 are the distances to the apexes of the respective cones. At the interface z=d the arguments of the three functions f, g and h are the same, $t-d/c_p^L$. The upwave g will reflect back at the free surface and then propagate downwards along the cone (apex 4) shown in Fig. 2. Upon reaching the interface of the layer and the rock, a refraction and a reflection again take place, etc. The reflection coefficient -α, defined as the ratio of the reflected wave g to the incident wave f, is determined by formulating compatibility and equilibrium at the interface.

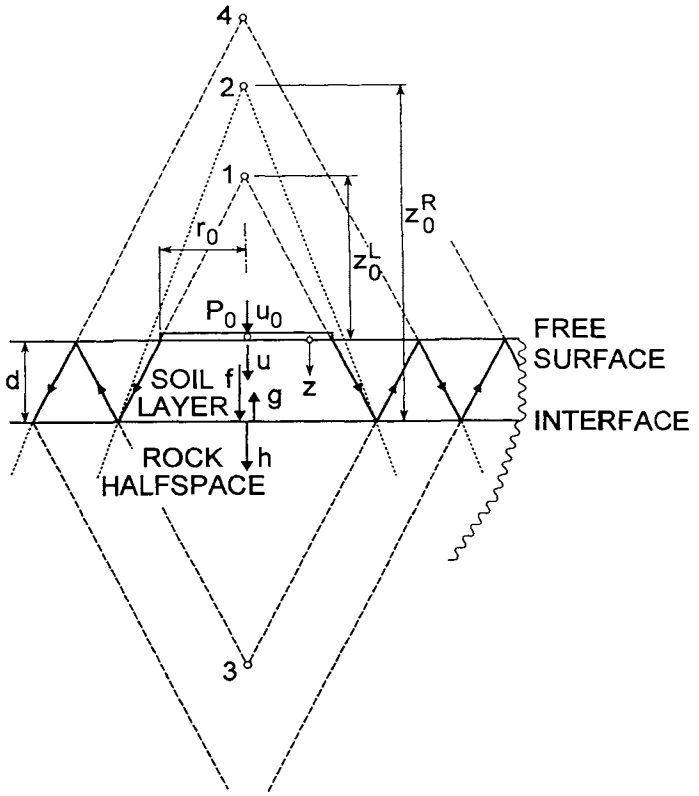

Fig. 2 Wave patterns of corresponding cones in soil layer and rock halfspace.

From a practical point of view sufficient accuracy results from using the high-frequency limit which corresponds to replacing the cone by a prismatic bar.

$$-\alpha=\frac{\rho_L c_p^L-\rho_R c_p^R}{\rho_L c_p^L+\rho_R c_p^R} \qquad (5)$$

The resulting displacement in the layer $u_L(t,z)$ is equal to the superposition of the contributions of all cones; i.e. the displacements of the incident wave and of all subsequent upwaves and downwaves are summed. Denoting the incident wave at z=0 as $\bar{u}_0(t)(=f(t))$ the displacement $u_L(z,t)$ of the layer at depth z and time t may be expressed as the wave pattern

incident wave

$$u_L(z,t)=\frac{z_0^L}{z_0^L+z}\,\bar{u}_0\left(t-\frac{z}{c_p^L}\right)$$

upwave from rock downwave from surface

$$+\sum_{j=1}^{k}(-\alpha)^j\left[\frac{z_0^L\bar{u}_0\left(t-\frac{2jd}{c_p^L}+\frac{z}{c_p^L}\right)}{z_0^L+2jd-z}+\frac{z_0^L\bar{u}_0\left(t-\frac{2jd}{c_p^L}-\frac{z}{c_p^L}\right)}{z_0^L+2jd+z}\right] \qquad (6)$$

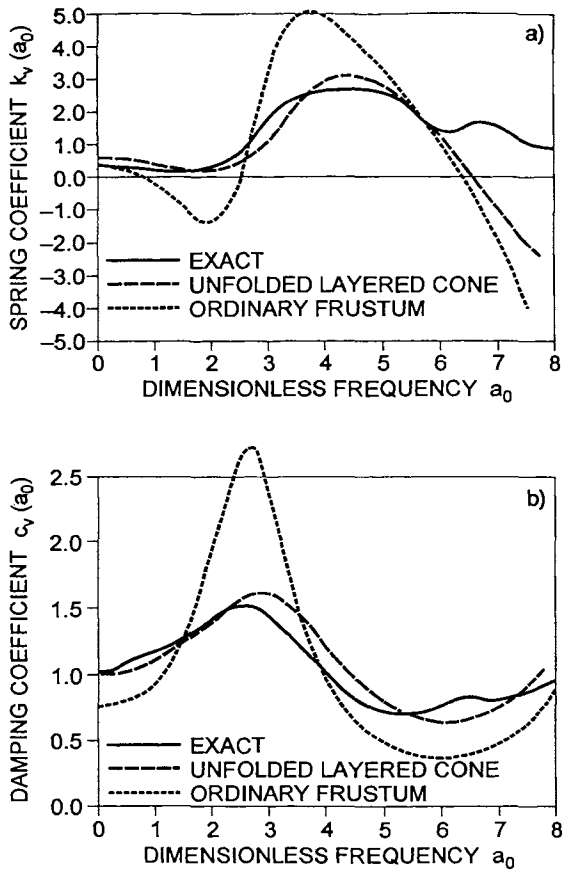

Fig. 3 Vertical dynamic-stiffness coefficient for disk on soil layer stiffer than rock halfspace.

The integer k is equal to the largest j for which at least one of the arguments of $\bar{u}_0$ for a specific z and t is positive.

The cones describing the wave propagation in the layer can be unfolded to form a single layered cone. This generalized *unfolded layered cone* represents a wave pattern whose amplitude decays with distance, that considers the reflections at the free surface and the reflections and refractions at the layer-rock interface and that spreads resulting in radiation of energy in the horizontal direction. Through the choice of the cone as a physical model, the complicated three-dimensional wave pattern with body and surface waves and three different velocities is replaced by the simple one-dimensional wave propagation governed by the one constant dilatational wave velocity of the conical rod, whereby *plane sections remain plane* (theory of strength of materials). Only the (one) unknown u_0 needs to be introduced.

As an example, the vertical dynamic-stiffness coefficient for harmonic loading of the disk on the soil layer-rock halfspace based on the refolded layered cone equals [44]

$$S(\omega) = K \frac{1 + i\frac{\omega T}{K}}{1 + 2\sum_{j=1}^{\infty}(-\alpha)^j \frac{e^{-ij\omega T}}{1 + j\kappa}} \qquad (7)$$

where $K=4G_L r_0/(1-\upsilon_L)$ denotes the static-stiffness coefficient of the disk on a homogeneous halfspace with the properties of the layer, $T=2d/c_p^L$ and $\kappa=2d/z_0^L$. The numerator is equal to the dynamic-stiffness coefficient of the truncated semi-infinite cone modeling the halfspace which is multiplied by the transfer function $\bar{u}_0(\omega)/u_0(\omega)$ determined from Eq. 6 which introduces the reflections of the layered system. Equation 7 represents a compact expression with a clear physical interpretation.

To check the accuracy, the case of a stiffer and denser layer than the halfspace is examined. This situation can occur for a new sand fill over soft alluvial virgin soil. It is typical for some sea coast areas. The ratios $d/r_0=1$, $G_L/G_R=5$, $\rho_L/\rho_R=1.25$ and $\upsilon_L=\upsilon_R=1/3$ are selected, resulting in an impedance ratio $\rho_L c_L/(\rho_R c_R)=2.5$. The apex ratio for the vertical motion equals $z_0^L/r_0=2.094$ (Eq. 2) and the reflection coefficient $-\alpha=+3/7$ (Eq. 5). In this case $z_0^R=z_0^L+d$. The non-dimensionalized vertical dynamic-stiffness coefficient $S(\omega)/K$ (Eq. 7) is decomposed as $k_v(a_0)+ia_0 c_v(a_0)$ with $a_0=\omega r_0/c_s^L$ (shear-wave velocity c_s). The spring and damping coefficients $k_v(a_0)$, $c_v(a_0)$ of the unfolded layered cone agree well with the rigorous result using the consistent-boundary formulation [37] denoted as exact in Fig. 3.

To capture the horizontal radiation of energy through a layer with cones, the sum in Eq. 7 must be evaluated up to a large j. The sum may be avoided if the layer is idealized by an ordinary non-radiating cone frustum (finite element of a tapered bar) with vertical dynamic-stiffness coefficients (index 1 for top ($r_1=r_0$), index 2 for bottom [25])

$$S_{11}(\omega) = \rho\left(c_p^L\right)^2 \pi r_1^2 \left[\frac{1}{z_0^L} + \frac{1}{d}\frac{\omega d / c_p^L}{\tan\left(\omega d / c_p^L\right)}\right] \qquad (8a)$$

$$S_{12}(\omega) = S_{21}(\omega) = -\rho\left(c_p^L\right)^2 \pi r_1^2 \left[\frac{z_0^L + d}{z_0^L d}\frac{\omega d / c_p^L}{\sin\left(\omega d / c_p^L\right)}\right] \qquad (8b)$$

$$S_{22}(\omega) = \rho\left(c_p^L\right)^2 \pi r_1^2 \left[\left(\frac{z_0^L + d}{z_0^L}\right)^2 \frac{1}{d}\frac{\omega d / c_p^L}{\tan\left(\omega d / c_p^L\right)} - \frac{z_0^L + d}{\left(z_0^L\right)^2}\right] \qquad (8c)$$

In this ordinary frustum, waves reflected at the layer-rock interface cannot spread and radiate energy horizontally as they propagate back upwards. Instead, they are focused in the narrowing neck of the frustum. This disadvantage makes the ordinary frustum used to model the soil layer whose dynamic-stiffness matrix (Eq. 8) can be assembled with the dynamic-stiffness coefficient of the cone representing the rock halfspace to calculate the layered system clearly inferior (Fig. 3). The spring and damping coefficients of the ordinary frustum oscillate more than they should.

The simple physical models such as the unfolded layered cone easily fit the size and economics of a project, and no

sophisticated computer code needs to be available. Use of these procedures leads to some loss of precision, which is more than compensated for by their many advantages. It cannot be the aim of the engineer to calculate the complex reality as closely as possible. For a well balanced design which is both safe and economical rigorous results are not called for in a standard project. Their accuracy is anyhow limited because of the many uncertainties (for instance in defining the soil profile), some of which can never be eliminated.

As the simple physical models cannot cover all cases, they do not supplant the more generally applicable rigorous boundary-element method, but rather supplement it. It should also be stressed that an improved understanding can be gained from the results of a rigorous analysis, which should thus be developed to enable progress. As experience increases, the key aspects of the behavior can be identified. This then leads to the development of simplified procedures which, however, still capture the salient features of the phenomenon. These physical models for soil dynamics are not the first attempt to capture the physics which has not been properly evaluated yet. On the contrary they make full use of the experience gained from the rigorous state-of-the-art formulations. The physical models are thus not only simple to use and lead to valuable physical insight, but they are also quite dependable incorporating implicitly much more know-how than meets the eye.

As described by Roesset in the foreword covering the early work on simple models of [49], the same researchers engaged in the derivation of rigorous procedures based on elasto-dynamics have at the same time tried to explain their results with simple models. These attempts dating back to the thirties were not always successful. Summaries, written by Roesset [29, 30], who contributed significantly to the advancement of the state of the art, influenced the development significantly. A brief historical review with a classification of the methods concentrating on certain key aspects influenced by the preferences of the author follows. For a more complete evaluation of the rich tradition the reader is referred to the literature mentioned in the references of this paragraph. The first group to calculate the interaction force-displacement relationship of a foundation on the surface of a halfspace consists of *truncated semi-infinite cones* introduced by Ehlers [5] for translational motion and much later by Meek and Veletsos [15] for rotational motion. An application to the torsional motion is described in Veletsos and Nair [35]. Wedges for plane-strain conditions are examined by Gazetas and Dobry [7]. It is important to stress that in a practical application the (one dimensional) wave propagation does not have to be addressed as the dynamic stiffness of the semi-infinite cone is exactly equal to that of a simple discrete-element model consisting of a spring and a dashpot (for rotation also of a mass moment of inertia with its own internal degree of freedom) with frequency-independent coefficients. Based on this arrangement the coefficients of the discrete elements are determined not from the cone model - but as an extension - from calibration with rigorous solutions of elasto-dynamics. This permits not only material damping to be considered (Veletsos and Nair [36]), but allows generalizations to embedded and inhomogeneous sites (Wolf and Somaini [39]) whereby also an additional discrete-element (a spring) can be introduced (de Barros and Luco [2]). In this second group, the *lumped-parameter models*, the early single-degree-of-freedom systems determined in an ad-hoc manner (Whitman [38], Richart, Hall and Woods [28]) are also included. Starting from the discrete-element model of the rotational cone, a family of lumped-parameter models can be constructed systematically for any dynamic-stiffness coefficient (Wolf [40]). In the third group, *wave patterns in the horizontal plane* are prescribed. Dobry and Gazetas [4] assume simple cylindrical waves to calculate dynamic-interaction factors which permit a pile group to be analysed considering dynamic pile-soil-pile interaction. Finally, the fourth group consists of calibration procedures to determine *approximate expressions for the dynamic-stiffness coefficients in the frequency domain* and the static-stiffness coefficients for a wide range of foundations (Gazetas [9], [11], Pais and Kausel [27]), in many cases also being guided by the dynamic-stiffness coefficient of the rotational cone.

This paper concentrates on summarizing the research and development performed in an informal, enthusiastic, and collegial atmosphere during the past fours years with Dr. J.W. Meek. His role as leader and his significant contributions in generalizing the concept of cones (group 1 [18, 22]) and the wave pattern in the horizontal plane (group 3 [21]) are acknowledged. In addition, the extension of the systematic formulation to construct consistent lumped-parameter models (group 2 [41, 43]) is addressed. For details the reader can consult the references cited above or the book [49] which contains easy-to-follow derivations, many examples and engineering applications.

2. CONCEPTS, CLASSIFICATION AND EXAMPLES

2.1 Applications

The simple models to be summarized can be used in the majority of cases for the final dynamic analyses of foundation vibration and soil-structure interaction. In addition, the following considerations are appropriate. In certain cases, the effect of the interaction of the soil and the structure on the response of the latter will be negligible and need thus not be considered. This applies, for example, to a flexible high structure with small mass where the influence of the higher modes (which are actually affected significantly by soil-structure interaction) on the seismic response remains small. It is then possible to excite the base of the structure with the prescribed earthquake motion. For loads applied directly to the structure, the soil can in this case be represented by a static spring or the structure can even be regarded as built-in. In other cases, which include many everyday building structures, ignoring the interaction analysis can lead to an overly conservative design. It should be remembered that seismic-design provisions [26] allow for a significant *reduction* of the equivalent static lateral force (up to 30%) *for soil-structure interaction effects*. For these two categories, to determine if a dynamic interaction

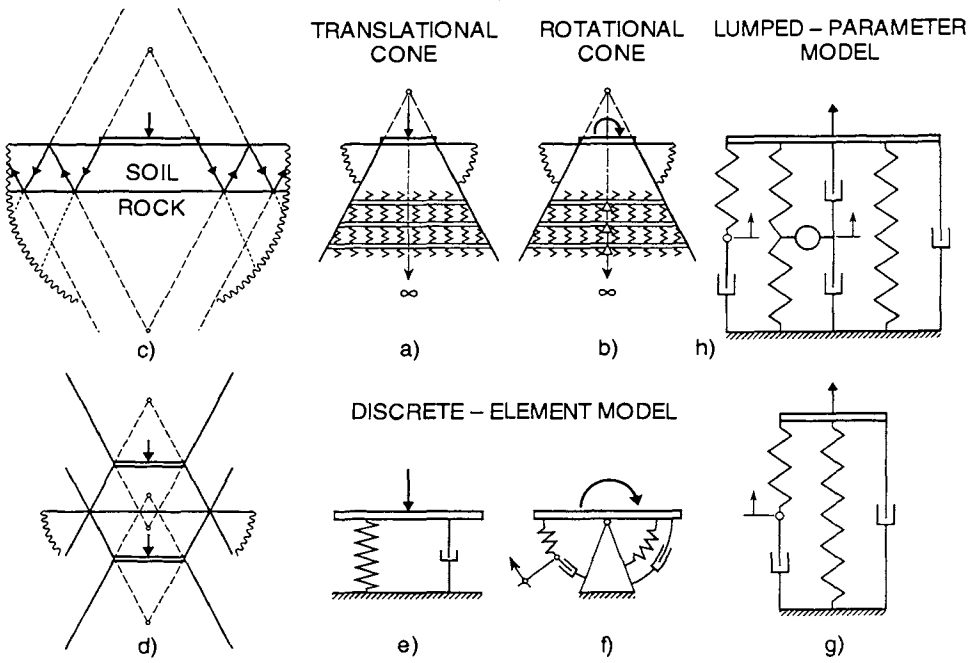

Fig. 4 Physical models to represent dynamic stiffness.
a) Disk on surface of halfspace with truncated semi-infinite translational cone.
b) Disk on surface of halfspace with truncated semi-infinite rotational cone.
c) Disk on surface of soil layer resting on flexible rock halfspace with corresponding cones.
d) Anti-symmetry condition with respect to free surface for disk and mirror-image disk with corresponding double cones to calculate Green's function.
e) Discrete-element model for translational cone.
f) Discrete-element model for rotational cone.
g) Lumped-parameter model consisting of springs and dashpots with one internal degree of freedom corresponding to f.
h) Lumped-parameter model consisting of springs, dashpots and a mass with two internal degrees of freedom.

analysis is meaningful or not and to calculate the reduction in the response of everyday structures, i.e. to perform the actual dynamic analysis, physical models are well suited. They are also appropriate to help the analyst to identify the key parameters of the dynamic system, for preliminary design, to investigate alternative designs, to perform parametric studies varying the parameters with large uncertainties such as the soil properties or the contact conditions on the structure-soil interface. Finally, simple models are used to check the results of more rigorous procedures determined with sophisticated computer codes.

2.2 Overview

To construct a physical model, physical approximations are introduced for the cone models and the assumed wave patterns in the horizontal plane, which at the same time simplify the mathematical formulation. The latter can then be solved rigorously, in general in closed form. These assumptions of mechanics permit a much better evaluation of the consequences than when mathematical approximations are introduced, such as e.g. neglecting certain higher-order derivatives in the differential equations of the rigorous formulation. For the lumped-parameter models, which for more complicated cases does involve curve fitting, a visual check of the accuracy is possible by comparing the dynamic-stiffness coefficients of the rigorous procedure and the physical model.

An overview of the physical models to calculate the interaction force-displacement relationship (dynamic stiffness) of the unbounded soil and the effective foundation input motion for seismic excitation is presented.

A summary of the key expressions used to model the various foundations is specified in the Appendix.

The simplest case consists of a rigid massless circular *basemat*, called disk in the following, resting *on the surface of a homogeneous soil halfspace*. A translational degree of freedom, e.g. the vertical motion, is examined (Fig. 4a). To determine the interaction force-displacement relationship of the disk and thus its dynamic stiffness, the disk's displacement (as a function of time) is prescribed and the corresponding interaction force, the load acting on the disk (as a function of time), is calculated. The halfspace below the disk is modeled as a *truncated semi-infinite rod (bar) with its area varying as in a cone* with the same material

properties. A load applied to the disk on the free surface of a halfspace leads to stresses, due to geometric spreading, acting on an area that increases with depth, which is also the case for the translational cone. As already mentioned, by equating the static stiffness of the *translational cone* to that of the disk on a halfspace, the cone's opening angle is calculated. It turns out that the opening angle for a given degree of freedom depends only on Poisson's ratio of the soil. Through the choice of the physical model, the complicated three-dimensional wave pattern of the halfspace with body and surface waves and three different velocities is replaced by the simple one-dimensional wave propagation governed by the one constant dilatational-wave velocity of the conical rod, whereby plane cross-sections remain plane. The radiation condition (outwardly propagating waves only) is enforced straightforwardly by admitting waves traveling downwards only. For the horizontal motion a translational cone in shear with the shear-wave velocity is constructed analogously. For the rocking and torsional degrees of freedom, rotational cones can be identified using the same concepts (Fig. 4b).

The same cones can also be used to examine a *surface foundation* for a site consisting *of a soil layer resting on flexible rock halfspace*, as already discussed in the Introduction. The vertical degree of freedom is addressed in Fig. 4c using the corresponding translational cone. The same approach can be applied for the horizontal and rotational degrees of freedom. The vertical force applied to the disk produces dilatational waves propagating downwards from the disk. The opening angle of this cone follows again from equating the static stiffness of the truncated semi-infinite cone to that of the disk on a homogeneous halfspace with the material properties of the layer. At the interface of the soil layer and the rock halfspace the incident wave will lead to a refracted wave propagating in the rock in the same direction as the incident wave along its own cone (dotted lines). In addition, a reflected wave is created propagating back through the soil layer along the indicated cone (dashed lines) in the opposite upward direction. The latter will reflect back at the free surface and then propagate downwards along the cone shown in Fig. 4c. Upon reaching the interface of the layer and the rock, a refraction and a reflection again take place, etc. The waves in the layer thus decrease in amplitude and spread resulting in radiation of energy in the layer in the horizontal direction (in addition to the energy loss through the rock halfspace).

The concepts of cone models can be expanded to the analysis of *embedded cylindrical foundations*. Again, the vertical degree of freedom of a foundation embedded *in* a *halfspace* is addressed in Fig. 4d, but the following argumentation is just as valid for the horizontal, rocking or torsional ones. The embedded part is discretized with disks. To represent a disk within an elastic fullspace, a double-cone model is introduced. Its displacement field defines an approximate Green's function for use in an uncomplicated (one-dimensional) version of the boundary-element method. To enforce the stress-free condition at the free surface of the halfspace (Fig. 4d), a mirror-image disk (again modeled as a double cone) placed symmetrically (with respect to the free surface) and excited simultaneously by the same force is considered. Indeed, any halfspace problem amenable to a solution via cone models may also be solved in the full-space. It is only necessary to augment the actual foundation in the lower halfspace by its mirror image in the upper halfspace. By exploiting principles of antisymmetry and superposition, the soil's flexibility matrix defined at the disks located within the embedded part of the foundation can be set up. The rest of the analysis follows via conventional matrix methods of structural analysis. The concept can be expanded to a fixed boundary and also to an interface with another halfspace. This permits *cylindrical foundations embedded in a soil layer resting on a rigid or flexible rock halfspace* to be calculated using cones. The methodology points towards a general *strength-of-materials approach to foundation dynamics* using the approximate *Green's functions of the double-cone models.*

A generalization is possible, enabling the dynamic-stiffness coefficients of a *foundation on the surface of or embedded in a layered halfspace* to be calculated. For each layer a dynamic-stiffness matrix based on cones is established. Assembling the dynamic-stiffness coefficients of the underlying halfspace and the dynamic-stiffness matrices of the layers yields that of the layered site.

Returning to the translational and rotational cones of Figs. 4a and b, it should be emphasized that in an actual soil-structure-interaction or foundation vibration analysis the cones are not represented physically by finite elements of a tapered rod. For practical applications it is not necessary to compute explicitly the displacements of the waves propagating along the cone. The attention can be restricted to the interaction force-displacement relationship at the disk. The translational cone's dynamic stiffness can rigorously be represented by the *discrete-element model* shown in Fig. 4e. It consists of a spring with the static stiffness (of the disk on a halfspace) in parallel with a dashpot with its coefficient determined as the product of the density, the dilatational-wave velocity (for the vertical degree of freedom) and the area of the disk. As the latter is equal to the disk on a halfspace's limit of the dynamic stiffness as the frequency approaches infinity, the cone's dynamic stiffness will be exact for the static case and for the limit of infinite frequencies (*doubly-asymptotic approximation*). For intermediate frequencies the cone is only an approximation of the disk on a halfspace. One rigorous representation of the rotational cone's dynamic stiffness is shown in Fig. 4f. The model again consists of a spring with the static stiffness in parallel with a dashpot with as coefficient the exact high-frequency limit of the dynamic stiffness (density times dilatational-wave velocity times disk's moment of inertia for the rocking degree of freedom). An additional internal degree of freedom is introduced, connected by a spring (with a coefficient equal to minus a third of the static-stiffness coefficient) to the footing and by a dashpot (with a coefficient equal to minus the high-frequency limit) to the rigid support. Again, the rotational cone's dynamic stiffness is doubly asymptotic. This is easily verified by noting that the internal degree of freedom of the discrete-element model is not activated in the two limits.

The model of Fig. 4f is shown for a translational degree

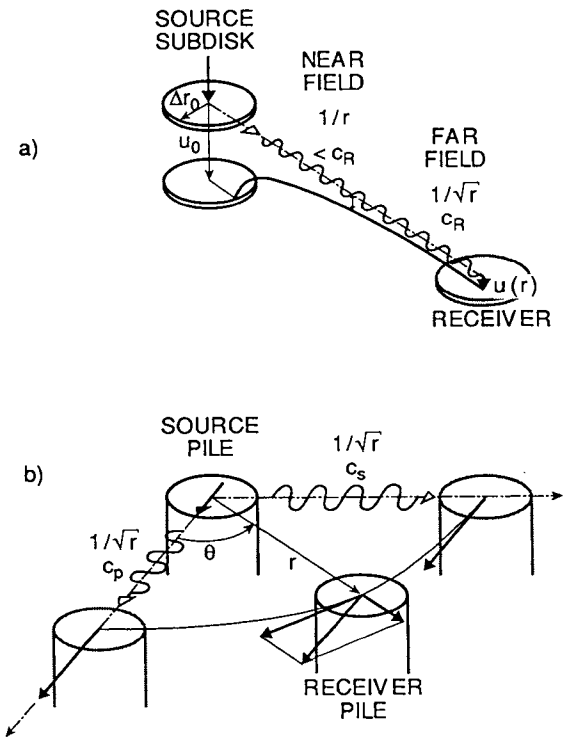

Fig. 5 Displacement patterns in horizontal plane.
a) Vertical displacement on free surface from loaded source subdisk.
b) Horizontal displacement from loaded source pile.

of freedom in Fig. 4g, which forms the starting point to develop systematically a family of consistent *lumped-parameter models*. The direct spring is chosen to represent the static stiffness. The coefficients of the other spring and of the two dashpots are selected so as to achieve *an optimum fit* between the dynamic stiffness of the lumped-parameter model and the corresponding exact value (originally determined by a rigorous procedure such as the boundary-element method). If the direct dashpot is used to represent the high-frequency limit of the dynamic stiffness, the number of coefficients available for the optimum fit is reduced to two. To increase the number of coefficients and thus the accuracy, several systems of Fig. 4g can be placed in parallel. Figure 4h shows the lumped-parameter model for three such systems, whereby two of them are combined to form a new system consisting of two springs, one independent dashpot (the two dashpots in series have the same coefficient) and a mass. A total of six coefficients keeping the doubly-asymptotic approximation thus results. It can be shown that these six frequency-independent coefficients, which can be determined using curve fitting applied to the dynamic stiffnesses (involving the solution of a linear system of equations only) will be real (but not necessarily positive). The *springs, dashpots and mass* will represent a *stable lumped-parameter model with only two additional internal degrees of freedom*. The fundamental lumped-parameter model of Fig. 4g is easy to interpret physically. This physical insight is, however, lost to a large extent in

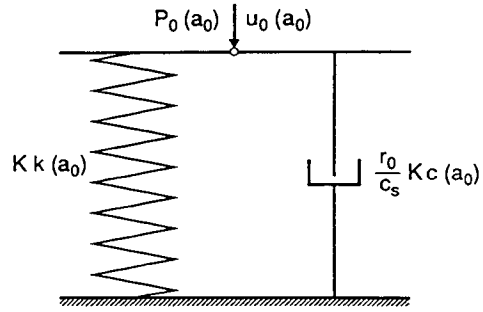

Fig. 6 Interpretation of dynamic-stiffness coefficient for harmonic excitation as spring and as dashpot in parallel with frequency-dependent coefficients.

the model shown in Fig. 4h. But the latter does allow the analyst to model quite complicated cases, as will be demonstrated, such as a foundation embedded in a soil layer resting on rigid rock. Use is implicitly made of the results obtained with the state-of-the-art formulation which leads to the rigorous dynamic stiffnesses used in the optimum fit. By comparing visually the dynamic stiffness of the lumped-parameter model with the rigorous solution, the accuracy can be evaluated.

Summarizing, two types of physical models are described in connection with Fig. 4: the translational and rotational cones [truncated semi-infinite single or double cones based on rod (bar) theory with the corresponding one-dimensional displacement and wave propagation] and the lumped-parameter models. The latter can conceptionally be constructed from the former by assembling the exact discrete-element models of the cones in parallel and using calibration with rigorous solutions.

The models shown in Fig. 4 prescribe a displacement pattern varying with depth along the axis of the cone. To extend the application, *displacement patterns in the horizontal plane* other than those corresponding to the strength-of-materials assumption of plane cross-sections remain plane are introduced as a third type of physical models in this text. One-dimensional wave propagation is again prescribed.

Two examples follow. For a vertical point load on the surface of an elastic halfspace the displacement in form of a Green's function may be deduced via non-mathematical physical reasoning, then calibrated with a few constants taken from a rigorous solution. By superposing point loads, an approximate *Green's function* is constructed for a subdisk of radius Δr_0 (Fig. 5a). In the near field the displacement amplitude is inversely proportional to the distance r from the center of the loaded source *subdisk* (body wave), and the wave propagates with a velocity which is slightly less than the Rayleigh-wave velocity c_R. In the far field the displacement amplitude decays inversely proportional to the square root of r (surface wave), and the wave propagates with c_R. Arbitrary shaped foundations can be treated as an assemblage of subdisks. The through-soil coupling of neighboring foundations can also be analyzed using subdisks.

To analyze a *pile group*, the *dynamic-interaction factor* describing the effect of the loaded source pile on the recei-

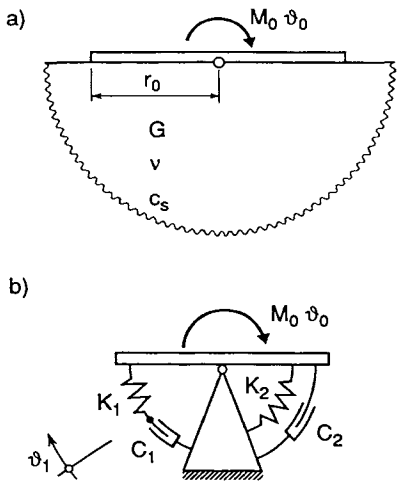

Fig. 7 Rocking of surface foundation on homogeneous soil halfspace.
a) Disk with halfspace (υ=1/3).
b) Discrete-element model (K_1/K_2= -1/3, C_1/C_2 =-1) and fundamental lumped-parameter model (K_1/K_2=-0.47,C_1/C_2=-1).
c) Dynamic-stiffness coefficient for harmonic excitation.

ver pile is applied (Fig. 5b). To calculate the interaction factor e.g. for a horizontal motion of a source pile, it is assumed that dilatational waves propagating with the corresponding velocity c_p are generated in the direction of motion and shear waves propagating with the velocity c_s in the perpendicular direction. The amplitudes of both types of these cylindrical waves decay inversely proportional to the square root of the radius.

2.3. Examples

To illustrate the concepts of constructing physical models, some examples with selected results are presented, which also allow the accuracy to be evaluated.

Harmonic excitation with frequency ω is addressed. Complex-variable notation is used in the following. From the complex response u(ω)=Reu(ω)+iImu(ω), the magnitude is calculated as $\sqrt{\mathrm{Re}u^2(\omega)+\mathrm{Im}u^2(\omega)}$ and the phase angle as arctan [Imu(ω)/Reu(ω)]. Applying a displacement with amplitude $u_0(\omega)$, the corresponding force amplitude $P_0(\omega)$ is formulated as

$$P_0(\omega)=S(\omega)u_0(\omega) \tag{9}$$

with the (complex) dynamic-stiffness coefficient S(ω). In foundation dynamics it is appropriate to introduce the dimensionless frequency a_0

$$a_0=\frac{\omega r_0}{c_s} \tag{10}$$

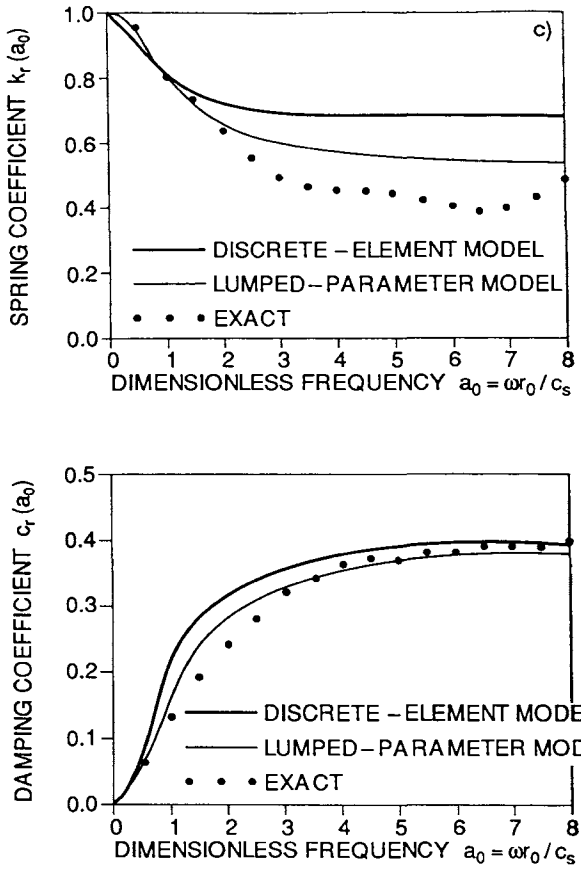

with r_0 representing a characteristic length of the foundation, for example, the radius of a disk, and c_s the shear-wave velocity. Using the static-stiffness coefficient K to nondimensionalize the dynamic-stiffness coefficient

$$S(a_0)=K[k(a_0)+ia_0c(a_0)] \tag{11}$$

is formulated. The spring coefficient $k(a_0)$ governs the force which is in phase with the displacement, and the damping coefficient $c(a_0)$ describes the force which is 90° out of phase. The dynamic-stiffness coefficient $S(a_0)$ can thus be interpreted as a spring with the frequency-dependent coefficient $Kk(a_0)$ and a dashpot in parallel with the frequency-dependent coefficient $(r_0/c_s)Kc(a_0)$ (Fig. 6).

First, the rocking degree of freedom of a rigid disk with radius r_0 (Fig. 7a) resting on the surface of an undamped homogeneous soil halfspace with shear modulus G, Poisson's ratio υ and c_s is addressed. The rigorous result denoted as exact is specified in [32]. The discrete-element model representing exactly the rotational cone (which is a doubly-asymptotic approximation of the disk on a halfspace) is shown in Fig. 7b with $K_2=8Gr_0^3/(3(1-\upsilon))$, $C_2=\rho c_p\pi r_0^4/4$ (ρ=mass density, c_p=dilatational-wave velocity). The accuracy of the corresponding dynamic-stiffness coefficient (Fig. 7c) is acceptable. Better agreement is achieved when the coefficients of K_1 and C_1 are determined by an optimum fit based on the exact values, leading to the fundamental lumped-parameter model with the same arran-

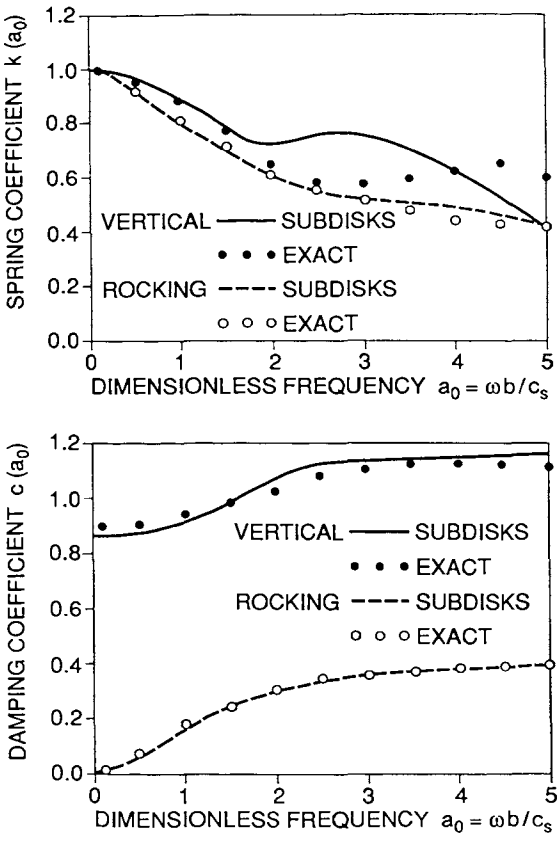

Fig. 8 Dynamic-stiffness coefficients of square foundation on surface of homogeneous soil halfspace modeled with subdisks (υ=1/3).

gement of the springs and dashpots. The coefficients K_1, C_1 are presented in the caption.

Second, the Green's function illustrated in Fig. 5a is applied. The vertical and rocking degrees of freedom of a rigid square foundation of length 2b resting on the surface of a soil halfspace is investigated with the exact result given in [50]. One quadrant is discretized with 7x7 subdisks. Figure 8 shows the dynamic-stiffness coefficients. The agreement is good.

As another application of the subdisks, the through-soil coupling in the vertical direction of two square rigid basemats of length 2b and distance d=2b on a halfspace is addressed (Fig. 9a). Each basemat is discretized into 10x10 subdisks. The dynamic-stiffness coefficient $S_{12}(a_0)$ representing the through-soil coupling of the two basemats in their centers of gravity points 1 and 2 in the vertical direction is normalized as

$$S_{12}(a_0)=Gb[k_{v12}(a_0)+ia_0c_{v12}(a_0)] \qquad (12)$$

with $a_0=\omega b/c_s$. A good agreement (Fig. 9b) exists with the exact solution of [51].

Third, the vertical degree of freedom of a rigid disk on the surface of an undamped soil layer of depth d resting on rigid rock (Fig. 10a) is examined (with the exact solution specified in [12]). The cone model with the wave pattern

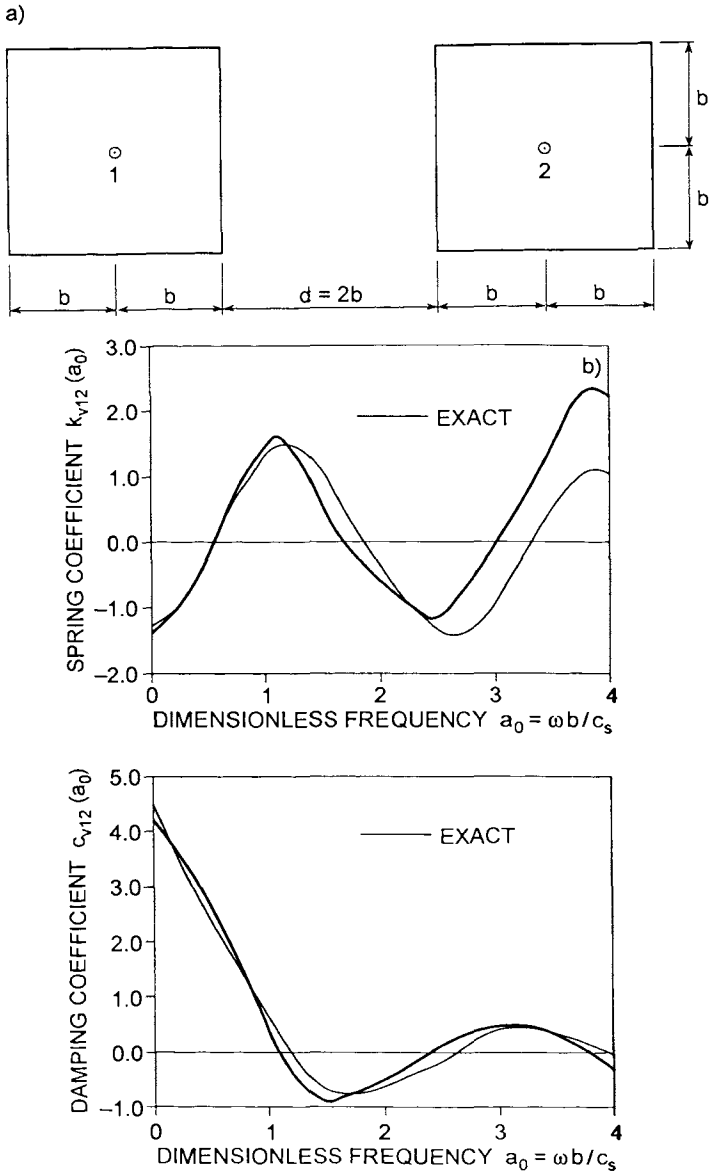

Fig. 9 Through-soil-coupling of two foundations modeled with subdisks.
a) Plan view of two square foundations (υ=1/3).
b) Vertical through-soil coupling dynamic-stiffness coefficient for harmonic excitation.

representing the reflections at the rigid interface and the free surface is shown in Fig. 10b. The corresponding dynamic-stiffness coefficient (Fig. 10c) yields a smooth approximation in the sense of an average fit to the exact solution, which becomes increasingly irregular. The unit-impulse response function shown in Fig. 10d exhibits jump discontinuities from the reflected waves at the travel times from the disk at the surface to the rock and back and at multiples thereof. The unit-impulse response function of the halfspace is also shown. The lumped-parameter model of Fig. 10e based on an optimum fit leads to the results shown in Fig. 10f.

Fourth, a rigid cylindrical foundation embedded with the depth e in a halfspace is addressed (Fig. 11a). In the

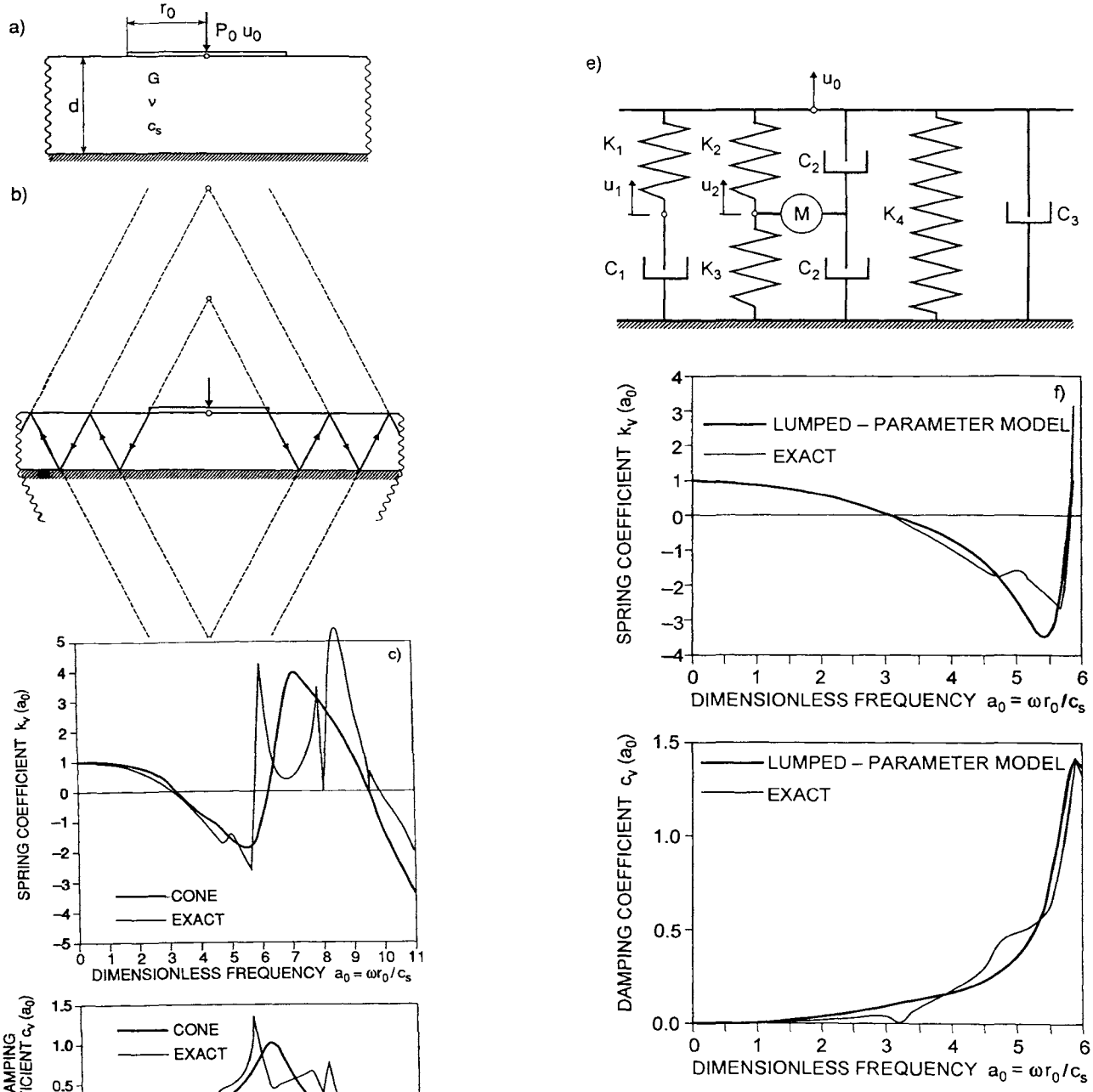

Fig. 10 Vertical motion of surface foundation on soil layer on rigid rock.

a) Disk with layer built-in at its base ($r_0/d=1$, $\upsilon=1/3$).

b) Wave pattern in layered cone model.

c) Dynamic-stiffness coefficient for harmonic excitation determined with layered cone model.

d) Vertical unit-impulse response function.

e) Lumped-parameter model ($K_1=-31.26\ Gr_0$, $K_2=5.65\ Gr_0$, $K_3=-2975.70\ Gr_0$, $K_4=10.10\ Gr_0$, $C_1=-6.20\ Gr_0^2/c_s$, $C_2=-37.29\ Gr_0^2/c_s$, $C_3=43.57\ Gr_0^2/c_s$, $M=-89.68\ Gr_0^3/c_s^2$).

f) Dynamic-stiffness coefficient for harmonic excitation determined with lumped-parameter model.

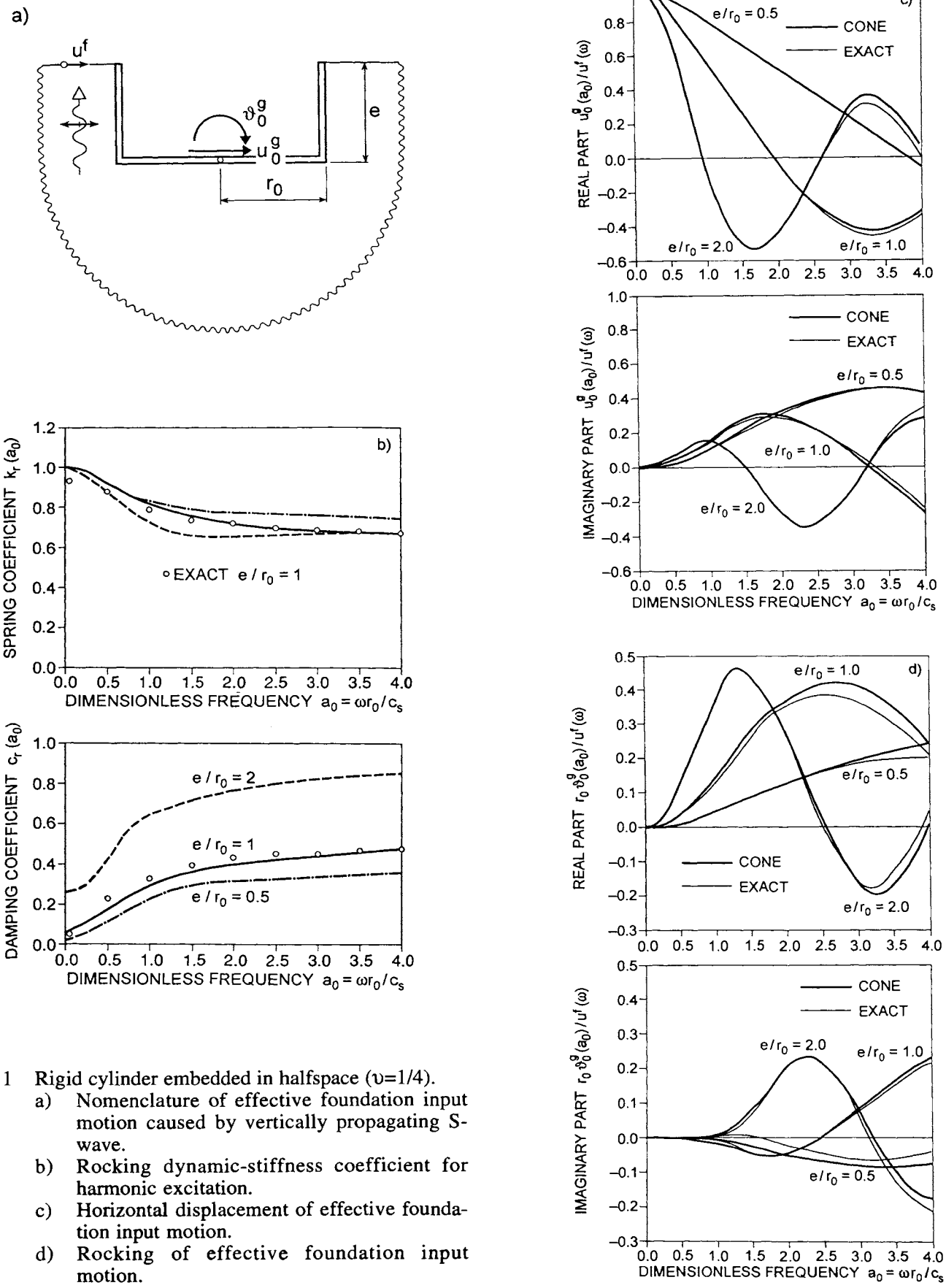

Fig. 11 Rigid cylinder embedded in halfspace (υ=1/4).

a) Nomenclature of effective foundation input motion caused by vertically propagating S-wave.

b) Rocking dynamic-stiffness coefficient for harmonic excitation.

c) Horizontal displacement of effective foundation input motion.

d) Rocking of effective foundation input motion.

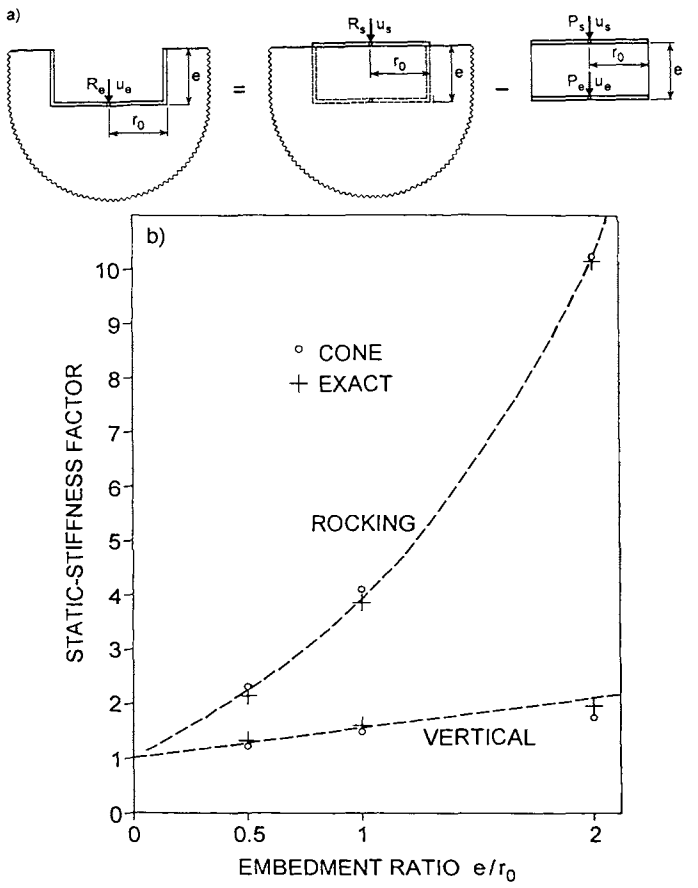

Fig. 12 Excavation-deletion method for rigid cylinder embedded in halfspace.
a) Nomenclature for vertical motion.
b) Static-stiffness factors.

embedded part of the foundation, 8 disks with their double cones are selected. For the rocking motion, the dynamic-stiffness coefficient is presented for three embedment ratios in Fig. 11b. The derivation from the exact result of [1] shown for $e/r_0=1$ is less than 10%. For vertically propagating S-waves with the amplitude $u^f(\omega)$ at the free surface (Fig. 11a) the effective foundation imput motion consisting of the horizontal component with amplitude $u_0^g(\omega)$ defined at the center of the basemat and of the rocking component with amplitude $\vartheta_0^g(\omega)$ are calculated (Fig. 11c and d). The agreement with the exact solution [14] is excellent.

Diverting somewhat, it is instructive to derive an approximate expression for the vertical static-stiffness coefficient of the embedded cylindrical foundation. The substructure-deletion method [3] is used which expresses the stiffness coefficient of the embedded foundation as a function of that of the surface foundation and of the stiffness matrix of the excavated part (Fig. 12a). Applying the strength-of-materials concept, the stiffness coefficient of the disk on the surface of the halfspace is calculated based on the cone (Eq. 13) and the stiffness matrix of the excavated part is determined for a cylindrical rod (Eq. 14)

$$R_s = K_s^\infty u_s \tag{13a}$$

where (Table A-1)

$$K_s^\infty = \frac{E_c}{z_0}\pi r_0^2 \tag{13b}$$

$$\begin{Bmatrix} P_s \\ P_e \end{Bmatrix} = \begin{bmatrix} K & -K \\ -K & K \end{bmatrix} \begin{Bmatrix} u_s \\ u_e \end{Bmatrix} \tag{14a}$$

where

$$K = \frac{E_c \pi r_0^2}{e} = K_s^\infty \frac{z_0}{e} \tag{14b}$$

with the interaction forces R and P, the displacement u, the constrained modulus E_c and the apex height of the cone z_0 (Fig. A-2). The subscripts s and e denote the surface and the embedded cases and the superscript ∞ the infinite halfspace. The stiffness coefficient of the embedded foundation is defined as

$$R_e = K_e^\infty u_e \tag{15}$$

Formulating equilibrium

$$R_s = P_s \tag{16a}$$

$$R_e = -P_e \tag{16b}$$

and eliminating all interaction forces and u_s yields

$$\left(-K\left(K - K_s^\infty\right)^{-1} K + K + K_e^\infty\right) u_e = 0 \tag{17}$$

Setting the coefficient equal to zero leads to

$$K_e^\infty = \frac{K^2}{K - K_s^\infty} - K \tag{18}$$

Substituting Eq. 14b results in

$$K_e^\infty = K_s^\infty \left[\frac{\frac{z_0}{e}}{1 - \frac{e}{z_0}} - \frac{z_0}{e} \right] \tag{19}$$

Applying a Taylor expansion for $e/z_0 \ll 1$ yields

$$K_e^\infty = K_s^\infty \left(1 + \frac{e}{z_0}\right) \tag{20}$$

For $\upsilon=0.25$, $e/z_0=(e/r_0)(r_0/z_0)=0.566e/r_0$, with z_0/r_0 specified in Table A-1 leading to

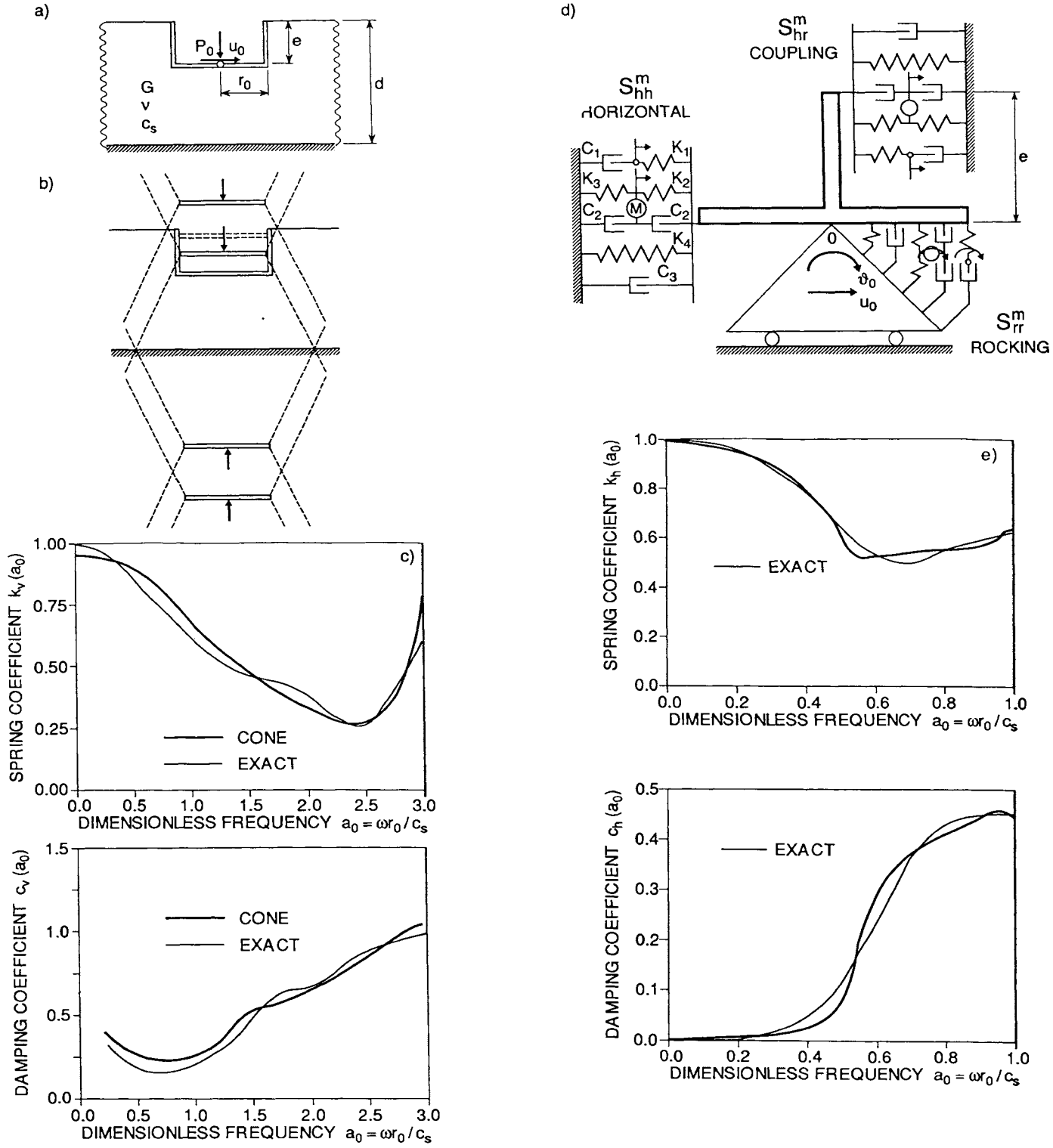

Fig. 13 Rigid cylinder embedded in soil layer on rigid rock.

a) Cylindrical foundation with layer fixed at its base ($r_0/e=1$, $r_0/d=1/3$, $\upsilon=1/3$).

b) Array of disks with double-cone models and mirror-image disks for vertical motion.

c) Vertical dynamic-stiffness coefficient for harmonic excitation with cone model (5% material damping).

d) Lumped-parameter model with coupling of horizontal and rocking motions (coefficients see Table A-7).

e) Horizontal dynamic-stiffness coefficient for harmonic excitation with lumped-parameter model (undamped).

$$K_e^\infty = K_s^\infty\left(1+0.566\frac{e}{r_0}\right) \qquad (21)$$

which hardly deviates from the expression determined from curve fitting [27] shown in Table A-6

$$K_e^\infty = K_s^\infty\left(1+0.54\frac{e}{r_0}\right) \qquad (22)$$

In Fig. 12b, the vertical static-stiffness factor $1+0.566e/r_0$ is compared to that determined with cones and with the exact value. For the rocking motion, the solution using cones is very close to the exact result and the equation specified in Table A-6 (dashed line).

Fifth, a rigid cylindrical foundation embedded with the depth e in a soil layer resting on rigid rock (Fig. 13a) is discussed. The cones are applied to calculate the dynamic-stiffness coefficient of the vertical degree of freedom and the lumped-parameter model that of the horizontal motion. In the embedded part of the foundation (Fig. 13b), 8 disks with doubles cones are selected (two are shown in the figure, one with a solid and one with a dashed line). To enforce approximately the stress-free condition at the free surface and the fixed boundary condition at the base of the layer, mirror images of the disk with the loads acting in the indicated directions with the corresponding double cones (dashed lines) are introduced. The dynamic-stiffness coefficient (Fig. 13c) is surprisingly accurate, as can be seen from a comparison with the exact solution determined with a very fine mesh of boundary elements [6]. The lumped-parameter model for the coupled horizontal and rocking degrees of freedom is shown in Fig. 13d. The coupling term is represented by placing the lumped-parameter model of Fig. 4h at the eccentricity e. The agreement for the horizontal dynamic-stiffness coefficient in Fig. 13e with the exact value [31] is good.

Finally, a rigidly capped floating pile group taking pile-soil-pile interaction into consideration is addressed. The 3x3 pile group in a halfspace is shown in Fig. 14a (s=distance between axes of two neighboring piles, ℓ=length of pile, $2r_0$=diameter of pile, E=Young's modulus of elasticity, ρ=density). To model the single pile, 25 disks with the corresponding double cones are used. To calculate pile-soil-pile interaction, the dynamic-interaction factor based on the sound physical approximation illustrated in Fig. 5b - but for vertical motion - is determined. The dynamic-stiffness coefficient in the vertical direction of the pile group (normalized with the sum of the static-stiffness coefficients of the single piles) calculated with cones is astonishingly accurate (Fig. 14b) with the exact solution specified in [13]. Even details of the strong dependency on frequency are well represented.

2.4 Requirements

1. Physical insight. The mathematical complexity of rigorous solutions in elastodynamics often obscures physical insight and intimidates practitioners. By simplifying the physics of the problem, *conceptual clarity* with *physical insight* results. As an example, the calculation of the dynamic stiffness of a disk on the surface of a soil layer resting on rigid rock (Fig. 10a) - a complicated three-dimensional mixed boundary-value problem with dispersive waves - is addressed. In the physical model made up of truncated cones (Fig. 10b), for which the familiar strength-of-materials theory applies, the wave pattern is clearly postulated. The one-dimensional waves propagate with the dilatational-wave velocity (a material constant), reflecting back and forth, spreading and decreasing in amplitude, and thus radiating energy towards infinity in the horizontal direction.

2. Simplicity. Due to the simplification of the physical problem, the physical model can be rigorously mathematically solved. The fundamental principles of wave propagation and dynamics are thus satisfied exactly for the simple physical model. Closed-form solutions (even in the time domain) exist for the (one-dimensional) cones. For instance, to calculate the dynamic stiffness of the disk on the soil layer resting on rigid rock with cones (Fig. 10b), the analysis can be performed with a hand calculator as no system of equations is solved; for the embedded cylindrical foundation with cones (Fig. 13b), a special-purpose computer code can easily be written; and when lumped-parameter models are applied (Figs. 10e, 13d), a standard general-purpose structural dynamics program which permits springs, dashpots, and masses as input can be used directly. The *practical application* of the physical models is thus also *simple*, together with the *physics* and the rigorous *mathematical solution.*

3. Generality. To be able to provide engineering solutions to reasonably complicated practical cases and not just to address academic examples, the physical models must reflect the following key aspects of the foundation-soil system for all translational and rotational degrees of freedom [8].

- *The shape of the foundation-soil (structure-soil) interface*: Besides the circle, the rectangle and the arbitrary shape, which can be modeled as an equivalent disk or directly (Fig. 8) without "smearing", can be represented as a three-dimensional case or, if applicable, as a two-dimensional slice of a strip foundation.
- *The nature of the soil profile*: The homogeneous halfspace, the layer resting on a flexible halfspace, and the layer resting of a rigid halfspace as well as the layered halfspace with many layers can be modeled.
- *The amount of embedment*: Surface, embedded (with soil contact along the total height of the wall or only on part of it), and pile foundations can be represented.

The physical models must also allow the calculation of the effective foundation input motion for seismic excitation. They must work well for the static case, for the low- and intermediate-frequency ranges important for machine vibrations and earthquakes, and for the limit of very high frequencies as occurring in impact loads.

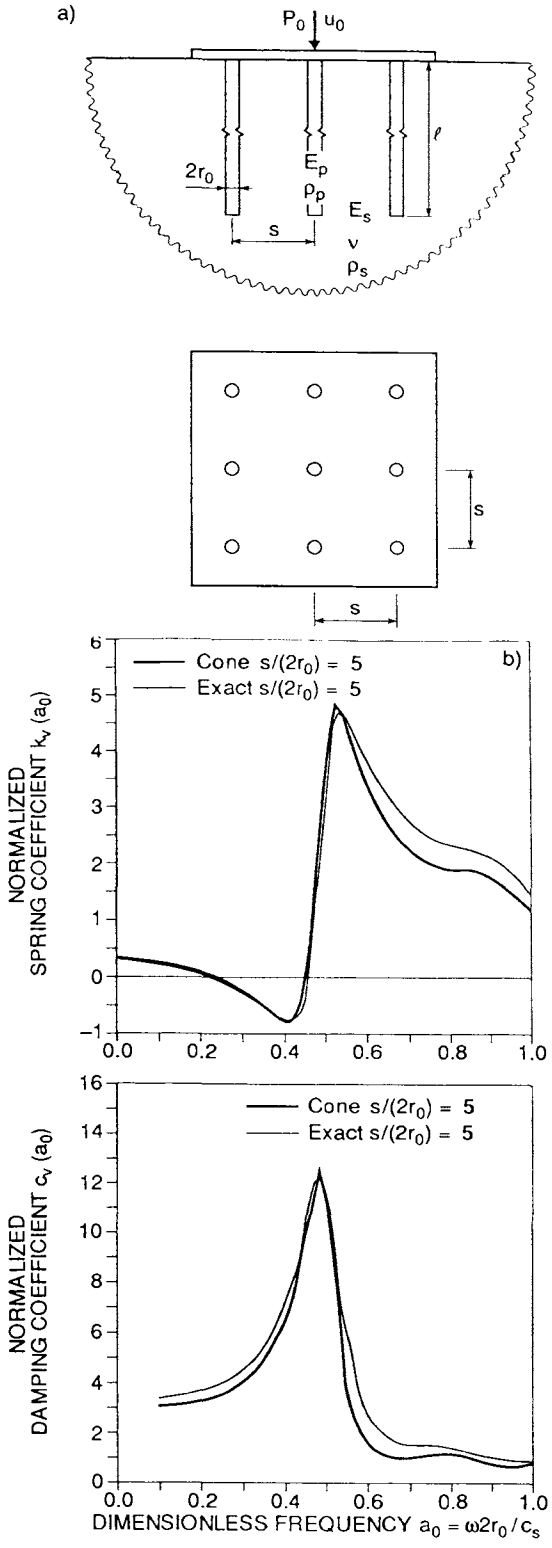

Fig. 14 Vertical motion of floating pile group in homogeneous soil halfspace.
a) Elevation and plan view of 3x3 pile group ($s/(2r_0)=5$, $\ell/(2r_0)=15$, $\upsilon=0.4$, $E_p/E_s=1000$, $\rho_p/\rho_s=1.43$, 5% material damping).
b) Dynamic-stiffness coefficient for harmonic excitation with cone model and dynamic-interaction coefficient.

4. Accuracy. Due to many uncertainties, the accuracy of any analysis will always be limited. A deviation of ±20% of the results of the physical models from those of the rigorous solution for one set of input parameters is, in general, acceptable. This *engineering accuracy* criterion is, in general, satisfied, as can be verified by examining the dynamic-stiffness coefficients shown in Figs. 7, 11, 13 and 14. It should also be remembered that for a transient loading such as an earthquake the deviations (with both signs) are "smeared" over the frequency range of the excitation and thus further reduced compared to the larger error for one frequency.

The use of the physical models does indeed lead to some loss of precision compared to applying the rigorous boundary-element procedure or the sophisticated finite-element-based method; however, this is more than compensated by the many advantages discussed in this section.

5. Demonstration of physical features. Besides leading (by construction of the physical model) to physical insight of the mechanisms involved in foundation vibration (item 1), the physical models are also well suited to demonstrate certain unexpected features and to derive further results. Four examples follow.

1. Placing a row of an infinite number of identical vertical point loads (Fig. 1-5a) on the surface of a half-space as a simple physical model, the vertical dynamic stiffness of a two-dimensional slice of a rigid surface strip foundation can be determined. An analytical solution can be derived. The static stiffness is zero, but the spring coefficient increases abruptly to a more or less constant value for larger frequencies. By contrast, the damping coefficient begins from infinity at zero frequency and then diminishes asymptotically for increasing frequency. The same features exist in the rigorous solution.
2. As can be shown, the radiation damping ratio in a two-dimensional model is significantly larger than in the corresponding three-dimensional case (just the contrary of what is expected intuitively). To model a two-dimensional slice of a strip foundation on a half-plane, wedges can be used which are again based on rod theory, just as cones represent a disk on a half-space (three-dimensional situation). For both the translational and rotational motions, the damping ratios $\zeta=b_0c(b_0)/[2k(b_0)]$ of the wedges are significantly larger than those of the cones (Fig. 15). The dimensionless frequency parameter is defined as $b_0=\omega z_0/c$ with z_0 denoting the apex height of the cone or wedge and c the appropriate wave velocity. The multipliers are also specified in the figure.
3. For the frequency range below the cutoff frequency of the soil layer resting on rigid rock, the radiation damping and thus the damping coefficient of the dynamic stiffness vanish, which is well simulated using cones and lumped-parameter models. See Figs. 10c and 10f, where below the cutoff frequency for dilatational waves, $a_0=\pi$, $c(a_0)$ is very small.
4. The combined structure-soil system can be modeled approximately as an equivalent one-degree-of-free-

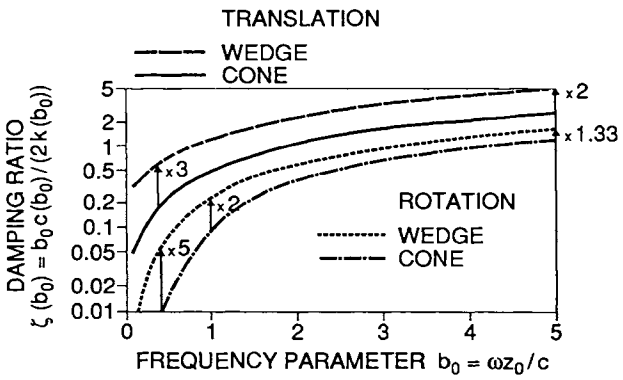

Fig. 15 Overestimation of radiation damping ratio of two-dimensional modeling with wedges when compared to that of three-dimensional modeling with cones for translational and rotational motions.

dom system. The corresponding effective natural frequency and damping ratio can be determined by modeling the soil as cones.

6. Suitability for everyday practical foundation-vibration analysis. Especially the ease in use, the sufficient generality and the good accuracy allow the physical models to be applied for foundation vibration and dynamic soil-structure-interaction analyses in a design office.

7. Potential for generalization. The *concepts and certain features of the physical models can be generalized* and the results applied in much more sophisticated calculations. Three examples of such extensions are listed.

1. The cone models lead to simple Green's functions, and the analysis of an embedded foundation can be interpreted as a straightforward application of the one-dimensional boundary-element method. The rigorous calculation can be performed also with a boundary-element method based on the same concept, the major difference being that the Green's function of the three-dimensional fullspace is used and not the one-dimensional solution derived from the rod theory of cones.
2. A consistent lumped-parameter model for the dynamic-stiffness matrix of any general flexible foundation can be systematically constructed starting from the same fundamental lumped-parameter model (Fig. 4g). In general, a large number of these building blocks are assembled in parallel for each coefficient of the matrix to be represented.
3. The interaction force-displacement relationship of some physical models will involve convolution integrals which can be evaluated exactly very efficiently using a recursive formulation. The same procedure can also be applied to the corresponding relationship of any general flexible foundation.

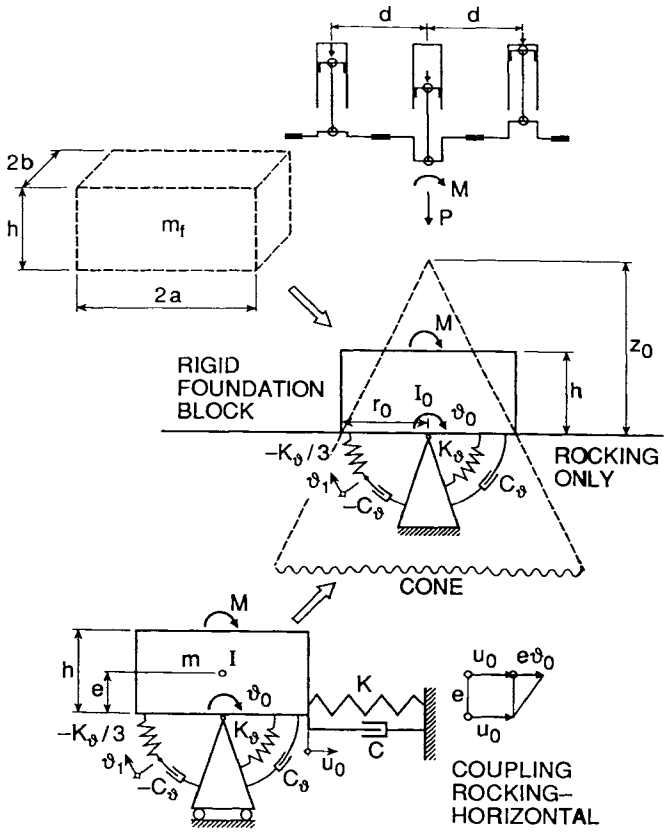

Fig. 16 Foundation of three-cylinder compressor with cranks at 120° with dynamic models.

Summarizing, the cone models with the prescribed deformation of rod (bar) theory, the lumped-parameter models based on them, and the displacement patterns in the horizontal plane present a major step towards developing a *strength-of-materials approach to foundation dynamics*. The aim is the same as in stress analysis of structural engineering, where, for instance for very complicated skew-curved prestressed concrete bridges, beam theory is applied successively and the general three-dimensional theory of elasticity is not needed. As in stress analysis, each specific case has to be calculated based on the strength-of-materials approach. It is not sufficient just to use tables of dynamic-stiffness coefficients calculated for certain cases based on the rigorous formulation of elastodynamics. As the soil is a three-dimensional body without a dominant axial direction, the strength-of-materials approach, with prescribed displacement behavior taking all essential features into account, will be more difficult to formulate in foundation engineering than in structural engineering. Concluding, the dynamic analyst should always "make things as simple as possible but no simpler (H. Einstein). Or to state it differently: "*Simplicity that is based on rationality is the ultimate sophistication*" (A.S. Veletsos).

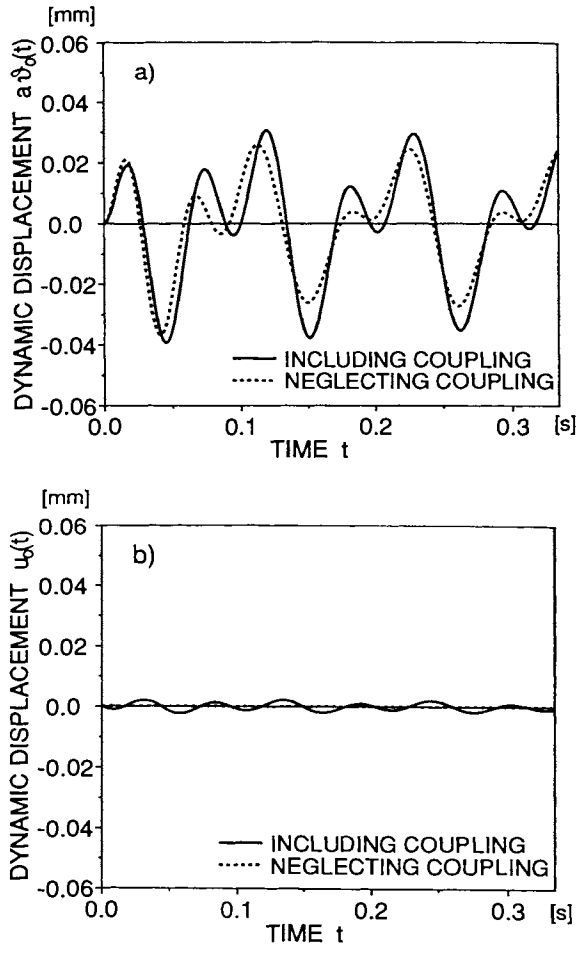

Fig. 17 Response including coupling of rocking motion with horizontal motion.
a) Vertical displacement at edge of foundation block.
b) Horizontal displacement.

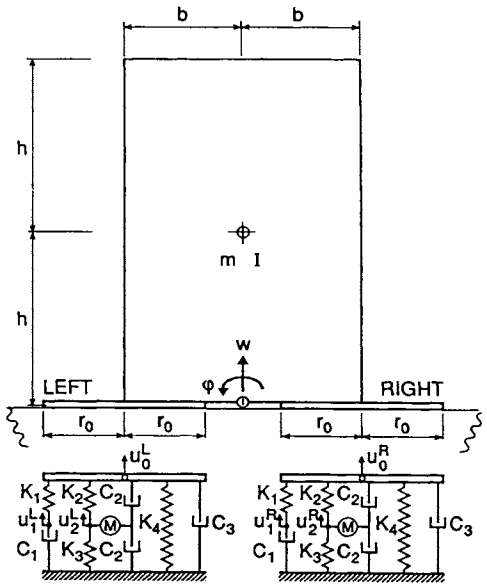

Fig. 18 Rigid block on disks with lumped-parameter models of disks on surface of soil layer resting on rigid rock.

3. ENGINEERING APPLICATIONS

Selected simple engineering applications taken from [49] follow.

As a first example, a machine foundation on the surface of a soil halfspace excited by a three-cylinder compressor operating at 9 Hz with the cranks at 120° resulting in a moment (Fig. 16) is investigated. The discrete-element models of the cones shown in Figs. 4f and 4e are used to represent the soil in the rocking and horizontal motions. Including the coupling between the horizontal and rocking motions increases the rocking response (Fig. 17a).

The second example examines non-linear soil-structure-interaction analysis. A rigid block with individual footings, which can uplift, resting on the surface of a soil layer with c_s=750 m/s and d/r_0=1 is discussed (Fig. 18). An idealized horizontal earthquake acts during 2s. Only the vertical and rocking motions of the block's bottom center are considered in the calculation. The lumped-parameter model of Fig. 4h is used to represent the soil neglecting through-soil coupling. As the fundamental frequency in rocking lies below the cutoff frequency of the layer, no radiation damping occurs during the free vibration phase after 2s. This leads to no decay occurring in the gaps (Fig. 19a). If the soil is a halfspace, the gaps are much smaller and decay rapidly after 2s (Fig. 19b).

The third example, also addressing nonlinear soil-structure-interaction analysis, discusses the vibration of a hammer foundation embedded in a soil layer on rigid rock (d/r_0=2) with an excentrically mounted anvil (Fig. 20). The head impacts with a velocity c_h=5 m/s against the anvil. As a tension-resistant connection for the pads of the anvil is not provided, the anvil will partially uplift from the block, when the dynamic stress in tension exceeds the static stress. The dynamic system with 14 degrees of freedom (Fig. 21) is constructed using the lumped-parameter models of Figs. 13d and 4h. As expected, the partial uplift of the anvil increases the motion significantly when compared with the result of a linear analysis (Fig. 22). The response for a soil halfspace is also plotted.

As a final example, the vertical seismic motion of a structure founded on the surface of a soil layer on rigid rock (Fig. 23) for a record of the Loma Prieta earthquake is investigated. Two radius-to-depth ratios are addressed. For d/r_0=1, the vertical fundamental frequency of the structure-soil system is smaller than the corresponding fundamental frequency of the layer (=cutoff frequency) which eliminates radiation damping. For d/r_0=4, the opposite applies which results in radiation damping occurring. The analyses are performed with the layered cone model (Fig. 10b) and with the lumped-parameter model (Fig. 10e). From the structural distortion $u^t - u_0^t$ plotted for the

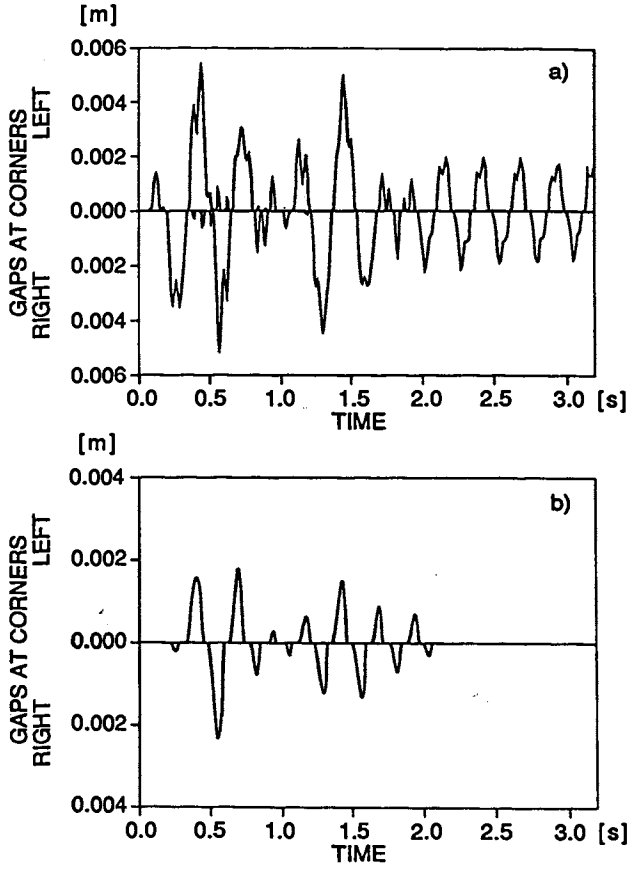

Fig. 19 Vertical gap between block and disk for soil modeled as
a) Layer.
b) Halfspace.

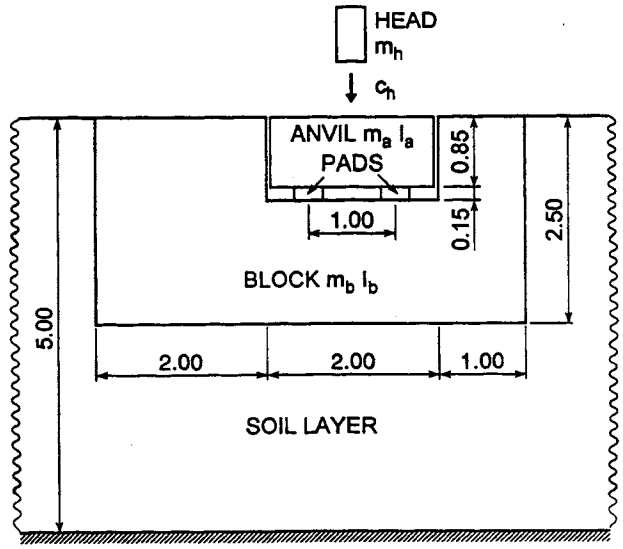

Fig. 20 Hammer foundation with inertial block embedded in soil layer resting on rigid rock.

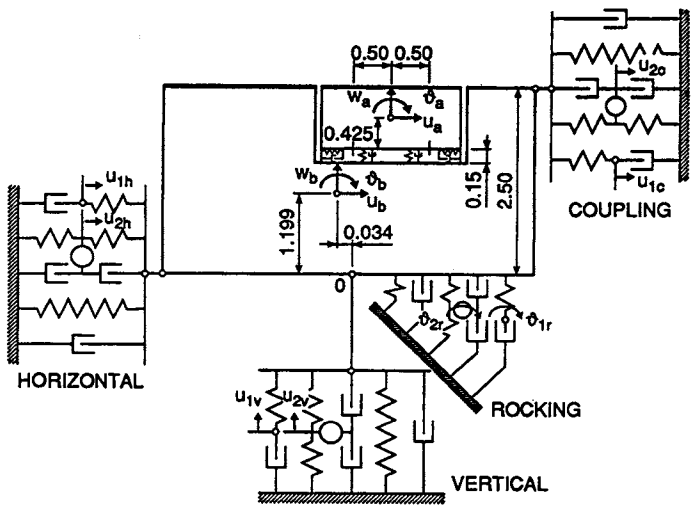

Fig. 21 Dynamic model of hammer foundation with lumped-parameter models of soil layer.

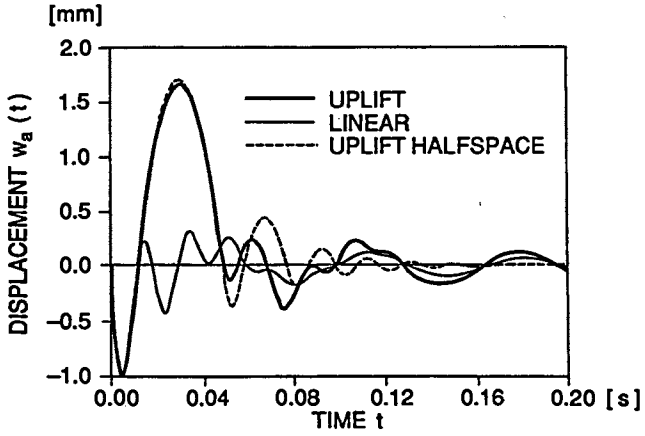

Fig. 22 Vertical displacement at center of anvil for load transmitted as initial velocity of anvil.

shallow and the deep layers in Fig. 24, the significant influence of radiation damping resulting in smaller peaks and a larger decay is clearly visible.

The same effect is also present for the coupled horizontal and rocking motions (see Fig. A-30) of a structure of height h, fixed-base frequency ω_s, mass m and material damping ratio ζ on a soil layer. While the natural frequency ratio $\tilde{\omega}/\omega_s$ of the equivalent one-degree-of-freedom system (Fig. A-31) is hardly effected by

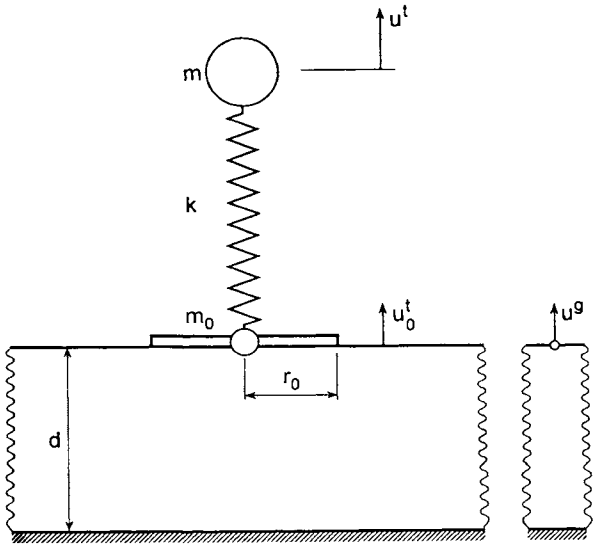

Fig. 23 Dynamic system with two degrees of freedom for vertical motion of structure on soil layer.

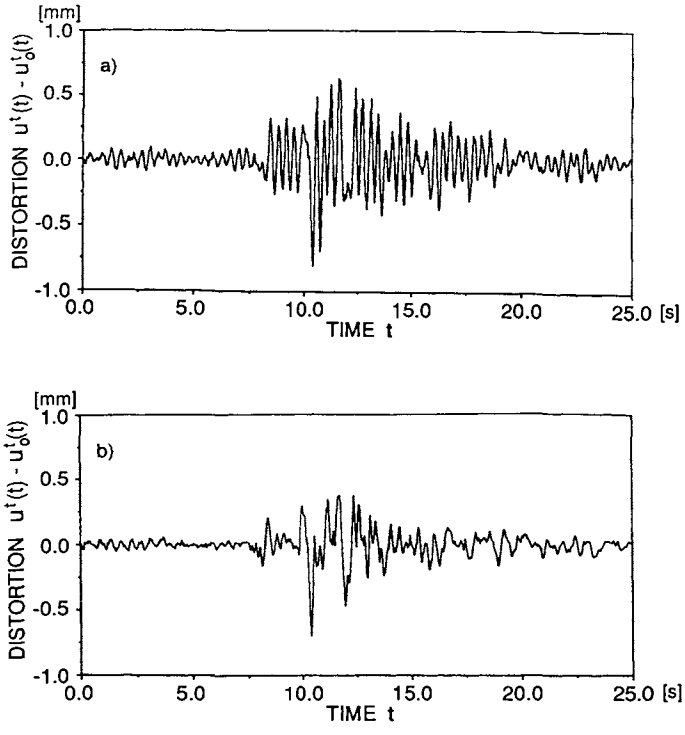

Fig. 24 Structural distortion.
a) Fundamental frequency of dynamic system below fundamental frequency of soil layer (cutoff frequency).
b) Fundamental frequency of dynamic system above fundamental frequency of soil layer (cutoff frequency).

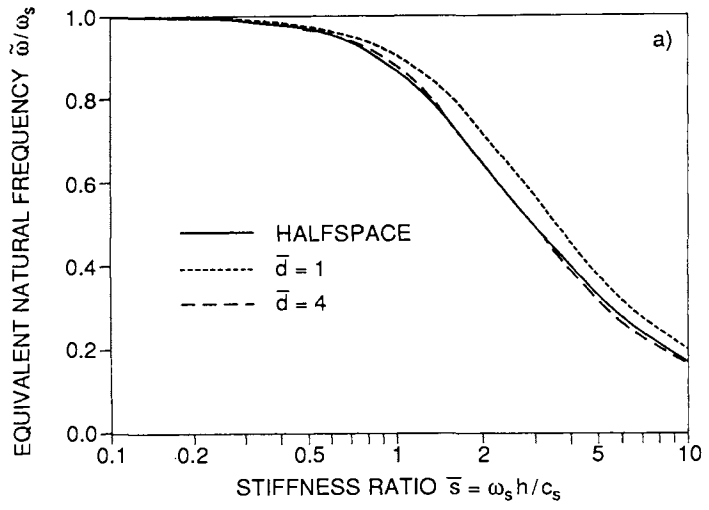

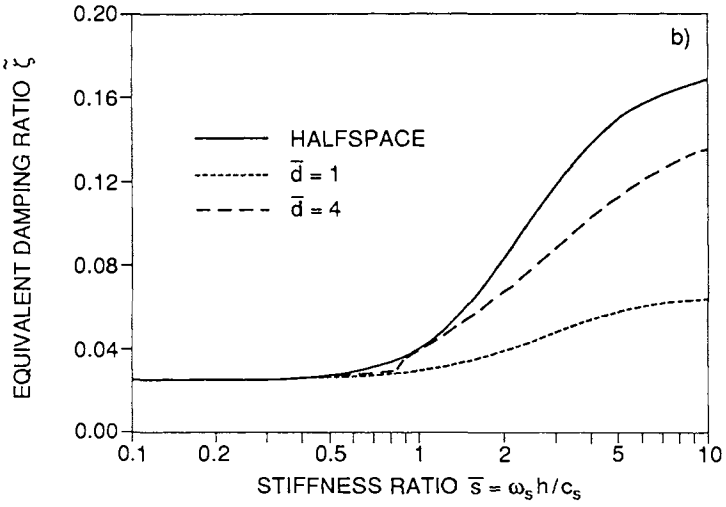

Fig. 25 Properties of equivalent one-degree-of-freedom system modeling coupled horizontal and rocking motions for horizontal earthquake varying depth of soil layer (see Fig. A-30, $h/r_0=2$, $m/(\rho r_0^3)=1$, $\upsilon=1/3$, $\zeta=0.025$, $\zeta_g=0.05$).

$\bar{d} = d / r_0 =$ (Fig. 25a), the equivalent damping ratio $\tilde{\zeta}$ depends for large $\bar{s}(=\omega_s h / c_s)$, i.e. for a significant soil-structure interaction effect, strongly on $\bar{d}$ (Fig. 25b). For the shallow layer $\bar{d}=1$, no radiation damping is activated, as $\tilde{\zeta}$ converges for large $\bar{s}$ essentially to the material damping of the soil $\zeta_g=0.05$. For the halfspace shown for comparison, $\tilde{\zeta}$ increases significantly for increasing $\bar{s}$, due to the large effect of radiation damping. For the intermediate site with $\bar{d}=4$, a transmission occurs.

APPENDIX. BARE ESSENTIALS FOR PRACTICAL APPLICATION

The book *Foundation Vibration Analysis Using Simple Physical Models* [49] contains a summary at the end of each chapter with the key findings and relations. Of the latter those equations which are necessary to analyze practical cases are listed in the following. The subdivision corresponds to the chapters of the book [49] which should be consulted for a complete description including derivations and examples. Other tables for the analysis of foundations concentrating on harmonic loading are specified in the handbook [9].

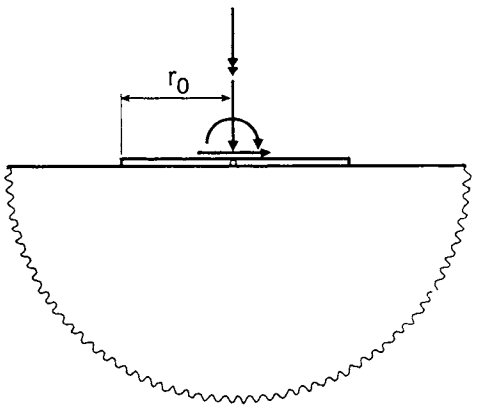

Fig. A-1 Disk on surface of homogeneous soil halfspace.

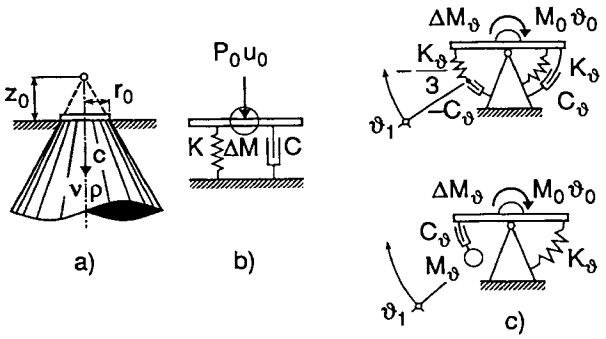

Fig. A-2 Cone model and equivalent discrete-element model.
a) Cone.
b) Discrete-element model for translation.
c) Discrete-element models for rotation.

A1 FOUNDATION ON SURFACE OF HOMOGENEOUS SOIL HALFSPACE

A1.1 Cone Model

For all components of motion a rigid basemat with area A_0 and (polar) moment of inertia I_0 on the surface of a homogeneous soil halfspace (three-dimensional foundation) with Poisson's ratio υ, shear-wave velocity c_s, dilatational-wave velocity c_p and density ρ (Fig. A-1) can be modeled as a truncated semi-infinite cone of equivalent radius r_0, apex height z_0 and wave velocity c (Fig. A-2a and Fig. A-3). For the horizontal and torsional cones deforming in shear the appropriate wave velocity c equals c_s. For the vertical and rocking cones deforming axially c equals c_p for $\upsilon \le 1/3$ and is limited to $2c_s$ for $1/3 < \upsilon \le 1/2$. The translational cone model for the displacement u_0 is dynamically equivalent to the spring K- and dashpot C-system (Fig. A-2b). The rotational cone for the rotation ϑ_0 corresponds exactly to the discrete-element models with one internal degree of freedom ϑ_1 and a small number of springs(s) K_ϑ, dashpot(s) C_ϑ and in the monkey-tail configuration a mass moment of inertia M_ϑ (Fig. A-2c). All coefficients are frequency independent. For the vertical and rocking motions in the case of nearly-incompressible soil ($1/3 < \upsilon \le 1/2$), a trapped mass ΔM and a trapped mass moment of inertia ΔM_ϑ assigned to the basemat arise. The properties of the cones and the discrete-element models which are all that is necessary for the modeling of a basemat of arbitrary shape on the surface of the soil (e.g. in a general-purpose structural dynamics program working directly in the time domain) are summarized in a nutshell in Table A-1.

$$c_s = \sqrt{\frac{G}{\rho}} = \sqrt{\frac{E_c}{2\rho}\frac{1-2\upsilon}{1-\upsilon}} \qquad \text{shear modulus G}$$

$$c_p = \sqrt{\frac{E_c}{\rho}} = \sqrt{2\frac{G}{\rho}\frac{1-\upsilon}{1-2\upsilon}} \qquad \text{constrained modulus } E_c$$

Static-Stiffness Coefficient

$$K_h = \frac{8Gr_0}{2-\upsilon} \quad \text{horizontal} \qquad K_v = \frac{4Gr_0}{1-\upsilon} \quad \text{vertical}$$

$$K_r = \frac{8Gr_0^3}{3(1-\upsilon)} \quad \text{rocking} \qquad K_t = \frac{16}{3}Gr_0^3 \quad \text{torsional}$$

Radiation-Dashpot Coefficient (high-frequency behavior)

$C = \rho c A_0$ translational $\qquad C_\vartheta = \rho c I_0$ rotational

Translational Cone

Stiffness Formulation

Interaction force-displacement relationship (Fig. A-2b)

$$P_0(t) = Ku_0(t) + C\dot{u}_0(t) + \Delta M\ddot{u}_0(t)$$

($\Delta M = 0$ for horizontal motion and for vertical motion when $\upsilon \le 1/3$)

Table A-1: Key Expressions to Model a Three-Dimensional Foundation on the Surface of a Homogeneous Soil Halfspace with a Cone

Motion	Horizontal	Vertical		Rocking		Torsional
Equivalent Radius r_0	$\sqrt{\frac{A_0}{\pi}}$	$\sqrt{\frac{A_0}{\pi}}$		$\sqrt[4]{\frac{4I_0}{\pi}}$		$\sqrt[4]{\frac{2I_0}{\pi}}$
Aspect Ratio $\frac{z_0}{r_0}$	$\frac{\pi}{8}(2-\upsilon)$	$\frac{\pi}{4}(1-\upsilon)\left(\frac{c}{c_s}\right)^2$		$\frac{9\pi}{32}(1-\upsilon)\left(\frac{c}{c_s}\right)^2$		$\frac{9\pi}{32}$
Poisson's Ratio υ	all υ	$\leq\frac{1}{3}$	$\frac{1}{3}<\upsilon\leq\frac{1}{2}$	$\leq\frac{1}{3}$	$\frac{1}{3}<\upsilon\leq\frac{1}{2}$	all υ
Wave Velocity c	c_s	c_p	$2c_s$	c_p	$2c_s$	c_s
Trapped Mass ΔM ΔM_ϑ	0	0	$2.4\left(\upsilon-\frac{1}{3}\right)\rho A_0 r_0$	0	$1.2\left(\upsilon-\frac{1}{3}\right)\rho I_0 r_0$	0
Discrete-Element Model	$K=\rho c^2\frac{A_0}{z_0}$ $C=\rho c A_0$			$K_\vartheta=3\rho c^2\frac{I_0}{z_0}$ $C_\vartheta=\rho c I_0$ $M_\vartheta=\rho I_0 z_0$		

Dynamic-stiffness coefficient for harmonic loading

$$S(a_0)=K[k(a_0)+ia_0c(a_0)]$$

with dimensionless spring coefficient $k(a_0)$ for horizontal motion and for vertical motion when $\upsilon\leq 1/3$

$$k(a_0)=1$$

for vertical motion when $1/3<\upsilon\leq 1/2$

$$k(a_0)=1-0.6\pi(1-\upsilon)\left(\upsilon-\frac{1}{3}\right)a_0^2$$

dimensionless damping coefficient

$$c(a_0)=\frac{z_0}{r_0}\frac{c_s}{c}$$

and dimensionless frequency

$$a_0=\frac{\omega r_0}{c_s}$$

Flexibility Formulation

Displacement-interaction force relationship (Fig. A-2b)
For horizontal motion and for vertical motion when $\upsilon\leq 1/3$

$$u_0(t)=\int_0^t h_1(t-\tau)\frac{P_0(\tau)}{K}d\tau$$

with unit-impulse response function

$$h_1(t)=\frac{c}{z_0}e^{-\frac{c}{z_0}t} \qquad t\geq 0$$

$$=0 \qquad t<0$$

The convolution integral with the first-order term $h_1(t)$ (Duhamel integral) at time station n can be evaluated efficiently by the recursive procedure expressing the displacement at time station n as a linear function of the displacement at the previous time station n-1 and of the normalized interaction forces at the same two time stations

$$u_{0n}=au_{0n-1}+b_0\frac{P_{0n}}{K}+b_1\frac{P_{0n-1}}{K}$$

where the recursive coefficients are specified as (Δt=time step)

$$a = e^{-\frac{c\Delta t}{z_0}}$$

$$b_0 = 1 + \frac{e^{-\frac{c\Delta t}{z_0}} - 1}{\frac{c\Delta t}{z_0}} \qquad b_1 = \frac{-e^{-\frac{c\Delta t}{z_0}} + 1}{\frac{c\Delta t}{z_0}} - e^{-\frac{c\Delta t}{z_0}}$$

The unconditionally stable recursive evaluation which is suitable even for a hand calculation is exact when $P_0(t)$ is piecewise linear.
For vertical motion when $1/3<\upsilon\leq 1/2$

$$u_0(t) = \int_0^t h_4(t-\tau)\frac{P(\tau)}{K}d\tau$$

with $\left(\gamma = \frac{\pi}{2.4}\frac{1-\upsilon}{\upsilon-\frac{1}{3}}\right)$

$$h_4(t) = \frac{4}{\pi(1-\upsilon)}\frac{c_s}{r_0}\frac{1}{\sqrt{1-\frac{4}{\gamma}}}e^{-\frac{1}{2.4\left(\upsilon-\frac{1}{3}\right)}\frac{c_s}{r_0}t}$$

$$*\sinh\frac{1}{2.4\left(\upsilon-\frac{1}{3}\right)}\frac{c_s}{r_0}\sqrt{1-\frac{4}{\gamma}}t \qquad t\geq 0$$

$$=0 \qquad t<0$$

The recursive evaluation with the second-order term $h_4(t)$ proceeds as

$$u_{0n} = a_1 u_{0n-1} + a_2 u_{0n-2} + b_0\frac{P_{0n}}{K} + b_1\frac{P_{0n-1}}{K} + b_2\frac{P_{0n-2}}{K}$$

where

$$a_1 = 2e^{-\frac{1}{2.4\left(\upsilon-\frac{1}{3}\right)}\frac{c_s}{r_0}\Delta t}\cosh\frac{1}{2.4\left(\upsilon-\frac{1}{3}\right)}\frac{c_s}{r_0}\sqrt{1-\frac{4}{\gamma}}\Delta t$$

$$a_2 = -e^{-\frac{1}{1.2\left(\upsilon-\frac{1}{3}\right)}\frac{c_s}{r_0}\Delta t}$$

and

$$b_0 = \frac{r(\Delta t)}{\Delta t} \qquad b_1 = \frac{r(2\Delta t) - (2+a_1)r(\Delta t)}{\Delta t}$$

$$b_2 = \frac{r(3\Delta t) - (2+a_1)r(2\Delta t) + (1+2a_1-a_2)r(\Delta t)}{\Delta t}$$

with $r(t)=r_4(t)$

$$r_4(t) = -\frac{\pi(1-\upsilon)}{2}\frac{r_0}{c_s} + t + \frac{1-\frac{2}{\gamma}}{\sqrt{1-\frac{4}{\gamma}}}\frac{\pi(1-\upsilon)}{2}\frac{r_0}{c_s}e^{-\frac{1}{2.4\left(\upsilon-\frac{1}{3}\right)}\frac{c_s}{r_0}t}$$

$$*\sinh\frac{1}{2.4\left(\upsilon-\frac{1}{3}\right)}\frac{c_s}{r_0}\sqrt{1-\frac{4}{\gamma}}\ t$$

$$+\frac{\pi(1-\upsilon)}{2}\frac{r_0}{c_s}e^{-\frac{1}{2.4\left(\upsilon-\frac{1}{3}\right)}\frac{c_s}{r_0}t} \qquad t\geq 0$$

$$*\cosh\frac{1}{2.4\left(\upsilon-\frac{1}{3}\right)}\frac{c_s}{r_0}\sqrt{1-\frac{4}{\gamma}}\ t$$

$$=0 \qquad t<0$$

Rotational Cone

Stiffness Formulation

Interaction moment-rotation relationship (Fig. A-2c)

$$M_0(t) = K_\vartheta\vartheta_0(t) + C_\vartheta\dot{\vartheta}_0(t) + \Delta M_\vartheta\ddot{\vartheta}_0(t) - \int_0^t h_1(t-\tau)\ C_\vartheta\dot{\vartheta}_0(\tau)d\tau$$

(ΔM_ϑ=0 for torsional motion and for rocking motion when $\upsilon\leq 1/3$)

The recursive evaluation of the convolution integral with $h_1(t)$ is described above.

Dynamic-stiffness coefficient for harmonic loading

$$S_\vartheta(a_0) = K_\vartheta\left[k_\vartheta(a_0) + ia_0c_\vartheta(a_0)\right]$$

with dimensionless spring coefficient $k_\vartheta(a_0)$ for torsional motion and for rocking motion when $\upsilon\leq 1/3$

$$k_\vartheta(a_0) = 1 - \frac{1}{3}\frac{a_0^2}{\left(\frac{r_0c}{z_0c_s}\right)^2 + a_0^2}$$

for rocking motion when $1/3<\upsilon\leq 1/2$

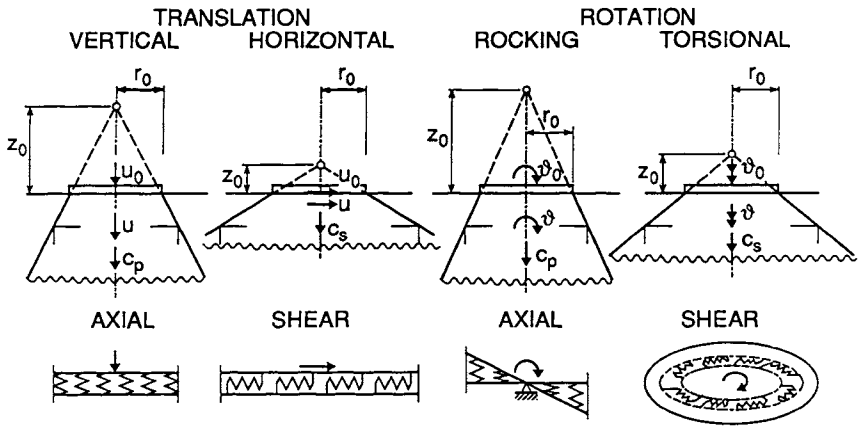

Fig. A-3 Cones for various degrees of freedom with corresponding apex ratio (opening angle), wave-propagation velocity and distortion.

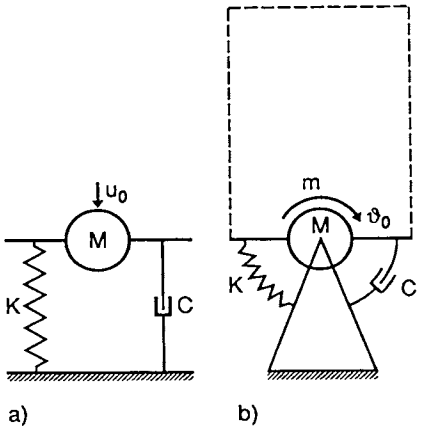

Fig. A-4 Standard lumped-parameter model with no internal degree of freedom for
a) Translational motion.
b) Rotational motion.

$$k_\vartheta(a_0) = 1 - \frac{1}{3}\frac{a_0^2}{\left(\frac{16}{9\pi(1-\upsilon)}\right)^2 + a_0^2} - \frac{0.9\pi(1-\upsilon)\left(\upsilon - \frac{1}{3}\right)}{8}\, a_0^2$$

and dimensionless damping coefficient

$$c_\vartheta(a_0) = \frac{z_0 c_s}{3 r_0 c}\,\frac{a_0^2}{\left(\frac{r_0 c}{z_0 c_s}\right)^2 + a_0^2}$$

Flexibility Formulation

Rotation-interaction moment relationship (Fig. A-2c)
For torsional motion and for rocking motion when $\upsilon \le 1/3$

$$\vartheta_0(t) = \int_0^t h_2(t-\tau)\frac{M_0(\tau)}{K_\vartheta}\,d\tau$$

with unit-impulse response function

$$h_2(t) = \frac{c}{z_0} e^{-\frac{3}{2}\frac{c}{z_0}t} * \left(3\cos\frac{\sqrt{3}}{2}\frac{c}{z_0}t - \sqrt{3}\sin\frac{\sqrt{3}}{2}\frac{c}{z_0}t\right) \quad t \ge 0$$
$$= 0 \quad t < 0$$

The recursive evaluation with the second order term $h_2(t)$ proceeds as:

$$\vartheta_{0n} = a_1\vartheta_{0n-1} + a_2\vartheta_{0n-2} + b_0\frac{M_{0n}}{K_\vartheta} + b_1\frac{M_{0n-1}}{K_\vartheta} + b_2\frac{M_{0n-2}}{K_\vartheta}$$

where

$$a_1 = 2e^{-\frac{3}{2}\frac{c\Delta t}{z_0}}\cos\frac{\sqrt{3}}{2}\frac{c\Delta t}{z_0}$$

$$a_2 = -e^{-3\frac{c\Delta t}{z_0}}$$

and substituting $r(t) = r_2(t)$

$$r_2(t) = t - \frac{2\sqrt{3}}{3}\frac{z_0}{c}e^{-\frac{3}{2}\frac{ct}{z_0}}\sin\frac{\sqrt{3}}{2}\frac{ct}{z_0} \quad t \ge 0$$
$$= 0 \quad t < 0$$

b_0, b_1 and b_2 follow from the equations specified in connection with the convolution with $h_4(t)$(end of Section Translational Cone).

A1.2 Lumped-Parameter Model

Standard Lumped-Parameter Model

Besides a spring with the static-stiffness coefficient K (=K_ϑ for rotational motion) a dashpot and a mass (mass moment of inertia for rotational motion) are present (Fig. A-4) with the coefficients

$$C = \frac{r_0}{c_s}\,\gamma\,K \qquad M = \frac{r_0^2}{c_s^2}\,\mu\,K$$

γ and μ are specified in Table A-2 with the mass moment of inertia of the disk (rigid structure) m.

Table A-2: Static Stiffness and Dimensionless Coefficients of the Standard Lumped-Parameter Model for a Disk with Mass on a Homogeneous Halfspace

	Static Stiffness K	Dimensionless Coefficients of Dashpot γ	Dimensionless Coefficients of Mass μ
Horizontal	$\frac{8Gr_0}{2-\upsilon}$	0.58	0.095
Vertical	$\frac{4Gr_0}{1-\upsilon}$	0.85	0.27
Rocking	$\frac{8Gr_0^3}{3(1-\upsilon)}$	$\frac{0.3}{1+\frac{3(1-\upsilon)m}{8r_0^5\rho}}$	0.24
Torsional	$\frac{16Gr_0^3}{3}$	$\frac{0.433}{1+\frac{2m}{r_0^5\rho}}\sqrt{\frac{m}{r_0^5\rho}}$	0.045

Fundamental Lumped-Parameter Model

Besides a spring with the static-stiffness coefficient K (= K_ϑ for rotational motion) and a direct dashpot C_0 connecting the basemat node with mass M_0 (mass moment of inertia for rotational motion) to the rigid support (Fig. A-5), an internal degree of freedom with its own mass M_1 (mass moment of inertia for rotational motion) is introduced which is attached to the disk node by a dashpot C_1

$$C_0 = \frac{r_0}{c_s}\gamma_0 K \qquad C_1 = \frac{r_0}{c_s}\gamma_1 K$$

$$M_0 = \frac{r_0^2}{c_s^2}\mu_0 K \qquad M_1 = \frac{r_0^2}{c_s^2}\mu_1 K$$

γ_0, γ_1, μ_0 and μ_1 are specified in Table A-3.

A 1.3 Wedge Model

For the horizontal and rocking motions a rigid basemat with width 2b on the surface of a homogeneous soil halfplane (two-dimensional strip foundation) can be modeled with a truncated semi-infinite wedge with apex height z_0 and wave velocity c (Fig. A-6). For the horizontal wedge deforming in shear c equals c_s and for the rocking wedge

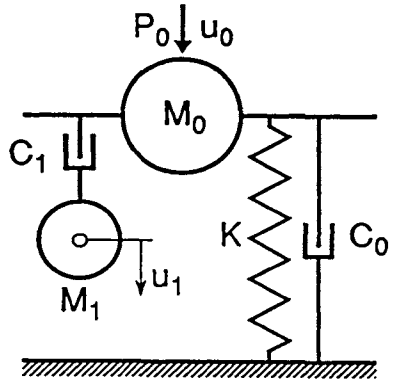

Fig. A-5 Fundamental lumped-parameter model (monkey-tail arrangement) with one internal degree of freedom.

deforming axially c equals c_p for $\upsilon<1/3$ and is limited to $2c_s$ for $1/3<\upsilon\leq 1/2$. For the rocking motion in the case of the nearly-incompressible soil ($1/3<\upsilon\leq 1/2$) a trapped mass moment of inertia ΔM_ϑ assigned to the basemat arises. The properties are summarized in Table A-4.

Static-Stiffness Coefficient

$$K_h = 0 \quad \text{horizontal} \qquad K_r = \frac{\pi G b^2}{2(1-\upsilon)} \quad \text{rocking}$$

Radiation-Dashpot Coefficient (high-frequency behavior)

$$C_h = \rho c_s 2b \quad \text{horizontal} \qquad C_r = \rho c \frac{8b^3}{12} \quad \text{rocking}$$

Dynamic-Stiffness Coefficient for Harmonic Loading

$$\text{horizontal} \quad S(b_0) = \frac{b_0 H_1^{(2)}(b_0)}{H_0^{(2)}(b_0)} \frac{\rho c_s^2 2b}{z_0}$$

$$\text{rocking} \quad S(b_0) = \frac{b_0 H_2^{(2)}(b_0)}{H_1^{(2)}(b_0)} \frac{\rho c^2}{z_0}\frac{8b^3}{12}$$

with dimensionless frequency parameter defined with respect to properties of wedge

$$b_0 = \frac{\omega z_0}{c}$$

and Hankel functions of second kind $H^{(2)}$.

A 1.4 Material Damping

Material damping is introduced in the frequency domain based on the correspondence principle applied to the elastic solution. For non-causal linear-hysteretic damping the shear

Table A-3: Static Stiffness and Dimensionless Coefficients of the Fundamental Lumped-Parameter Model (Monkey-Tail Arrangement) for a Disk on a Homogeneous Halfspace

		Dimensionless Coefficients of			
		Dashpots		Masses	
	Static Stiffness K	γ_0	γ_1	μ_0	μ_1
Horizontal	$\frac{8Gr_0}{2-\upsilon}$	0.78–0.4υ	——	——	——
Vertical	$\frac{4Gr_0}{1-\upsilon}$	0.8	0.34–4.3 υ^4	$\upsilon<\frac{1}{3}$ 0 $\upsilon>\frac{1}{3}$ $0.9\left(\upsilon-\frac{1}{3}\right)$	0.4–4 υ^4
Rocking	$\frac{8Gr_0^3}{3(1-\upsilon)}$	——	0.42–0.3 υ^2	$\upsilon<\frac{1}{3}$ 0 $\upsilon>\frac{1}{3}$ $0.16\left(\upsilon-\frac{1}{3}\right)$	0.34–0.2 υ^2
Torsional	$\frac{16Gr_0^3}{3}$	—— (0.017)	0.29 (0.291)	—— (——)	0.2 (0.171)

Table A-4: Key Expressions to Model a Two-Dimensional Foundation on the Surface of a Homogeneous Soil Halfplane with a Wedge

Motion	Horizontal	Rocking	
Aspect Ratio $\frac{z_0}{b}$	$\frac{2-\upsilon}{\pi}$	$\frac{8(1-\upsilon)}{3\pi}$ $\frac{c^2}{c_s^2}$	
Poisson's Ratio υ	all υ	$\leq\frac{1}{3}$	$\frac{1}{3}<\upsilon\leq\frac{1}{2}$
Wave Velocity c	c_s	c_p	$2c_s$
Trapped Mass Moment of Inertia ΔM_ϑ	0	0	$\frac{3}{4}\left(\upsilon-\frac{1}{3}\right)\rho\frac{8b^3}{12}b$

modulus G and constrained modulus E_c are multiplied by $1 + 2i\zeta_g$ (ζ_g = hysteretic-damping ratio), resulting in the solution for the damped case. The corresponding spring and damping coefficients $k_\zeta(a_0)$, $c_\zeta(a_0)$ are expressed approximately as a function of the elastic values $k(a_0)$, $c(a_0)$

$$k_\zeta(a_0) = k(a_0) - \zeta_g a_0 c(a_0)$$

$$c_\zeta(a_0) = c(a_0) + \frac{2\zeta_g}{a_0} k(a_0)$$

For Voigt visco-elasticity with damping proportional to frequency (defined as the ratio ζ_0 at ω_0) the factor equals $1+i\omega 2\zeta_0/\omega_0$, and the correspondence principle is applied directly to the discrete-element model (or lumped-parameter model). Each original spring with coefficient K is augmented by a dashpot with coefficient $C = 2(\zeta_0/\omega_0)K$ in parallel, and each original dashpot with coefficient C by a pulley-mass with coefficient $(\zeta_0/\omega_0)C$ (Fig. A-7). Masses in the original model remain unchanged.

For frictional (hysteretic) material damping which preserves causality, non-linear frictional elements replace the augmenting dashpot and pulley-mass. The correspon-

Table A-5: Dimensionless Coefficients of the Basic Lumped-Parameter Model for a Disk on the Surface of a Soil Layer on Rigid Rock

Ratio of Radius to Depth r_0/d			Horizontal			Vertical			Rocking			Torsional
			Poisson's Ratio υ									
			0	1/3	0.45	0	1/3	0.45	0	1/3	0.45	
	1.00	k_1	-.109636 E+02	-.125658 E+02	-.107091 E+02	-.185216 E+02	-.312572 E+02	-.585650 E+02	-.538137 E+01	-.127100 E+02	-.125057 E+02	-.920277 E+01
		k_2	-.199616 E+02	-.100143 E+02	-.277613 E+02	-.689058 E+02	+.564651 E+01	+.533868 E+02	-.118019 E+02	-.127000 E+01	-.102097 E+02	-.488643 E+01
		k_3	-.596293 E+03	-.236814 E+03	-.837270 E+03	-.803915 E+04	-.297570 E+04	-.972054 E+05	-.370561 E+03	-.106411 E+03	-.114401 E+05	-.762034 E+02
		k_4	+.262006 E+02	+.172890 E+02	+.350886 E+02	+.781698 E+02	+.101028 E+02	-.297301 E+02	+.152717 E+02	+.665102 E+01	+.171002 E+02	+.104850 E+02
		c_1	-.423955 E+01	-.391585 E+01	-.443420 E+01	-.564579 E+01	-.620122 E+01	-.533597 E+01	-.152562 E+01	-.168764 E+01	-.159579 E+01	-.209847 E+01
		c_2	-.144980 E+02	-.969345 E+01	-.164981 E+02	-.573623 E+02	-.372925 E+02	-.162817 E+03	-.511671 E+01	-.464871 E+01	-.205038 E+02	-.424955 E+01
		c_3	+.176380 E+02	+.128349 E+02	+.196381 E+02	+.618023 E+02	+.435725 E+02	+.173237 E+03	+.622671 E+01	+.621871 E+01	+.231038 E+02	+.581955 E+01
		m	-.444888 E+02	-.177585 E+02	-.804875 E+02	-.355432 E+03	-.896786 E+02	-.759400 E+03	-.136958 E+02	-.294864 E+01	-.748688 E+02	-.501042 E+01
	0.50	k_1	-.101741 E+02	-.756096 E+01	-.103098 E+02	-.869429 E+01	-.178038 E+02	-.211241 E+02	-.558202 E+01	-.315920 E+01	-.544861 E+01	-.584813 E+01
		k_2	-.711128 E+01	+.221036 E+01	+.353643 E+00	-.211429 E+02	+.869558 E+01	+.237930 E+02	-.260867 E+01	+.429538 E+00	+.544528 E+01	+.779373 E+00
		k_3	-.376551 E+02	-.183990 E+02	-.386290 E+02	-.301954 E+03	-.648930 E+02	-.574768 E+04	-.120186 E+02	-.563639 E+00	-.495529 E+02	-.267204 E+01
		k_4	+.114651 E+02	+.370791 E+01	+.631911 E+01	+.266455 E+02	+.167960 E+00	-.104560 E+02	+.553603 E+01	+.268680 E+01	-.714571 E+00	+.448746 E+01
		c_1	-.563146 E+01	-.169515 E+01	-.312323 E+01	-.635435 E+01	-.300736 E+01	-.885920 E+01	-.180105 E+01	-.217449 E+00	-.226588 E+01	-.873265 E+00
		c_2	-.853329 E+01	-.484337 E+01	-.900332 E+01	-.118278 E+02	-.967485 E+01	-.348879 E+02	-.209944 E+01	-.485884 E-01	-.872006 E+00	-.664093 E+00
		c_3	+.116733 E+02	+.798337 E+01	+.121433 E+02	+.162678 E+02	+.159548 E+02	+.453079 E+02	+.320944 E+01	+.161859 E+01	+.347201 E+01	+.223409 E+01
		m	-.125108 E+02	-.142805 E+02	-.222875 E+02	-.438319 E+02	-.104698 E+02	-.156304 E+03	-.166034 E+01	-.550887 E-01	-.105920 E+01	-.758683 E+00
	0.25	k_1	-.500393 E+01	-.569922 E+01	-.635602 E+01	-.650348 E+01	-.866267 E+01	-.939217 E+01	-.197103 E+01	-.131566 E+01	-.185845 E+01	-.317223 E+01
		k_2	+.117908 E+01	+.113372 E+01	+.126563 E+01	+.212837 E+01	+.360033 E+01	+.591506 E+01	-.908392 E+00	-.159178 E+01	+.140842 E+01	-.110204 E+02
		k_3	-.531658 E+01	-.627809 E+01	-.861155 E+01	-.111486 E+02	-.206851 E+02	-.294639 E+02	+.320667 E+00	+.889908 E+00	-.198123 E+01	-.272014 E+02
		k_4	+.330564 E+01	+.414181 E+01	+.444955 E+01	+.290606 E+01	+.353509 E+01	+.239510 E+01	+.280516 E+01	+.228996 E+01	+.228257 E+00	+.133791 E+02
		c_1	-.753687 E+00	-.123420 E+01	-.118324 E+01	-.147587 E+01	-.301652 E+01	-.652332 E+01	-.111891 E+01	-.117566 E+01	-.166191 E+01	-.175255 E+01
		c_2	-.320391 E+01	-.343160 E+01	-.476257 E+01	-.545496 E+01	-.633133 E+01	-.153512 E+01	-.192001 E-01	-.120420 E+00	-.608065 E-01	-.576183 E+00
		c_3	+.634391 E+01	+.657160 E+01	+.790257 E+01	+.989496 E+01	+.126113 E+02	+.119551 E+02	+.131920 E+01	+.199042 E+01	+.266081 E+01	+.214618 E+01
		m	-.197705 E+02	-.277938 E+02	-.353939 E+02	-.202557 E+02	-.262470 E+02	-.217797 E+01	-.496405 E-02	-.234838 E-01	-.166728 E-01	-.408057 E+00
	0.00	k_1	-.135004 E+02	-.388471 E+01	-.517262 E+01	-.196175 E+01	-.741830 E+01	-.174454 E+02	-.177328 E+01	-.371794 E+01	-.398695 E+01	-.347454 E+01
		k_2	-.953646 E+01	-.159784 E+02	+.239313 E+00	-.586095 E+00	+.149859 E+01	+.318590 E+01	-.825315 E+01	-.530262 E+01	+.488296 E+01	+.161189 E+00
		k_3	-.152937 E+02	-.214052 E+02	-.491200 E+01	+.418313 E+00	-.108130 E+02	-.145871 E+03	-.960129 E+00	-.456729 E+01	-.157465 E+02	-.175021 E+00
		k_4	+.100318 E+02	+.139890 E+02	+.491843 E+01	+.253876 E+01	+.426031 E+01	+.401297 E+01	+.363207 E+01	+.648378 E+01	-.222776 E+01	+.329151 E+01
		c_1	-.108173 E+01	-.406936 E+00	-.431719 E-01	-.540639 E+00	-.308148 E+00	-.287195 E+01	-.105544 E+01	-.150532 E+01	-.158356 E+01	-.257114 E-01
		c_2	-.164199 E+01	-.441082 E+00	-.433318 E-01	-.316451 E-02	-.760091 E+00	-.496738 E+01	-.396130 E+00	-.400894 E+00	-.408329 E+00	-.525606 E-02
		c_3	+.478349 E+01	+.358258 E+01	+.318483 E+01	+.470316 E+01	+.704009 E+01	+.153874 E+02	+.150613 E+01	+.197089 E+01	+.300833 E+01	+.157526 E+01
		m	-.207315 E+00	-.331202 E-01	-.126178 E+00	-.110135 E-02	-.348161 E+00	-.240813 E+01	-.245402 E-01	-.633544 E-01	-.125199 E+00	-.126499 E-02

ding forces acting between the nodes with displacements u_0 and u_1 are equal to (sgn () returns the algebraic sign of the argument)

$$P = K|\overline{u_0 - u_1}| \tan\delta \ \text{sgn}\ (\dot{u}_0 - \dot{u}_1)$$

$$P = C|\overline{\dot{u}_0 - \dot{u}_1}| \ 0.5 \ \tan\delta \ \text{sgn}\ (\ddot{u}_0 - \ddot{u}_1)$$

with the overbar denoting the short-term memory (current or last peak value) and $\tan\delta = 2\zeta_g$ (δ=friction angle). Incorporation of these frictional elements in the discrete-element model (or lumped-parameter model) permits causal analysis in the time domain taking hysteretic damping independent of frequency into consideration.

These concepts also apply to the lumped-parameter models for a foundation on the surface of a layer on rigid rock (Appendix A2) and for a foundation embedded in a halfspace or in a layer (Appendix A3).

A2 FOUNDATION ON SURFACE OF SOIL LAYER ON RIGID ROCK

A2.1 Unfolded Layered Cone Model

For all components of motion a rigid basemat with equivalent radius r_0 on the surface of a soil layer of depth d resting on rigid rock (Fig. A-8) can be visualized as a folded cone. When unfolded, this layered cone enables a wave pattern to be postulated which incorporates the decay of amplitude as the waves propagate away from the basemat as well as the reflections at rock interface and at the free surface. The aspect ratio z_0/r_0 (opening angle) of the unfolded layered cone is the same as that of the truncated semi-infinite cone used to model a disk on a homogeneous halfspace with the same material properties as the layer (Table A-1).

From the wave pattern it follows that the translation $u_0(t)$ (or rotation $\vartheta_0(t)$) of the basemat on a layer is equal to that of the basemat, with the same load acting, on a

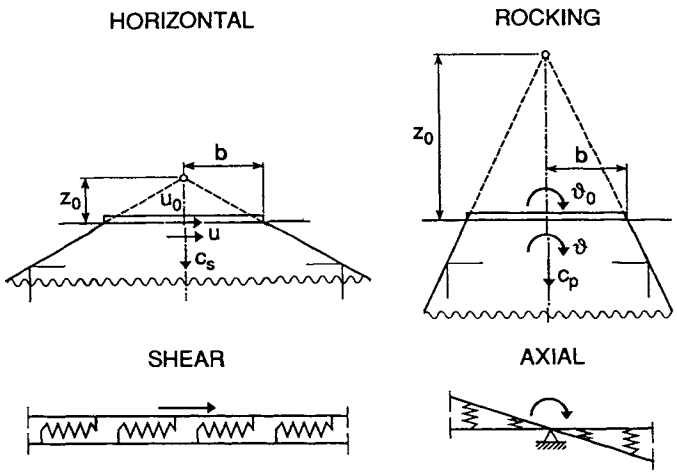

Fig. A-6 Horizontal and rocking wedges with corresponding apex ratio (opening angle), wave-propagation velocity and distortion.

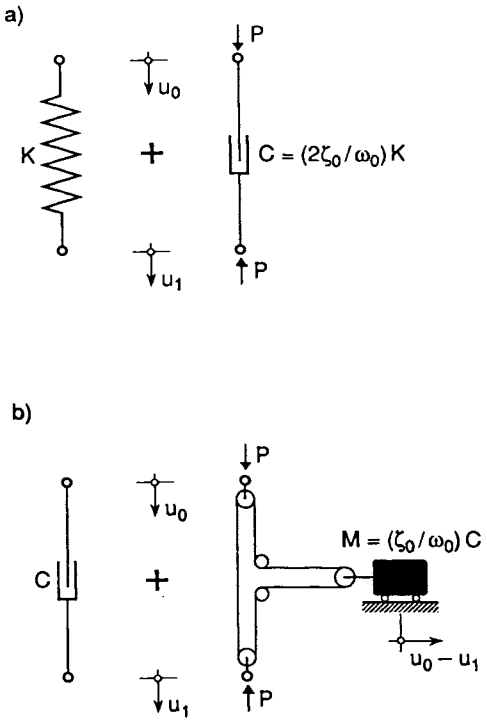

Fig. A-7 Augmenting elements to represent Voigt viscoelasticity.
a) Original spring with augmenting dashpot.
b) Original dashpot with augmenting pulley mass.

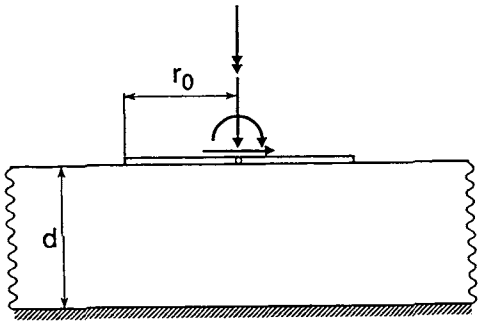

Fig. A-8 Disk on surface of soil layer resting on rigid rock.

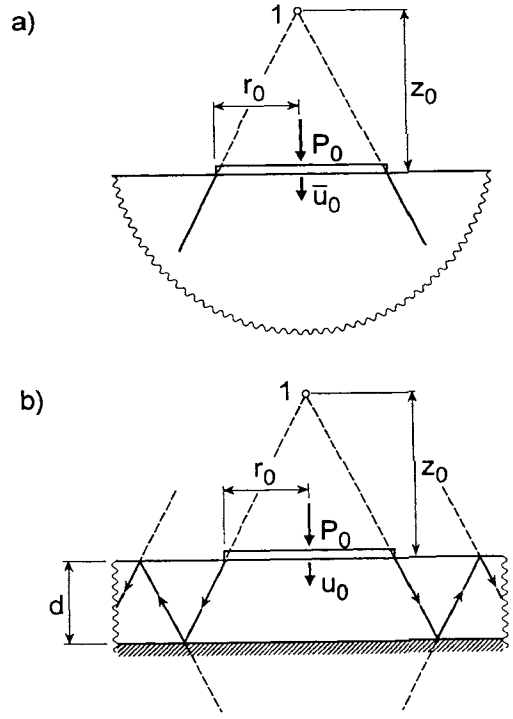

Fig. A-9 Nomenclature for loaded disk in vertical motion on surface of soil.
a) Halfspace with generating displacement.
b) Layer with resulting displacement.

homogeneous halfspace ($\bar{u}_0(t)$ or $\bar{\vartheta}_0(t)$) (generating function), augmented by echoes of the previous response (Fig. A-9). The appropriate echo constants are derived for the flexibility formulation, then inverted to obtain the echo constants of the stiffness formulation.

Echo Constant

Echo formula for translation in a flexibility formulation

$$u_0(t) = \sum_{j=0}^{k} e_j^F \bar{u}_0(t - jT)$$

with flexibility echo constants

$$e_0^F = 1 \qquad e_j^F = \frac{2(-1)^j}{1+j\kappa} \qquad j \geq 1$$

and $T = \frac{2d}{c}$ $\qquad \kappa = \frac{2d}{z_0}$

and appropriate wave velocity c and aspect height z_0 (Table A-1). The integer k is equal to the largest index j for which the argument t-jT of $\bar{u}_0$ is positive.

Echo formula for rotation in a flexibility formulation

$$\vartheta_0(t) = \sum_{j=0}^{k} e_{0j}^F \bar{\vartheta}_0(t-jT) + \sum_{j=0}^{k} e_{1j}^F \bar{\vartheta}_1(t-jT)$$

with flexibility echo constants

$$e_{00}^F = 1 \quad e_{0j}^F = \frac{2(-1)^j}{(1+j\kappa)^2} \qquad j \geq 1$$

$$e_{10}^F = 0 \quad e_{1j}^F = 2(-1)^j \left[\frac{1}{(1+j\kappa)^3} - \frac{1}{(1+j\kappa)^2} \right] \qquad j \geq 1$$

and $\bar{\vartheta}_1(t) = \int_0^t h_1(t-\tau)\bar{\vartheta}_0(\tau)\, d\tau$

with unit-impulse response function

$$h_1(t) = \frac{c}{z_0} e^{-\frac{c}{z_0} t} \qquad t \geq 0$$
$$= 0 \qquad t < 0$$

Alternatively, using pseudo-echo constants e_{rm}^F (influence functions) which follow from e_{0j}^F and e_{1j}^F (see [49], p. 175-177) the echo formula for rotation equals

$$\vartheta_0(t) = \sum_{m=0}^{k} e_{rm}^F \bar{\vartheta}_0(t-m\Delta t)$$

with time step Δt.

Echo formula for translation in a stiffness formulation

$$\bar{u}_0(t) = \sum_{j=0}^{k} e_j^K u_0(t-jT)$$

with stiffness echo constants

$$e_0^K = 1 \qquad e_j^K = -\sum_{\ell=0}^{j-1} e_\ell^K e_{j-\ell}^F \qquad j \geq 1$$

and for rotation

$$\bar{\vartheta}_0(t) = \sum_{m=0}^{k} e_{rm}^K \vartheta_0(t-m\Delta t)$$

with stiffness echo constants

$$e_{r0}^K = 1 \qquad e_{rm}^K = -\sum_{\ell=0}^{m-1} e_{r\ell}^K e_{rm-\ell}^F \qquad j \geq 1$$

Flexibility Formulation

In a flexibility formulation, in the first step, the prescribed interaction force $P_0(t)$ (or moment $M_0(t)$) is applied to the cone modeling a disk on the associated homogeneous halfspace with the same material properties as the layer, resulting in the surface displacement $\bar{u}_0(t)$ (or rotation $\bar{\vartheta}_0(t)$) using the procedure described in Section A1.1 (Fig. A-9a). In the second step, the displacement $u_0(t)$ (or rotation $\vartheta_0(t)$) of the basemat on the layer follows from $\bar{u}_0(t)$ (or $\bar{\vartheta}_0(t)$) using the corresponding echo formula.

Stiffness Formulation

In a stiffness formulation, in the first step, the prescribed surface displacement $u_0(t)$ (or rotation $\vartheta_0(t)$) is converted to the displacement $\bar{u}_0(t)$ (or rotation $\bar{\vartheta}_0(t)$) of a disk on the associated homogeneous halfspace using the corresponding echo formula. In the second step, insertion into the interaction force-displacement relationship of the cone modelling a disk on the associated homogeneous halfspace leads to the interaction force $P_0(t)$ (or moment $M_0(t)$) acting on the basemat using the procedure described in Section A1.1 (Fig. A-9a).

Static-Stiffness Coefficient

$$K^L = K \frac{1}{\sum_{j=0}^{\infty} e_j^F} \qquad K_\vartheta^L = K_\vartheta \frac{1}{\sum_{j=0}^{\infty} e_{0j}^F + \sum_{j=0}^{\infty} e_{1j}^F}$$

index L for disk on layer, no index for disk on homogeneous halfspace with material properties of layer

$$K_h^L = \frac{8Gr_0}{2-\upsilon}\left(1+\frac{1}{2}\frac{r_0}{d}\right) \quad \text{horizontal}$$
$$K_v^L = \frac{4Gr_0}{1-\upsilon}\left(1+1.3\frac{r_0}{d}\right) \quad \text{vertical}$$
$$K_r^L = \frac{8Gr_0^3}{3(1-\upsilon)}\left(1+\frac{1}{6}\frac{r_0}{d}\right) \quad \text{rocking}$$
$$K_t^L = \frac{16}{3}Gr_0^3\left(1+\frac{1}{10}\frac{r_0}{d}\right) \quad \text{torsional}$$

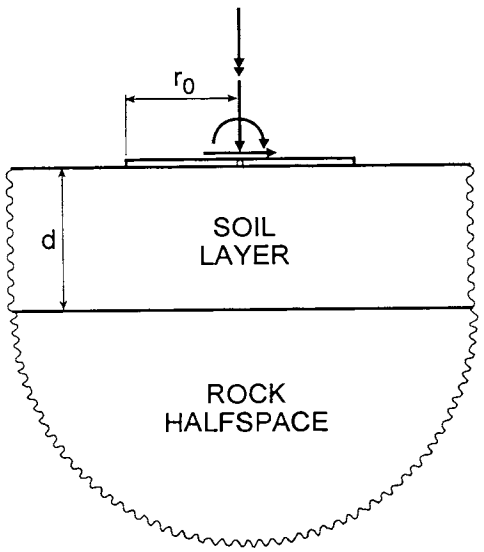

Fig. A-10 Disk on surface of soil layer resting on flexible rock halfspace.

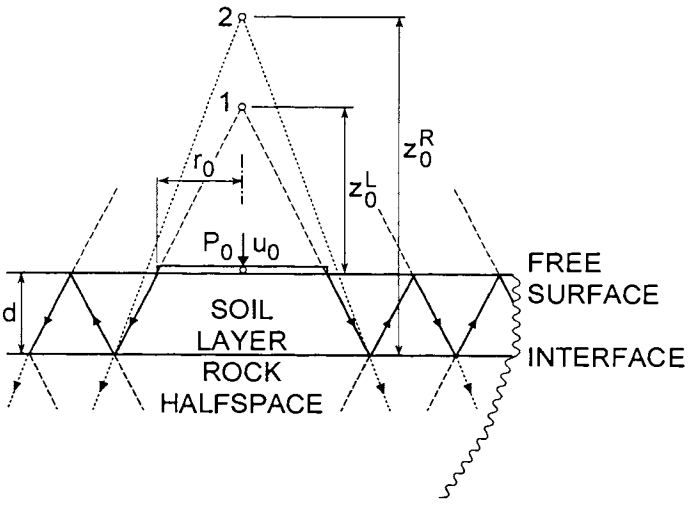

Fig. A-11 Disk in vertical motion on soil layer resting on flexible rock halfspace with wave pattern in corresponding cones.

Dynamic-Stiffness Coefficient for Harmonic Loading

translation

$$S(\omega) = K \frac{1 + i\frac{\omega T}{\kappa}}{1 + 2\sum_{j=1}^{\infty}(-1)^j \frac{e^{-ij\omega T}}{1 + j\kappa}}$$

rotation

$$S_\vartheta(\omega) = K_\vartheta * \frac{1 - \frac{1}{3}\frac{(\omega T)^2}{\kappa^2 + (\omega T)^2} + i\frac{\omega T}{3\kappa}\frac{(\omega T)^2}{\kappa^2 + (\omega T)^2}}{1 + \frac{2}{1 + i\frac{\omega T}{\kappa}}\left(\sum_{j=1}^{\infty}(-1)^j \frac{e^{-ij\omega T}}{(1 + j\kappa)^3} + i\frac{\omega T}{\kappa}\sum_{j=1}^{\infty}(-1)^j \frac{e^{-ij\omega T}}{(1 + j\kappa)^2}\right)}$$

with static-stiffness coefficients of homogeneous halfspace with material properties of layer K, K_ϑ (Table A-2).

Foundation on Surface of Soil Layer on Flexible Rock Halfspace

The unfolded cone can be generalized to the case of a layer on flexible rock (Fig. A-10) considering the refraction at the layer-rock interface. The only modification consists of replacing in the expressions for the echo constants the reflection coefficient associated with the rigid rock, -1, by the corresponding value $-\alpha$ for the flexible rock. All flexibility and stiffness formulations for the dynamic analysis remain valid.

$$-\alpha = \frac{\frac{\rho_L c_L^2}{z_0^L + d} - \frac{\rho_R c_R^2}{z_0^R}}{\frac{\rho_L c_L^2}{z_0^L + d} + \frac{\rho_R c_R^2}{z_0^R}} \quad \left(= \frac{\rho_L c_L^2 - \rho_R c_R^2}{\rho_L c_L^2 + \rho_R c_R^2} \text{ for } \upsilon_L = \upsilon_R\right)$$

Indices L and R refer to the layer and the rock. z_0^R measured from the interface determined with the properties of the rock halfspace (Table A-1) leads to the apex 2 of the rock's truncated semi-infinite cone (Fig. A-11).

For the dynamic-stiffness coefficients frequency-dependent reflection coefficients for translation and rotation $-\alpha(\omega)$ can also be used ([49], pages 193 and 196). A generalization to the halfspace with many layers exists ([49], Appendix D).

A2.2 Basic Lumped-Parameter Model

The basic lumped-parameter model can be used to represent the dynamic behavior for all components of motion of a disk on the surface of a soil layer on rigid rock in a standard finite-element program for structural dynamics in the time domain. The model (Fig. A-12) with two additional internal degrees of freedom (u_1, u_2) consists of four springs K_i, three dashpots C_i and one mass M whose real frequency-independent coefficients are specified for various ratios of the radius r_0 of the disk to the depth d of the layer and Poisson's ratio υ for the horizontal, vertical, rocking and torsional motions in Table A-5.

$$K_i = k_i G r_0 \quad i = 1, \ldots, 4$$

$$C_i = c_i G \frac{r_0^2}{c_s} \quad i = 1, \ldots 3, \quad M = mG\frac{r_0^3}{c_s^2}$$

To construct a lumped-parameter model for the rotational motions representing the relationship between the rotation and the moment, the right-hand side has to be multiplied by r_0^2.

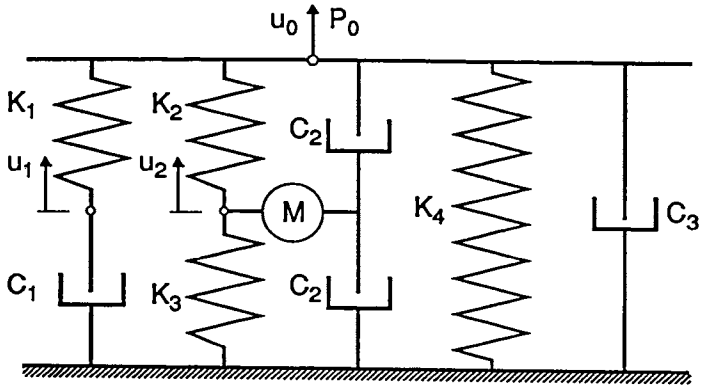

Fig. A-12 Basic lumped-parameter model with two internal degrees of freedom.

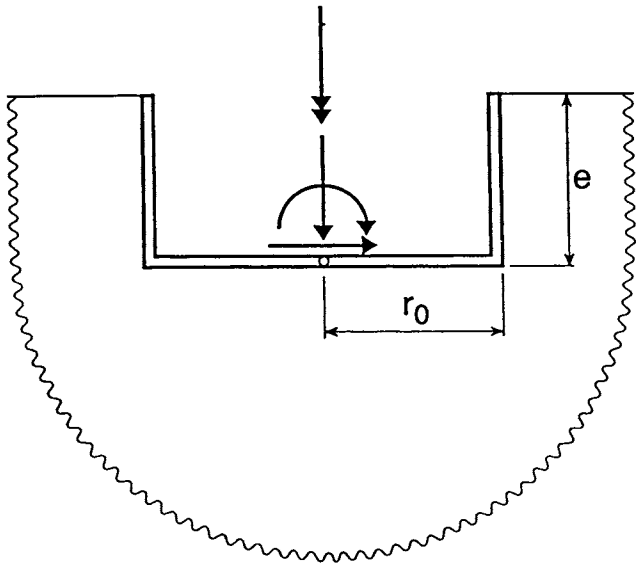

Fig. A-13 Cylindrical foundation embedded in soil half-space.

A3 EMBEDDED FOUNDATION AND PILE FOUNDATION

A3.1 Double-Cone Model

To analyze a foundation with embedment e for all components of motion (Fig. A-13), a rigid disk of radius r_0 embedded in a full-space, which is modeled with a double-cone model, is the building block (Fig. A-14). The aspect ratio z_0/r_0 and the wave velocity c are the same as for the one-sided cone used to model a surface disk (Table A-1). The only change consists of doubling the static-stiffness coefficients K and K_ϑ(Table A-2). The double cone's displacement field defines approximate Green's functions for use in a matrix formulation of structural mechanics.

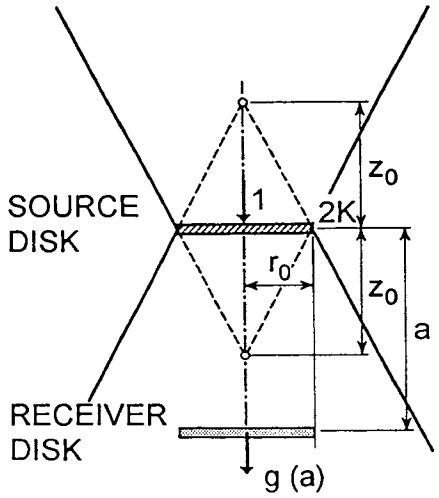

Fig. A-14 Green's function based on disk embedded in fullspace with double-cone model.

Green's Function

Translational Double Cone (Fig. A-14)

distance a

$$g(a,\ t) = \frac{1}{2K}\ \frac{1}{1+\frac{a}{z_0}}\ h_1\left(t-\frac{a}{c}\right)$$

with unit-impulse response function

$$h_1(t) = \frac{c}{z_0}\ e^{-\frac{c}{z_0}t} \qquad t \geq 0$$
$$= 0 \qquad t < 0$$

$$g(a,\omega) = \frac{1}{2K}\ \frac{1}{1+\frac{a}{z_0}}\ \frac{e^{-i\frac{\omega a}{c}}}{1+i\frac{\omega z_0}{c}}$$

Rotational Double Cone

$$g_\vartheta(a,t) = \frac{1}{2K_\vartheta}\ \frac{1}{\left(1+\frac{a}{z_0}\right)^2}\left[h_2\left(t-\frac{a}{c}\right)+\left(-1+\frac{1}{1+\frac{a}{z_0}}\right)h_3\left(t-\frac{a}{c}\right)\right]$$

with

$$h_2(t) = \frac{c}{z_0}e^{-\frac{3}{2}\frac{c}{z_0}t}\left(3\cos\frac{\sqrt{3}}{2}\ \frac{c}{z_0}t-\sqrt{3}\sin\frac{\sqrt{3}}{2}\ \frac{c}{z_0}t\right) \qquad t\geq 0$$
$$= 0 \qquad t<0$$

$$h_3(t) = 2\sqrt{3}\ \frac{c}{z_0}e^{-\frac{3}{2}\frac{c}{z_0}t}\sin\frac{\sqrt{3}}{2}\frac{c}{z_0}t \qquad t\geq 0$$
$$= 0 \qquad t<0$$

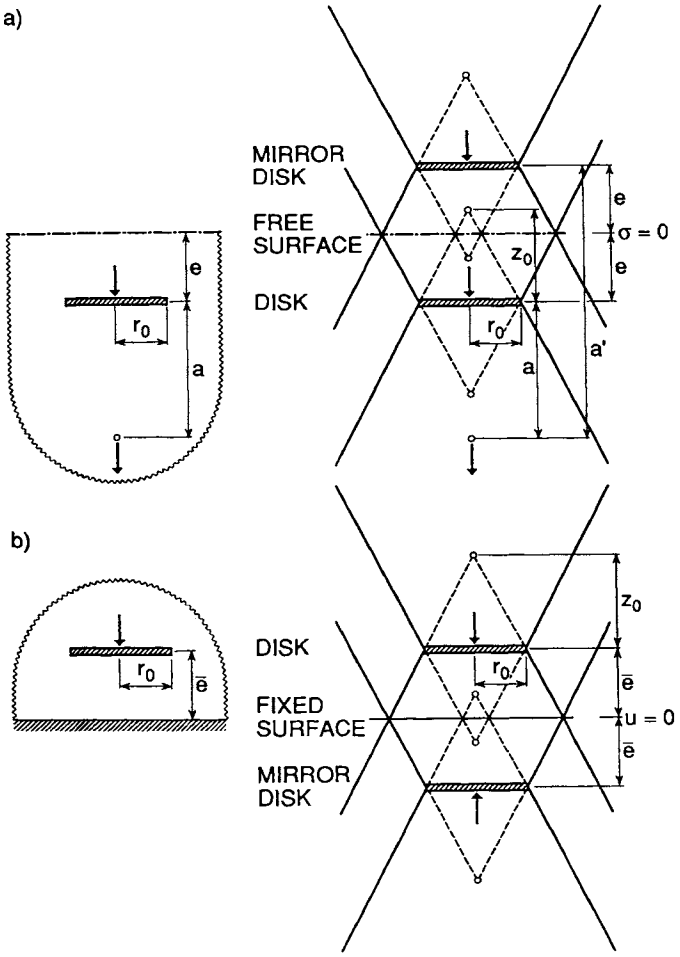

Fig. A-15 Modeling of free and fixed boundaries.
a) Disk embedded in halfspace with free boundary with anti-symmetrically loaded mirror-image disk to represent free surface.
b) Disk embedded in halfspace with fixed boundary with symmetrically loaded mirror-image disk to represent fixed boundary.

$$g_\vartheta(a,\omega) = \frac{3}{2K_\vartheta}\left(\frac{1}{\left(1+\frac{a}{z_0}\right)^3} + i\frac{\omega z_0}{c}\,\frac{1}{\left(1+\frac{a}{z_0}\right)^2}\right) * \frac{1}{3 + 3i\frac{\omega z_0}{c} + \left(i\frac{\omega z_0}{c}\right)^2}\, e^{-i\frac{\omega a}{c}}$$

For vertical motion of a *pile* the weighted Green's function of the double cone $g_{cone}(a,\omega)$ as above and of the fullspace for a point load $g_{fullspace}(a,\omega)$ is used

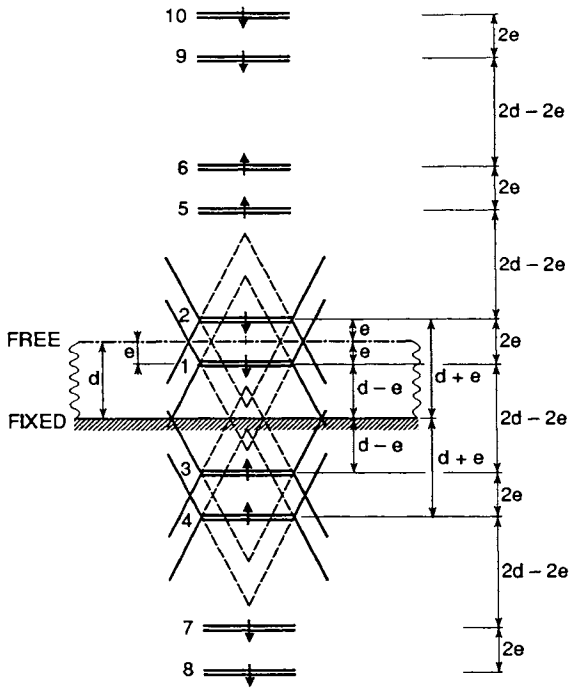

Fig. A-16 Arrangements of mirror-image disks embedded in fullspace with loads and double cones to model disk embedded in soil layer resting on rigid rock.

$$g(a,\omega) = w(a)\, g_{cone}(a,\omega) + (1-w(a))g_{fullspace}(a,\omega)$$

with the weighting function

$$w(a) = 1 \qquad a \le r_0$$
$$= e^{-0.8\,\frac{a-r_0}{r_0}} \qquad a > r_0$$

and where

$$g_{fullspace}(a,\omega) = \frac{1}{4\pi G}\left[\psi - \left(\frac{a}{r}\right)^2 \chi\right]$$

and with

$$\psi = \left(1 - i\frac{1}{a_0} - \frac{1}{a_0^2}\right)\frac{e^{-ia_0}}{r} + \left(i\frac{c_s}{c_p a_0} + \frac{1}{a_0^2}\right)\frac{e^{-i\frac{c_s}{c_p}a_0}}{r}$$

$$\chi = \left(1 - i\frac{3}{a_0} - \frac{3}{a_0^2}\right)\frac{e^{-ia_0}}{r} - \left(\frac{c_s^2}{c_p^2} - i\frac{3c_s}{c_p a_0} - \frac{3}{a_0^2}\right)\frac{e^{-i\frac{c_s}{c_p}a_0}}{r}$$

$$r = \sqrt{a^2 + r_0^2} \qquad a_0 = \frac{\omega r}{c_s}$$

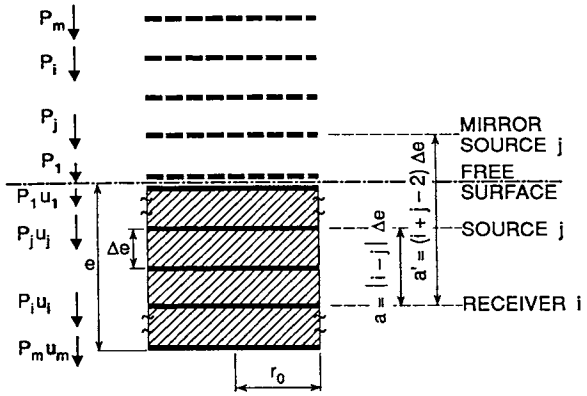

Fig. A-17 Stack of disks to model embedded cylindrical foundation with anti-symmetrically loaded mirror-image disks.

To model the free surface of a soil, a mirror-image disk (embedded in the fullspace and also represented by a double cone) loaded by the same time history of force as the original disk and with the same sign is introduced (Fig. A-15a). The same procedure can be used to model a fixed boundary, but the force on the mirror-image disk acts in the opposite direction (Fig. A-15b). To model a disk embedded in a soil layer resting on rigid rock, the concept of anti-symmetrically loaded mirror-image disks to represent the free surface and of symmetrically loaded mirror-image disks for the fixed boundary is applied repeatedly (Fig. A-16).

Matrix Formulation

Modeling the soil region which will later be excavated by a stack of rigid disks separated by soil (Fig. A-17), the dynamic-stiffness matrix for harmonic loading $\left[S^g_{00}(\omega)\right]$ of an embedded cylindrical foundation with respect to the rigid-body displacement amplitudes $\{u_0(\omega)\}$ and corresponding force amplitudes $\{P_0(\omega)\}$ is formulated with standard matrix methods of structural analysis as

$$\{P_0(\omega)\} = \left[S^g_{00}(\omega)\right] \{u_0(\omega)\}$$

where

$$\left[S^g_{00}(\omega)\right] = [A]^T \left[S^f(\omega)\right] [A] + \omega^2[M]$$

[A] is the kinematic-constraint matrix of the rigid foundation with $\{u(\omega)\}$ denoting the displacement amplitudes of the disks

$$\{u(\omega)\} = [A] \{u_0(\omega)\}$$

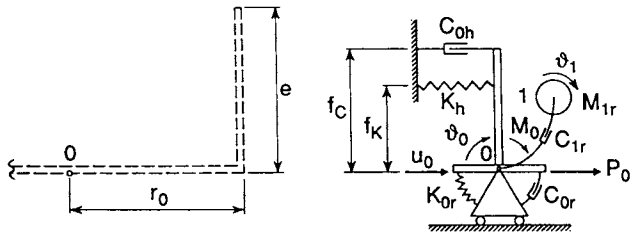

Fig. A-18 Fundamental lumped-parameter model for foundation embedded in halfspace with coupling of horizontal and rocking motions.

[M] is the rigid-body mass matrix of the excavated soil and $\left[S^f(\omega)\right]$ the dynamic-stiffness matrix of the free field

$$\left[S^f(\omega)\right] = [G(\omega)]^{-1}$$

where the dynamic-flexibility matrix of the disks embedded in the soil equals

$$\{u(\omega)\} = [G(\omega)] \{P(\omega)\}$$

with the corresponding force amplitudes $\{P(\omega)\}$. In $[G(\omega)]$ the sum of the Green's functions $g(a,\omega)$ of the source disk and $g(a',\omega)$ of the mirror-image disk appears (Fig. A-17).

In the time domain, the corresponding interaction force-displacement relationship of an embedded foundation at time $n\Delta t$ equals

$$\{P_0\}_n = [A]^T\left[S^f\right]_0[A]\{u_0\}_n - [A]^T\left[S^f\right]_0\{\bar{u}\}_n - [M]\{\ddot{u}_0\}_n$$

$\left[S^f\right]_0$ is the instantaneous dynamic-stiffness matrix of the free field

$$\left[S^f\right]_0 = [G]_0^{-1}$$

where the displacement-force relationship of the disks equals

$$\{u\}_n = \{\bar{u}\}_n + [G]_0\{P\}_n$$

with $$\{\bar{u}\}_n = \sum_{k=1}^{n-1}[G]_{n-k}\{P\}_k$$

$[G]_{n-k}$ is the dynamic-flexibility matrix in the time domain (displacements at time n caused by unit forces acting at time k).

Static-Stiffness Coefficient

cylindrical foundation of radius r_0 embedded with height e in a soil layer of depth d on rigid rock (d=∞: embedded in halfspace)

Table A-6: Static Stiffness and Dimensionless Coefficients of the Fundamental Lumped-Parameter Model (Monkey-Tail Arrangement) for a Cylinder Embedded in a Halfspace

	Static Stiffness K	Dimensionless Coefficients of		
		Dashpots		Mass
		γ_0	γ_1	μ_1
Horizontal	$\frac{8Gr_0}{2-\upsilon}\left(1+\frac{e}{r_0}\right)$	$0.68+0.57\sqrt{\frac{e}{r_0}}$	———	———
Vertical	$\frac{4Gr_0}{1-\upsilon}\left(1+0.54\frac{e}{r_0}\right)$	$0.80+0.35\frac{e}{r_0}$	$0.32-0.01\left(\frac{e}{r_0}\right)^4$	0.38
Rocking	$K_r=\frac{8Gr_0^3}{3(1-\upsilon)}\left[1+2.3\frac{e}{r_0}+0.58\left(\frac{e}{r_0}\right)^3\right]$	$0.15631\frac{e}{r_0}$	$0.40+0.03\left(\frac{e}{r_0}\right)^2$	$0.33+0.10\left(\frac{e}{r_0}\right)^2$
	$K_{0r}=K_r-\frac{Gr_0^3}{2(2-\upsilon)}\left(1+\frac{e}{r_0}\right)\left(\frac{e}{r_0}\right)^2$	$-0.08906\left(\frac{e}{r_0}\right)^2$ $-0.00874\left(\frac{e}{r_0}\right)^3$		
Torsional	$\frac{16Gr_0^3}{3}\left(1+2.67\frac{e}{r_0}\right)$	———	$0.29+0.09\sqrt{\frac{e}{r_0}}$	$0.20+0.25\sqrt{\frac{e}{r_0}}$

$$K_h = \frac{8Gr_0}{2-\upsilon}\left(1+\frac{1}{2}\frac{r_0}{d}\right)\left(1+\frac{e}{r_0}\right)\left(1+\frac{e}{d}\right) \quad \text{horizontal}$$

$$K_v = \frac{4Gr_0}{1-\upsilon}\left(1+1.3\frac{r_0}{d}\right)\left(1+0.54\frac{e}{r_0}\right) * \left[1+\left(0.85-0.28\frac{e}{r_0}\right)\frac{\frac{e}{d}}{1-\frac{e}{d}}\right] \quad \text{vertical}$$

$$K_r = \frac{8Gr_0^3}{3(1-\upsilon)}\left(1+\frac{1}{6}\frac{r_0}{d}\right) * \left[1+2.3\frac{e}{r_0}+0.58\left(\frac{e}{r_0}\right)^3\right]\left(1+0.7\frac{e}{d}\right) \quad \text{rocking}$$

$$K_t = \frac{16}{3}Gr_0^3\left(1+\frac{1}{10}\frac{r_0}{d}\right)\left(1+2.67\frac{e}{r_0}\right) \quad \text{torsional}$$

$$K_{hr} = \frac{e}{3}K_h \quad \text{coupling}$$

A3.2 Lumped-Parameter Model

Fundamental Lumped-Parameter Model

A cylindrical rigid foundation with embedment e in a *half-space* can be modeled with the fundamental lumped-parameter model described in Section A1.2 (Fig. A-5). The coupling between the horizontal and rocking motions is achieved by connecting the horizontal lumped-parameter model with eccentricities f_K, f_C to the base (Fig. A-18).

$$f_K = 0.25e \qquad f_C = 0.32e+0.03e\left(\frac{e}{r_0}\right)^2$$

The coefficients are specified as a function of the embedment ratio e/r_0 in Table A-6 (υ=1/4). Note that the coefficients of the rocking lumped-parameter model are defined with respect to K_r (and not K_{0r}), although K_{0r} is the coefficient of the direct spring (Fig. A-18).

$$C_{0r} = \frac{r_0}{c_s}\gamma_0 K_r \quad C_{1r} = \frac{r_0}{c_s}\gamma_1 K_r \quad M_{1r} = \frac{r_0^2}{c_s^2}\mu_1 K_r$$

Table A-7: Dimensionless Coefficients of the Basic Lumped-Parameter Model for a Cylinder Embedded in a Soil Layer on Rigid Rock (Embedment Ratio $e/r_0=1$)

Ratio of Radius to Depth r_0/d	Contact Ratio e_c/e		Vertical	Horizontal	Rocking	Coupling	Torsional
1/2	1.00	k_1	-.203759 E+02	-.124401 E+02	-.125229 E+02	-.618776 E+01	-.139252 E+02
		k_2	+.339543 E+01	+.286199 E+01	-.583152 E+00	+.202777 E+01	-.275441 E+01
		k_3	-.617014 E+01	-.208541 E+02	-.814822 E-01	-.141784 E+02	+.178780 E+01
		k_4	+.166202 E+02	+.794575 E+01	+.130945 E+02	+.337083 E+01	+.161164 E+02
		c_1	-.918456 E+01	-.590158 E+01	-.315268 E+01	-.333135 E+01	-.774712 E-02
		c_2	-.596381 E+00	-.516028 E+01	-.885823 E-01	-.340080 E+01	-.736101 E+00
		c_3	+.131164 E+02	+.130103 E+02	+.322858 E+01	+.811310 E+01	+.858610 E+01
		m	-.987169 E+00	-.163126 E+02	-.680666 E+00	-.146553 E+02	-.962102 E+00
	0.50	k_1	-.190169 E+02	-.123585 E+02	-.918010 E+01	-.311508 E+01	-.150459 E+02
		k_2	+.102770 E+02	+.382788 E+01	+.934512 E+00	+.786487 E+00	+.149201 E+01
		k_3	-.256293 E+02	-.116229 E+02	-.466308 E+01	-.869559 E+01	-.230599 E+01
		k_4	+.480379 E+01	+.697738 E+01	+.821627 E+01	+.184030 E+01	+.132374 E+02
		c_1	-.803919 E+00	-.129978 E+01	-.212247 E+01	-.715314 E+00	-.513171 E+00
		c_2	-.378972 E+01	-.357027 E+01	-.316747 E+00	-.208337 E+01	-.403901 E+00
		c_3	+.131677 E+02	+.102413 E+02	+.266675 E+01	+.326137 E+01	+.511390 E+01
		m	-.364874 E+01	-.820645 E+01	-.342125 E+01	-.888905 E+01	-.515523 E+00
	0.00	k_1	-.199866 E+02	-.113528 E+02	-.801960 E+01		-.820959 E+01
		k_2	+.324059 E+01	+.187819 E+01	+.103933 E+01		+.236828 E+00
		k_3	-.138239 E+03	-.141228 E+02	-.800817 E+01		-.295213 E+00
		k_4	+.151110 E+02	+.837372 E+01	+.584466 E+01		+.794727 E+01
		c_1	-.577181 E+01	-.169786 E+01	-.101867 E+01		-.288545 E+00
		c_2	-.891247 E+01	-.396633 E+01	-.157192 E+01		-.308176 E-01
		c_3	+.151425 E+02	+.710633 E+01	+.313092 E+01		+.160082 E+01
		m	-.485815 E+02	-.142894 E+02	-.217586 E+01		-.372596 E-01
1/3	1.00	k_1	-.215677 E+02	-.800686 E+01	-.112339 E+02	-.531331 E+01	-.158881 E+02
		k_2	+.995664 E+01	+.248098 E+01	+.271244 E+01	+.128879 E+01	-.216892 E+01
		k_3	-.299529 E+02	-.530555 E+01	-.112792 E+02	-.117090 E+02	+.122884 E+01
		k_4	+.122789 E+01	+.460883 E+01	+.830774 E+01	+.314281 E+01	+.175253 E+02
		c_1	-.214856 E+01	-.638370 E-01	-.185381 E+01	-.345899 E+01	-.770582 E+00
		c_2	-.703468 E+01	-.234186 E+01	-.147482 E+01	-.442673 E+01	-.114118 E+01
		c_3	+.195563 E+02	+.101919 E+02	+.461482 E+01	+.913903 E+01	+.899118 E+01
		m	-.476605 E+01	-.598035 E+01	-.101760 E+02	-.222249 E+02	-.244900 E+01
	0.50	k_1	-.263609 E+02	-.105510 E+02	-.812675 E+01	-.258694 E+01	-.164865 E+02
		k_2	+.106994 E+02	+.323771 E+01	+.327590 E+01	+.487010 E+00	+.162631 E+01
		k_3	-.415582 E+02	-.101866 E+02	-.183711 E+02	-.708382 E+01	-.359665 E+01
		k_4	+.391023 E+00	+.579774 E+01	+.434718 E+01	+.155304 E+01	+.138158 E+02
		c_1	-.734715 E-02	-.691681 E-01	-.831614 E+00	-.752538 E+00	-.786309 E+00
		c_2	-.101472 E+02	-.475156 E+01	-.272228 E+01	-.265221 E+01	-.129218 E+01
		c_3	+.195330 E+02	+.114226 E+02	+.507228 E+01	+.383021 E+01	+.600218 E+01
		m	-.674277 E+01	-.148975 E+02	-.147137 E+02	-.128622 E+02	-.159889 E+01
	0.00	k_1	-.147108 E+02	-.922525 E+01	-.736535 E+01		-.790274 E+01
		k_2	+.600489 E+01	+.187933 E+01	-.907967 E+00		+.176502 E-01
		k_3	-.355109 E+02	-.788239 E+01	-.157724 E+03		-.179897 E-01
		k_4	+.527313 E+01	+.637232 E+01	+.684877 E+01		+.788488 E+01
		c_1	-.203850 E+01	-.425306 E-01	-.168579 E+01		-.128670 E+00
		c_2	-.830045 E+01	-.368700 E+01	-.114538 E+02		-.263292 E-03
		c_3	+.145304 E+02	+.682700 E+01	+.130128 E+02		+.157125 E+01
		m	-.200705 E+02	-.139626 E+02	-.920928 E+02		-.331649 E-03

Basic Lumped-Parameter Model

To represent a cylindrical rigid foundation with embedment e in a *soil layer* resting on rigid rock (Fig. A-19), a lumped-parameter model for all degrees of freedom is described. For the vertical and torsional motions the basic lumped-parameter model with four springs, three dashpots and a mass introducing two internal degrees of freedom (Fig. A-12) is directly applicable (described in Section A2.2). For the coupled horizontal and rocking motions, a physical representation (Fig. A-20) exists, consisting of three basic lumped-parameter models, one of which is attached with the eccentricity e to take the coupling into consideration. For various ratios of the radius r_0 of the foundation to the depth d of the layer and lateral contact ratios e_c/e, the frequency-independent real coefficients for all springs, dashpots and masses are specified in Table A-7 (υ=1/3).

A3.3 Pile Foundation

Single Pile

The formulation based on disks embedded in a fullspace with their corresponding double cones and anti-symmetrically and symmetrically loaded mirror-image disks to model a free surface and a fixed boundary can straightforwardly be applied to the dynamic analysis of a single pile

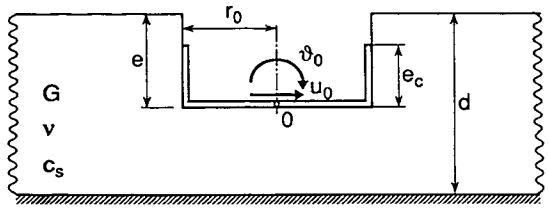

Fig. A-19 Cylindrical foundation with partial contact over embedment height embedded in soil layer resting on rigid rock.

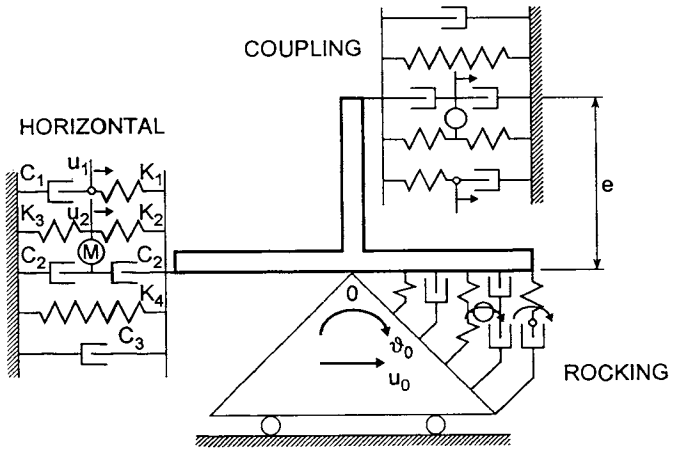

Fig. A-20 Basic lumped-parameter model for embedded foundation with coupling of horizontal and rocking motions.

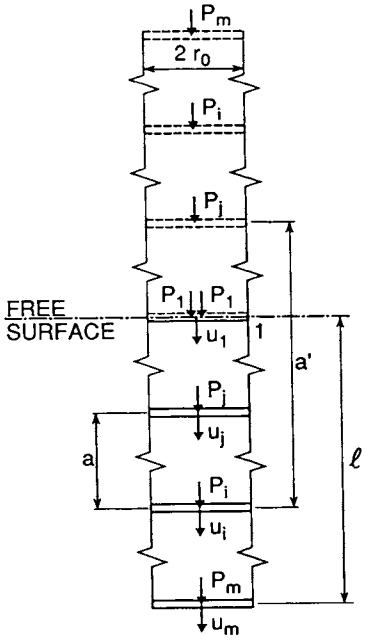

Fig. A-21 Stack of disks to model pile embedded in half-space with anti-symmetrically loaded mirror-image disks.

(Fig. A-21). The cylindrical soil region between the disks is not just analytically excavated as for an embedded foundation, but replaced by the difference of the material properties of the pile and the soil.

Pile Group

For a pile group, pile-soil-pile interaction can be considered with one dynamic-interaction factor in vertical direction and one in the lateral direction $\alpha(\omega)$, defined as the amplitude ratio of the displacement at the head of a receiver pile $u_r\omega)$ to the corresponding displacement of the loaded source pile $u_s(\omega)$ under its own dynamic load (Fig. A-22).

$$\alpha(\omega) = \frac{u_r(\omega)}{u_s(\omega)}$$

Dynamic-Interaction Factor

vertical (Fig. A-22 a)

$$\alpha_v(\omega) = \sqrt{\frac{r_0}{d}}\, e^{-\zeta_g \omega \frac{d}{c_s}}\, e^{-i\omega \frac{d}{c_s}}$$

with the radius r_0, pile distance d and material damping ratio ζ_g.

lateral (horizontal) (Fig. A-22 b)

$$\alpha_h^f(\omega) = \cos^2\theta \alpha_h^f(0°,\omega) + \sin^2\theta \alpha_h^f(90°,\omega)$$

with the angle θ between the horizontal load and the line connecting the source and the receiver piles.

$$\alpha_h^f(0°,\omega) = \sqrt{\frac{r_0}{d}} e^{-\zeta_g \omega \frac{d}{c_p}} e^{-i\omega \frac{d}{c_p}}$$

$$\alpha_h^f(90°,\omega) = \alpha_v(\omega)$$

The dynamic-interaction factor referred to the free-field of the soil (at the location of the receiver pile) $\alpha_h^f(\omega)$ can be transformed to the corresponding factor referred to the head of the receiver pile itself $\alpha_h(\omega)$ based on the concept of substructuring with replacement (see [49], p. 283).

Matrix Formulation

Dynamic-stiffness matrix for harmonic loading with rigid pile cap

$$[S(\omega)] = [A]^T [G(\omega)]^{-1} [A]$$

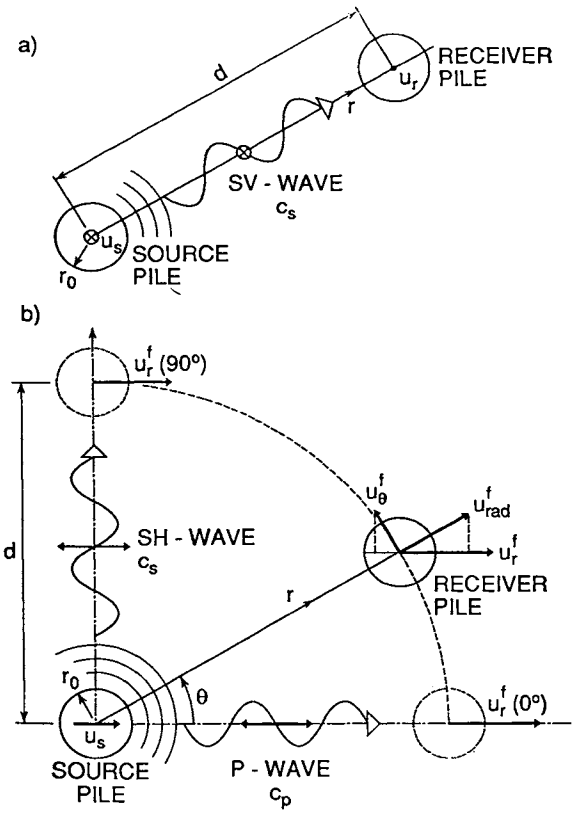

Fig. A-22 Cylindrical waves emitted from shaft of loaded source pile and propagating towards receiver pile determining dynamic-interaction factors.
a) Vertical.
b) Lateral (horizontal).

with kinematic-constraint matrix [A] and dynamic-flexibility matrix [G(ω)] discretized at pile heads. For instance, for vertical motion (Fig. A-23) and with the dynamic-stiffness coefficient S(ω) of a single pile

$$u_i(\omega) = \frac{1}{S(\omega)} * \left(\sum_{j=1}^{i-1} \alpha_v(d_{ij},\omega) P_j(\omega) + P_i(\omega) + \sum_{j=i+1}^{n} \alpha_v(d_{ij},\omega) P_j(\omega) \right)$$
$$i = 1, \ldots, n$$

which is generalized to

$$\{u(\omega)\} = [G(\omega)]\ \{P(\omega)\}$$

A4 SIMPLE VERTICAL DYNAMIC GREEN'S FUNCTION

To calculate the vertical and rocking dynamic-stiffness coefficients for harmonic loading of an irregular basemat which cannot by represented by an equivalent disk on the surface of a homogeneous halfspace, the basemat is modeled as an assemblage of subdisks.

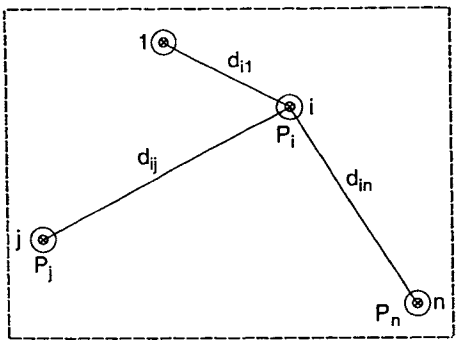

Fig. A-23 Plan view of arrangement of piles in group.

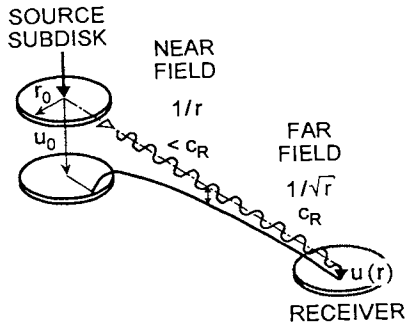

Fig. A-24 Vertical displacement on free surface from source subdisk loaded vertically.

A4.1 Dynamic-Flexibility Matrix of Subdisk

For small values of the dimensionless frequency $a_0 = \omega r_0 / c_s$, the amplitude of the vertical displacement $u_0(a_0)$ produced by a vertical load with amplitude $P(a_0)$ acting on the source disk of radius r_0 equals (Fig. A-24)

$$u_0(a_0) = \frac{P(a_0)}{K(1+0.74ia_0)}$$

with static-stiffness coefficient

$$K = 6Gr_0 \text{ for } \upsilon = 1/3$$

The Green's function outside the disk is approximated as

$$u(r,a_0) = u_0(a_0) A e^{-i\varphi(a_0)}$$

The amplitude-reduction factor A equals

$$A = \frac{2}{\pi}\frac{r_0}{r} \quad \text{for } r \le r_f \text{ (near field)}$$
$$A = \frac{2}{\pi}\frac{r_0}{\sqrt{r_f r}} \quad \text{for } r > r_f \text{ (far field)}$$

with (index R for Rayleigh wave)

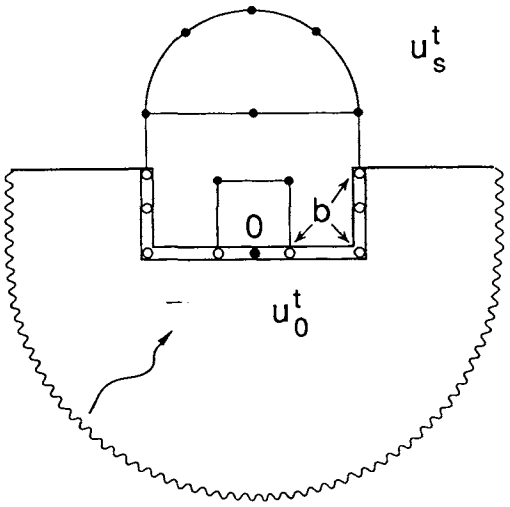

Fig. A-25 Structure-soil system with rigid base.

$$r_f = 0.3\lambda_R = \frac{1.76}{a_0} r_0$$

The phase angle $\varphi(a_0)$ equals

$$\varphi(a_0) = 1.16\, a_0\left(\frac{r}{r_0} - \frac{2}{\pi}\right) \qquad \text{for } r - \frac{2r_0}{\pi} \le 5r_f$$

$$\varphi(a_0) = \frac{\pi}{4} + 1.07\, a_0\left(\frac{r}{r_0} - \frac{2}{\pi}\right) \qquad \text{for } r - \frac{2r_0}{\pi} > 5r_f$$

With the amplitudes of the vertical forces $\{P(a_0)\}$ acting on the subdisks and of the vertical displacements $\{u(a_0)\}$

$$\{u(a_0)\} = [G(a_0)]\{P(a_0)\}$$

where the dynamic-flexibility matrix $[G(a_0)]$ is constructed based on the approximate Green's function of the subdisk.

A4.2 Matrix Formulation

The dynamic-stiffness matrix with respect to the displacement amplitudes of the rigid basemat $\{u_0(a_0)\}$ equals

$$[S(a_0)] = [A]^T[G(a_0)]^{-1}[A]$$

with the kinematic-constraint matrix [A] defined as

$$\{u(a_0)\} = [A]\{u_0(a_0)\}$$

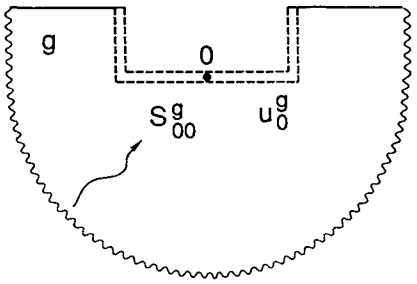

Fig. A-26 Soil system ground with excavation and rigid structure-soil interface.

A5 SEISMIC EXCITATION

A5.1 Basic Equation of Motion

Frequency Domain

Basic equation of motion of substructure method for harmonic loading for analysis of dynamic soil-structure interaction for seismic excitation (Fig. A-25)

$$\begin{bmatrix}[S_{ss}(\omega)] & [S_{s0}(\omega)] \\ [S_{0s}(\omega)] & [S_{00}^s(\omega)]\end{bmatrix}\begin{Bmatrix}\{u_s^t(\omega)\} \\ \{u_0^t(\omega)\}\end{Bmatrix} = \begin{Bmatrix}\{0\} \\ -\{P_0(\omega)\}\end{Bmatrix}$$

with amplitudes of total displacements in nodes within structure $\{u_s^t(\omega)\}$ and on rigid structure-soil interface $\{u_0^t(\omega)\}$ and dynamic-stiffness matrix of structure (static-stiffness matrix [K], mass matrix [M], hysteretic damping ratio ζ).

$$[S^s(\omega)] = [K](1+2i\zeta) - \omega^2[M]$$

$[S_{00}^g(\omega)]$ denotes the dynamic-stiffness matrix of unbounded soil with excavation (ground, Fig. A-26). Amplitudes of soil's interaction forces are formulated as

$$\{P_0(\omega)\} = [S_{00}^g(\omega)]\left(\{u_0^t(\omega)\} - \{u_0^g(\omega)\}\right)$$

with the effective foundation input motion $\{u_0^g(\omega)\}$ (Fig. A-26). Defining driving loads as

$$\{P_0^g(\omega)\} = [S_{00}^g(\omega)]\{u_0^g(\omega)\}$$

the equation of motion equals

$$\begin{bmatrix}[S_{ss}(\omega)] & [S_{s0}(\omega)] \\ [S_{0s}(\omega)] & [S_{00}^s(\omega)]+[S_{00}^g(\omega)]\end{bmatrix}\begin{Bmatrix}\{u_s^t(\omega)\} \\ \{u_0^t(\omega)\}\end{Bmatrix} = \begin{Bmatrix}\{0\} \\ \{P_0^g(\omega)\}\end{Bmatrix}$$

Time Domain

Basic equation in time domain (viscous damping matrix of structure)

$$\begin{bmatrix}[M_{ss}][M_{s0}]\\ [M_{0s}][M_{00}]\end{bmatrix}\begin{Bmatrix}\{\ddot{u}_s^t(t)\}\\ \{\ddot{u}_0^t(t)\}\end{Bmatrix}+\begin{bmatrix}[C_{ss}][C_{s0}]\\ [C_{0s}][C_{00}]\end{bmatrix}\begin{Bmatrix}\{\dot{u}_s^t(t)\}\\ \{\dot{u}_0^t(t)\}\end{Bmatrix}+$$
$$\begin{bmatrix}[K_{ss}][K_{s0}]\\ [K_{0s}][K_{00}]\end{bmatrix}\begin{Bmatrix}\{u_s^t(t)\}\\ \{u_0^t(t)\}\end{Bmatrix}=\begin{Bmatrix}\{0\}\\ -\{P_0(t)\}\end{Bmatrix}$$

A5.2 Interaction Force of Soil and Driving Load

Disk on Homogeneous Halfspace Modeled with Cones (Section A1.1)

translation

$$\begin{aligned}P_0(t) &= K\left(u_0^t(t)-u_0^g(t)\right)+C\left(\dot{u}_0^t(t)-\dot{u}_0^g(t)\right)\\ &= Ku_0^t(t)+C\dot{u}_0^t(t)-P_0^g(t)\\ \text{with}\quad P_0^g(t) &= Ku_0^g(t)+C\dot{u}_0^g(t)\end{aligned}$$

rotation

$$\begin{aligned}M_0(t) &= K_\vartheta\left(\vartheta_0^t(t)-\vartheta_0^g(t)\right)+C_\vartheta\left(\dot{\vartheta}_0^t(t)-\dot{\vartheta}_0^g(t)\right)\\ &\quad-\int_0^t h_1(t-\tau)C_\vartheta\left(\dot{\vartheta}_0^t(\tau)-\dot{\vartheta}_0^g(\tau)\right)d\tau\\ &= K_\vartheta\vartheta_0^t(t)+C_\vartheta\dot{\vartheta}_0^t(t)-\int_0^t h_1(t-\tau)\,C_\vartheta\dot{\vartheta}_0^t(\tau)d\tau-M_0^g(t)\end{aligned}$$

with

$$M_0^g(t)=K_\vartheta\vartheta_0^g(t)+C_\vartheta\dot{\vartheta}_0^g(t)-\int_0^t h_1(t-\tau)C_\vartheta\dot{\vartheta}_0^g(\tau)d\tau$$

Disk on Layer on Rock Modeled with Unfolded Layered Cone (Section A2.1)

translation

$$\begin{aligned}P_0(t) &= K\left(\sum_{j=0}^{k}e_j^K\left(u_0^t(t-jT)-u_0^g(t-jT)\right)\right)\\ &\quad+C\left(\sum_{j=0}^{k}e_j^K\left(\dot{u}_0^t(t-jT)-\dot{u}_0^g(t-jT)\right)\right)\\ &= K\sum_{j=0}^{k}e_j^Ku_0^t(t-jT)+C\sum_{j=0}^{k}e_j^K\dot{u}_0^t(t-jT)-P_0^g(t)\end{aligned}$$

with

$$P_0^g(t)=K\sum_{j=0}^{k}e_j^Ku_0^g(t-jT)+C\sum_{j=0}^{k}e_j^K\dot{u}_0^g(t-jT)$$

analogously for rocking unfolded layered cone

Embedded Foundation Modeled with Stack of Disks

for vertically propagating free-field motion $\{u^f(t)\}$

$$\begin{aligned}\{P_0\}_n &= [A]^T[S^f]_0[A]\{u_0^t\}_n-[A]^T[S^f]_0\{\bar{u}\}_n\\ &\quad-[M]\{\ddot{u}_0^t\}_n-[A]^T[S^f]_0\{u^f\}_n\\ &= [A]^T[S^f]_0[A]\{u_0^t\}_n-[A]^T[S^f]_0\{\bar{u}\}_n\\ &\quad-[M]\{\ddot{u}_0^t\}_n-\{P_0^g\}_n\end{aligned}$$

with $$\{P_0^g\}_n=[A]^T[S^f]_0\{u^f\}_n$$

A5.3 Effective Foundation Input Motion

Effective Foundation Input Motion for Harmonic Loading

$$\{u_0^g(\omega)\}=\left[S_{00}^g(\omega)\right]^{-1}[A]^T\left[S_{bb}^f(\omega)\right]\{u_b^f(\omega)\}$$

with dynamic-stiffness matrix $\left[S_{bb}^f(\omega)\right]$ and motion of free field $\{u_b^f(\omega)\}$ in those nodes (disks) b which will later lie on the structure-soil interface and with kinematic-constraint matrix [A] (see Fig. A-27).

Surface Foundation on Homogeneous Halfspace Modeled with Subdisks (Section A4)

vertical and rocking motions $\{u_0^g(\omega)\}$ caused by vertical free-field displacement with amplitude

$$u_z^f(x,\omega)=u_z^f(\omega)e^{-i\frac{\omega}{c_a}x}$$

propagating horizontally in x-direction with apparent velocity c_a

$$\{u_0^g(\omega)\}=\left([A]^T[G(a_0)]^{-1}[A]\right)^{-1}[A]^T[G(a_0)]^{-1}\{u_b^f(\omega)\}$$

with $\{u_b^f(\omega)\}$ equal to $\{u_z^f(x,\omega)\}$ evaluated in nodes b.

Surface Foundation Modeled with Distributed Springs

Vertical and rocking motions w_0^g, β_0^g caused by vertical free-field displacement propagating horizontally with apparent velocity c_a

$$u_z^f(x,t)=u^f\left(t-\frac{x}{c_a}\right)$$

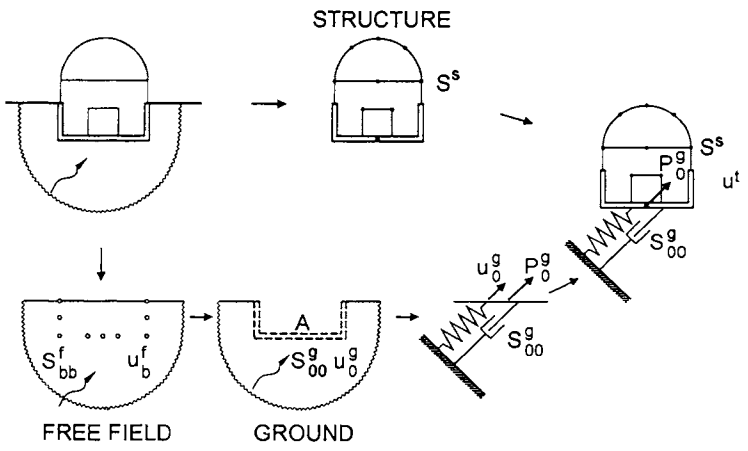

Fig. A-27 Physical interpretation of basic equation of motion in total displacements with effective foundation input motion and driving loads.

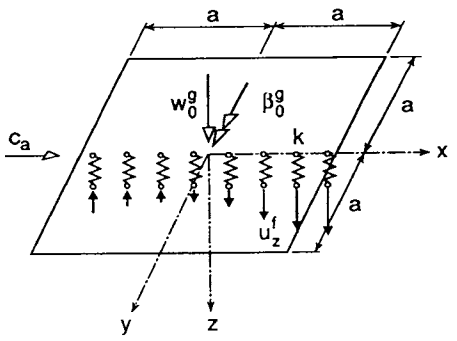

Fig. A-28 Effective foundation input motion for vertical component of horizontally propagating wave acting on rigid square basemat with distributed springs beneath.

for square foundation of length 2a and spring constant k (Fig. A-28)

$$w_0^g(t) = \frac{1}{k4a^2}\int_{-a}^{+a} k2a\; u^f\left(t-\frac{x}{c_a}\right)dx = \frac{c_a}{2a}\int_{t-a/c_a}^{t+a/c_a} u^f(\bar{x})d\bar{x}$$

$$\beta_0^g(t) = -\frac{1}{k\frac{4}{3}a^4}\int_{-a}^{+a} xk2a\; u^f\left(t-\frac{x}{c_a}\right)dx$$

$$= \frac{3}{2}\frac{c_a^2}{a^3}\left(\int_{t-a/c_a}^{t+a/c_a}\bar{x}u^f(\bar{x})d\bar{x} - t\int_{t-a/c_a}^{t+a/c_a}u^f(\bar{x})d\bar{x}\right)$$

Embedded Foundation Modeled with Stacks of Disks (Section A3.1)

for vertically propagating free-field motion with amplitude $\{u^f(\omega)\}$

$$\{u_0^g(\omega)\} = [S_{00}^g(\omega)]^{-1}[A]^T[S^f(\omega)]\{u^f(\omega)\}$$

A5.4 Foundation Represented by Lumped-Parameter Model

When a lumped-parameter model for the soil is used, the effective seismic input motion $\{u_0^g(t)\}$ is in a first step applied at the base (where the structure will later be connected) of the soil model, leading to the reaction forces (driving loads) $\{P_0^g(t)\}$. The latter are then applied to the total dynamic model in the second step, yielding the total dynamic response. The procedure is summarized in Fig. A-27. As an example the rocking motion of a rigid block on a homogeneous halfspace modeled with the lumped-parameter model (discrete-element model) of Fig. A-2c is addressed in Fig. A-29.

A6 DYNAMIC SOIL-STRUCTURE INTERACTION

A simple coupled dynamic model (Fig. A-30) consisting of a vertical rigid bar with the horizontal and rocking springs and dashpots with frequency-dependent coefficients $Kk(a_0)$, $(r_0/c_s)\,Kc(a_0)$ and $K_\vartheta k_\vartheta(a_0)$, $r_0/c_s)\,K_\vartheta c_\vartheta(a_0)$ representing the soil attached at one end and at the other one, at a distance equal to the height h, a spring with coefficient k connected to a mass m, which models the structure, correctly captures the essential effects of soil-structure interaction for a horizontal seismic excitation u^g. The dynamic-stiffness coefficients of the soil are calculated with cones for a halfspace (Section A1.1) and with unfolded layered cones for a layer resting on rigid or flexible rock (Section A2.1).

The coupled system can be replaced by an equivalent one-degree-of-freedom system (Fig. A-31) enforcing the same structural distortion u as in the coupled dynamic system with the same mass m, the effective natural frequency $\tilde{\omega}$, the effective damping ratio $\tilde{\zeta}$ and the effective input motion $\tilde{u}^g$.

$$\frac{1}{\tilde{\omega}^2} = \frac{1}{\omega_s^2} + \frac{1}{\omega_h^2(\tilde{a}_0)} + \frac{1}{\omega_r^2(\tilde{a}_0)}$$

$$\tilde{\zeta} = \frac{\tilde{\omega}^2}{\omega_s^2}\zeta + \left(1-\frac{\tilde{\omega}^2}{\omega_s^2}\right)\zeta_g + \frac{\tilde{\omega}^2}{\omega_h^2(\tilde{a}_0)}\zeta_h(\tilde{a}_0) + \frac{\tilde{\omega}^2}{\omega_r^2(\tilde{a}_0)}\zeta_r(\tilde{a}_0)$$

$$\tilde{u}^g = \frac{\tilde{\omega}^2}{\omega_s^2}u^g$$

with the natural frequencies

$$\omega_s = \sqrt{\frac{k}{m}}$$ fixed-base structure

$$\omega_h(\tilde{a}_0) = \sqrt{\frac{Kk(\tilde{a}_0)}{m}}$$ rigid structure and rocking motion prevented

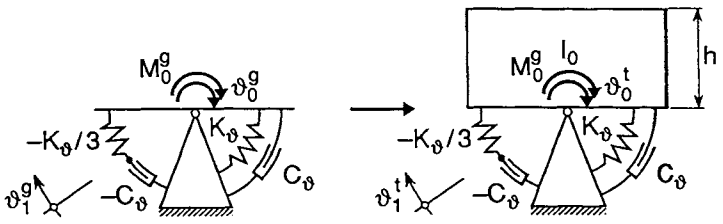

Fig. A-29 Rigid structure on soil halfspace. Lumped-parameter model of soil with applied effective foundation input rotational motion yielding reaction moment, which as driving moment acts on total dynamic system leading to total rotation.

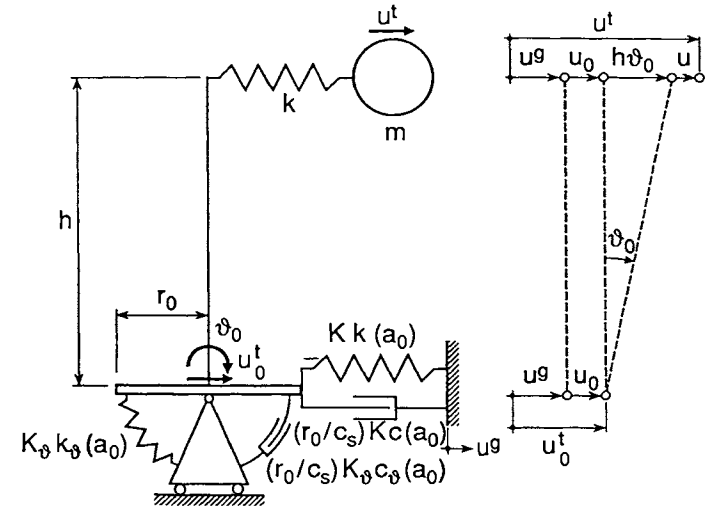

Fig. A-30 Coupled dynamic model of structure and soil for horizontal and rocking motions.

$$\omega_r(\tilde{a}_0) = \sqrt{\frac{K_\vartheta k_\vartheta(\tilde{a}_0)}{mh^2}}$$ rigid structure and horizontal motion prevented

the damping ratios

$$\zeta_h(\tilde{a}_0) = \frac{\tilde{a}_0 c(\tilde{a}_0)}{2k(\tilde{a}_0)}$$ horizontal radiation

$$\zeta_r(\tilde{a}_0) = \frac{\tilde{a}_0 c_\vartheta(\tilde{a}_0)}{2k_\vartheta(\tilde{a}_0)}$$ rocking radiation

and the hysteretic material damping of the structure ζ and of the soil ζ_g.

For a redundant coupled structure-soil system where the mass of the structure can only displace horizontally but not rotate (Fig. A-32), the equivalent one-degree-of-freedom system for horizontal seismic excitation is defined by the parameters

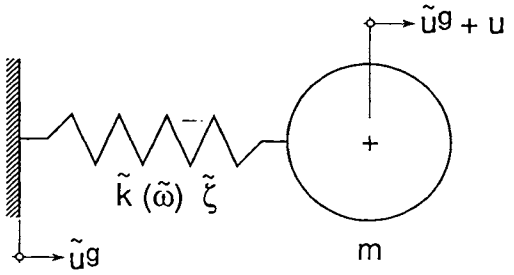

Fig. A-31 Equivalent one-degree-of-freedom system leading to same structural distortion with same mass, effective input motion, effective damping ratio and effective natural frequency determining effective spring.

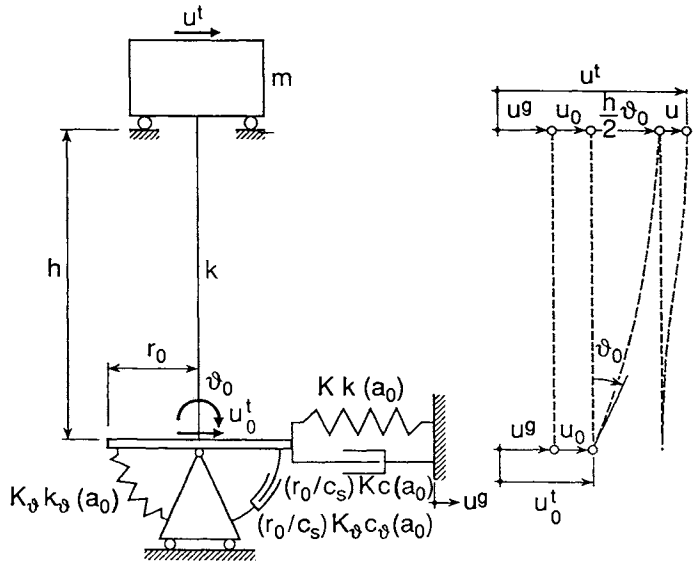

Fig. A-32 Redundant coupled dynamic model of structure with zero rotation of mass and of soil for horizontal and rocking motions.

$$\frac{1}{\tilde{\omega}^2} = \frac{1}{\omega_s^2} + \frac{1}{\omega_h^2(\tilde{a}_0)} + \frac{3}{\omega_s^2 + 12\omega_r^2(\tilde{a}_0)}$$

$$\tilde{\zeta} = \zeta - \frac{\tilde{\omega}^2}{\omega_h^2(\tilde{a}_0)}\left[\zeta - \zeta_g - \zeta_h(\tilde{a}_0)\right] - \frac{36\tilde{\omega}^2\omega_r^2(\tilde{a}_0)}{\left(\omega_s^2 + 12\omega_r^2(\tilde{a}_0)\right)^2}\left[\zeta - \zeta_g - \zeta_r(\tilde{a}_0)\right]$$

$$\tilde{u}^g = \frac{\tilde{\omega}^2}{\omega_s^2} u^g$$

REFERENCES

[1] R.J. Apsel and J.E. Luco, Impedance Functions for Foundations Embedded in a Layered Medium: An Integral Equation Approach, *Earthquake Engineering and Structural Dynamics*, 15 (1987): 213-231.

[2] F.C.P. de Barros and J.E. Luco, Discrete Models for Vertical Vibrations of Surface and Embedded Foundation, *Earthquake Engineering and Structural Dynamics*, 19 (1990), 289-303.

[3] G. Dasgupta, Foundation Impedance Matrices by Substructure Deletion, *Journal of the Engineering Mechanics Division*, ASCE, 106 (1980): 517-523.

[4] R. Dobry and G. Gazetas, Simple Method for Dynamic Stiffness and Damping of Floating Pile Groups, *Géotechnique*, 38 (1988): 557-574.

[5] G. Ehlers, The Effect of Soil Flexibility on Vibrating Systems, *Beton und Eisen*, 41 (1942): 197-203 [in German].

[6] J.M. Emperador and J. Dominguez, Dynamic Response of Axisymmetric Embedded Foundations, *Earthquake Engineering and Structural Dynamics*, 18 (1989): 1105-1117.

[7] G. Gazetas and R. Dobry, Simple Radiation Damping Model for Piles and Footings, *Journal of Engineering Mechanics*, ASCE, 110 (1984), 937-956.

[8] G. Gazetas, Simple Physical Methods for Foundation Impedances, in *Dynamic Behaviour of Foundations and Buried Structures* (Developments in Soil Mechanics and Foundation Engineering, Vol.3), edited by P.K. Banerjee and R. Butterfield, Chapter 2, pp. 45-93 (London: Elsevier Applied Science, 1987).

[9] G. Gazetas, Foundation Vibrations, in *Foundation Engineering Handbook*, 2nd Edition, edited by H.-J. Fang, Chapter 15, pp. 553-593 (New York: Van Nostrand Reinhold, 1991).

[10] G. Gazetas and N. Markis, Dynamic Pile-Soil-Pile Interaction, Part I: Analysis of Axial Vibration, *Earthquake Engineering and Structural Dynamics*, 20 (1991): 115-132.

[11] G. Gazetas, Formulas and Charts for Impedances of Surface and Embedded Foundations, *Journal of Geotechnical Engineering*, ASCE, 117 (1991): 1363-1381.

[12] E. Kausel, personal communication, 1990.

[13] A.M. Kaynia and E. Kausel, Dynamic Behavior of Pile Groups, *Proceedings of 2nd International Conference on Numerical Methods of Offshore Piling*, Austin, TX, 1982: 509-532.

[14] J.E. Luco and H.L. Wong, Seismic Response of Foundations Embedded in a Layered Half-space, *Earthquake Engineering and Structural Dynamics*, 15 (1987): 233-247.

[15] J.W. Meek and A.S. Veletsos, Simple Models for Foundations in Lateral and Rocking Motions, *Proceedings of the 5th World Conference on Earthquake Engineering*, Rome, 1974, Vol. 2: 2610-2613.

[16] J.W. Meek and J.P. Wolf, Insights on Cutoff Frequency for Foundation on Soil Layer, *Earthquake Engineering and Structural Dynamics*, 20 (1991): 651-665.

[17] J.W. Meek and J.P. Wolf, Cone Models for Homogeneous Soil, *Journal of Geotechnical Engineering*, ASCE, 118 (1992): 667-685.

[18] J.W. Meek and J.P. Wolf, Cone Models for Soil Layer on Rigid Rock, *Journal of Geotechnical Engineering*, ASCE, 118 (1992): 686-703.

[19] J.W. Meek and J.P. Wolf, Cone Models for Nearly Incompressible Soil, *Earthquake Engineering and Structural Dynamics*, 22 (1993): 649-663.

[20] J.W. Meek and J.P. Wolf, Why Cone Models Can Represent the Elastic Half-space, *Earthquake Engineering and Structural Dynamics*, 22 (1993): 759-771.

[21] J.W. Meek and J.P. Wolf, Approximate Green's Function for Surface Foundations, *Journal of Geotechnical Engineering*, ASCE, 119 (1993): 1499-1514.

[22] J.W. Meek and J.P. Wolf, Cone Models for an Embedded Foundation, *Journal of Geotechnical Engineering*, ASCE, 120 (1994): 60-80.

[23] J.W. Meek and J.P. Wolf, Material Damping for Lumped-Parameter Models of Foundations, *Earthquake Engineering and Structural Dynamics*, 23 (1994): 349-362.

[24] J.W. Meek and J.P. Wolf, Non-Linear Seismic Soil-Structure Interaction Using Simple Physical Models of the Soil, *Proceedings of the 8th International Conference on Computer Methods and Advances in Geomechanics*, Morgantown WV, 1994, edited by H.J. Siriwardane and M.M. Zaman, Vol. II: 943-948. (Rotterdam, Balkema, 1994).

[25] J.W. Meek and J.P. Wolf, Cones and Rigorous Solutions. A Good Marriage for Layered Systems? Radiating Versus Ordinary Cones, *Proceedings of Second International Conference on Earthquake Resistant Construction and Design*, Berlin, 1994, edited by S.A. Savidis, Vol. 1: 359-366 (Rotterdam, Balkema, 1994).

[26] National Earthquake Hazards Reduction Program (NEHRP), *Recommended Provisions for the Development of Seismic Regulations for New Buildings*, Building Seismic Safety Council, Washington DC, 1986.

[27] A. Pais and E. Kausel, Approximate Formulas for Dynamic Stiffnesses of Rigid Foundations, *Soil Dynamics and Earthquake Engineering*, 7 (1988): 213-227.

[28] F.E. Richart, J.R. Hall and R.D. Woods, *Vibrations of Soils and Foundations*. Englewood Cliffs, NJ: Prentice-Hall, 1970.

[29] J.M. Roesset, The Use of Simple Models in Soil-Structure Interaction, *Civil Engineering and Nuclear Power*, ASCE, N° 1/3, 1980, 1-25.

[30] J.M. Roesset, Stiffness and Damping Coefficients in Foundations, *Dynamic Response of Pile Foundations*, ed. M.O. Neil and R. Dobry, ASCE, 1980, 1-30.

[31] J.L. Tassoulas, *Elements for the Numerical Analysis of Wave Motion in Layered Media* (Research Report R81-2). Department of Civil Engineering, Massachusetts Institute of Technology, Cambridge, MA: 1981.

[32] A.S. Veletsos and Y.T. Wei, Lateral and Rocking Vibration of Footings, *Journal of the Soil Mechanics and Foundation Division*, ASCE, 97 (1971): 1227-1248.

[33] A.S. Veletsos and B. Verbic, Vibration of Viscoelastic Foundations, *Earthquake Engineering and Structural Dynamics*, 2 (1973):87-102.

[34] A.S. Veletsos and B. Verbic, Basic Response Functions for Elastic Foundations, *Journal of the Engineering Mechanics Division*, ASCE, 100 (1974): 189-202.

[35] A.S. Veletsos and V.D. Nair, Response of Torsionally Excited Foundations, *Journal of the Geotechnical Engineering Division*, ASCE, 100 (1974):476-482.

[36] A.S. Veletsos and V.D. Nair, Seismic Interaction of Structures on Hysteretic Foundations, *Journal of Structural Division*, ASCE, 101 (1975), 109-129.

[37] G. Waas, personal communication, 1992.

[38] R.V. Whitman, Soil-Platform Interaction, *Proceedings of Conference on Behaviour of Offshore Structures*, Vol. 1, Norwegian Geotechnical Institute, Oslo, 1976: 817-829.

[39] J.P. Wolf and D.R. Somaini, Approximate Dynamic Model of Embedded Foundation in Time Domain, *Earthquake Engineering and Structural Dynamics*, 14 (1986):683-703.

[40] J. P. Wolf, Consistent Lumped-Parameter Models for Unbounded Soil: Physical Representation, *Earthquake Engineering and Structural Dynamics*, 20 (1991): 11-32.

[41] J.P. Wolf and A. Paronesso, Lumped-Parameter Model for Foundation on Layer, *Proceedings of 2nd International Conference on Recent Advances in Geotechnical Earthquake Engineering and Soil Dynamics*, edited by S. Prakash, St. Louis MO, 1991; Vol. I: 895-905.

[42] J.P. Wolf, J.W. Meek and Ch. Song, Cone Models for a Pile Foundation, *Piles under Dynamic Loads*, Edited by S. Prakash. Geotechnical Special Publication No. 34, ASCE (1992): 94-113.

[43] J.P. Wolf and A. Paronesso, Lumped-Parameter Model for a Rigid Cylindrical Foundation Embedded in a Soil Layer on Rigid Rock, *Earthquake Engineering and Structural Dynamics*, 21 (1992): 1021-1038.

[44] J.P. Wolf and J.W. Meek, Cone Models for a Soil Layer on Flexible Rock Half-space, *Earthquake Engineering and Structural Dynamics*, 22 (1993): 185-193.

[45] J.P. Wolf and J.W. Meek, Insight on 2D- versus 3D-Modelling of Surface Foundations via Strength-of-Materials Solutions for Soil Dynamics, *Earthquake Engineering and Structural Dynamics*, 23 (1994): 91-112.

[46] J.P. Wolf and J.W. Meek, Rotational Cone Models for a Soil Layer on Flexible Rock Half-space, *Earthquake Engineering and Structural Dynamics*, 23 (1994), in press.

[47] J.P. Wolf and J.W. Meek, Dynamic Stiffness of Foundation on Layered Soil Halfspace Using Cone Frustums, *Earthquake Engineering and Structural Dynamics* , 23 (1994), in press.

[48] J.P. Wolf and J.W. Meek, Linear Seismic Soil-Structure Interaction Using Simple Physical Models of the Soil, *Proceedings of Fifth US National Conference on Earthquake Engineering*, Chicago 1994, Vol. IV: 5-14.

[49] J.P. Wolf, *Foundation Vibration Analysis Using Simple Physical Models*, Englewood Cliffs, NJ: Prentice-Hall, 1994.

[50] H.L. Wong and J.E. Luco, Tables of Influence Functions for Square Foundations on Layered Media, *Soil Dynamics and Earthquake Engineering*, 4 (1985): 64-81.

[51] H.L. Wong and J.E. Luco, Dynamic Interaction between Rigid Foundations in a Layered Half-space, *Soil Dynamics and Earthquake Engineering*, 5 (1986): 149-158.